UNIVERSITÀ DEGLI STUDI DI MESSINA

Dipartimento di Scienze Chimiche, Biologiche, Farmaceutiche ed Ambientali

---

DOTTORATO DI RICERCA IN SCIENZE CHIMICHE
XXIX CICLO

BINDING ABILITY OF SOME COMMERCIALLY AVAILABLE AND SYNTHESIZED LIGANDS TOWARDS METAL CATIONS OF ENVIRONMENTAL AND BIOLOGICAL INTEREST

Dott. Anna IRTO

Supervisore
Prof. Concetta DE STEFANO

Coordinatore
Prof. Sebastiano CAMPAGNA

Triennio 2014-2016

Summary

Chapter 1

Introduction

1.1. The Speciation

In the last years the increase of pollution and of the onset of diseases, led the scientific community to a great interest towards the study of the impact that some substances (*e.g.* metals, organic and inorganic compounds) could have on humans and the environment and the rulers to approve more specific laws to stem these types of problems.[1] It is already known that the biological and chemical activity of these substances can be attributed only to some of the chemical forms in which they are present in the natural fluids. To understand better their mechanism of action, it is necessary to know not only their analytical concentration, but also their "*speciation*". This term indicates the distribution of the physical and chemical forms (isotopic composition, electronic or oxidation state, inorganic compounds and complexes, organometallic compounds, organic and macromolecular complexes) in which a component is present in a system. The speciation analysis is so an analytic study for the identification and/or the measurement of the concentration of one or more individual physical or chemical species in a sample.[2]

Since the different forms of a substance may have various behavior towards humans and environment, the study of speciation becomes essential to have information about their bioavailability, toxicity and environmental impact.

This type of approach is diffused in the fields of food, clinical and environmental chemistry, biogeochemistry, medicine, pharmacy and industry.

Focusing on the investigation of the chemical species in a sample, the speciation can be performed in four different ways:

- screening speciation, with the determination of only one analyte;
- group speciation, with which the concentration of a group of compounds is determined;
- distribution speciation, mostly used for the analysis of biological samples;
- individual speciation, with the identification of chemical species through the use of fractionation and separation techniques.

Table 1.1 reports some examples of applications of the speciation studies, while in Figure 1.1 a description of the different type of speciation analysis performed in analytical chemistry is represented.[1]

When a substance is in a multicomponent system, the possible chemical species which could be present can be classified in:

- elements, with different oxidation states (*e.g.* As(III)/As(V), Cr(III)/Cr(VI)) or ionic (cationic, anionic) forms (NO_3^-/NO_2^-, SO_4^{2-}/SO_3^{2-});
- simple organometallic species characterized by alkyl- or aryl-metal bonds;
- organometallic complexes, usually with high molecular weights;
- ionic species and hydrated ions (like $[Ni(H_2O)_6]^{2+}$);
- highly dispersed colloids (such as $Fe(OH)_3$, Ag_2S);
- colloid-bonded metals (*e.g.* Fe-oxides).[3]

Some examples about the behavior of the substances according to their different forms are mentioned below. The As(III) and As(V) are toxic, but if they are characterized by a methyl group, the toxicity decreases, while the As-betaine complex is completely non toxic. Regarding the chromium, Cr(III) is essential and, as it is already known[4], participates in the metabolism of glucose, while Cr(VI) is highly toxic and carcinogenic.

Also the concentration of a substance could cause very different effects. Indeed, there are some trace elements that are essential for physiological roles and for the life on the Earth, but their excess or deficiency can be really dangerous for living organisms.

For example, iron trace in the human body have catalytic functions in cells and organisms.

Iron is present into proteins, which participate to the energy metabolism, like the cytochromes and some enzymes in the electron transport system. A deficiency of Fe provokes anemia, with problems of shortness of breath, dizziness, headache, coldness in hands and feet, pale skin, chest pain, weakness and tiredness.[3] People have the sensation of fatigue because there are not enough red blood cells to carry oxygen to the different parts of the human body.

On the contrary, an overload of iron could cause different types of symptoms, such as thyroid dysfunctions in women, the so-called "iron fist", with pain in the knuckles of the hand and at the base of the thumb, and the arise of the hemochromatosis, a disease that leads damages to organs such as liver, pancreas and heart. It was also found that an excess of iron may cause oxidative damages with hepatic lipid peroxidation, nuclear DNA harms and mitochondrial dysfunctions.[5]

Speciation studies can be performed using different approaches:

- in situ determination, that gives few information;
- determination on pretreated sample, which allows to work with a simplified system, but with the risk to not consider all the constituents into the model;
- chemical model, that use of a system "model" where a component is added and the behavior of this system in opportune conditions of pH, temperature and pressure is studied;
- biological model, that use the same approach of the chemical model, but in this case some nutrients are added in different conditions (*e.g.* light, contaminants) and the behavior of some organisms is monitored;
- thermodynamic approach, based on the determination of thermodynamic properties (*e.g.* equilibrium constants K_{eq}, dependence of thermodynamic parameters on ionic strength and temperature) related to the formation of the species in the matrix.

In this last case, to have a complete idea about the chemical speciation of a substance in a multicomponent system, it is necessary to consider the process of formation of all the possible chemical species and to evaluate the interactions with other species in the system.

Therefore, the consideration of reactions such as the protonation of the ligands, the hydrolysis of the metal cations, the metal-ligand complexation, redox, dissolution/precipitation reactions and adsorption processes should be considered.

Moreover, the effect of experimental conditions such as the metal-ligand concentration ratio (c_M / c_L), the temperature (T), the ionic medium and the ionic strength (I) are important for a correct study of speciation.

Different analytical techniques can be used to perform a complete speciation study, such as potentiometry (ISE-H^+), UV-Vis spectrophotometry, spectrofluorimetry, calorimetry, nuclear magnetic resonance (NMR), voltammetry, electrophoresis, gas chromatography (GC), high performance liquid chromatography (HPLC), hyphenated methods (*e.g.* GC-MS, LC-MS, GC-ICP-MS).

The most common procedures for the determination of stability constants are electrochemical and spectrophotometric titration techniques.

The experimental data usually are processed by suitable computer programs which allow to determine the equilibrium constants of the different species and the speciation model, considered the best possible on the base of some criteria such as simplicity, probability, statistical parameters, formation percentages and comparison of the results with the literature data.

To understand better the distribution of the metal-ligand complex species determined, it is possible to draw the speciation diagrams, where their formation percentages (or the mole fractions) are plotted *vs.* pH values, in the experimental conditions (*e.g.* concentration of metal cation and ligand, ionic strength, ionic medium, temperature) of the measurements.

Table 1.1. Examples of applications of the speciation studies.

Element (Symbol)	Application area of speciation analysis
Aluminium (Al)	Polymerization products. Forms of aluminium (*e.g.*, labile, complexed) in serum.
Antimony (Sb)	Redox forms and organoantimony compounds in the environment and food products.
Arsenic (As)	Redox forms and organoarsenic compounds in the environment. Arsenic-bound proteins in serum and hemoglobin. Arsenic in food products. Forms of arsine AsH_3 (arsenious hydride) in indoor air at the workplace.
Cadmium (Cd)	Complex organic cadmium compounds, metallothionine.
Chromium (Cr)	Redox forms of chromium, Cr(VI) in the environment. Chemical forms of chromium coupled with proteins.
Iodine (I)	Iodine forms in the environment and biological fluids.
Lead (Pb)	Forms of lead compounds in the environment, *e.g.*, trialkylated Pb compounds.
Phosphorus (P)	Phosphine (hydrogen phosphides) in indoor air at workplace
Mercury (Hg)	Forms of mercury compounds in the environment and food products (in particular methylmercury).
Platinum (Pt)	Inorganic forms in the environment. Metallo-organic forms of cis-platinum in medicine (therapeutic).
Selenium (Se)	Inorganic and organometallic selenium compounds in the environment and food products (*e.g.*, potatoes).
Tin (Sn)	Organometallic forms in the environment and food products (*e.g.*, shellfish)
Actinide series	Chemical forms of compounds in the environment and in radioactive waste storage places.

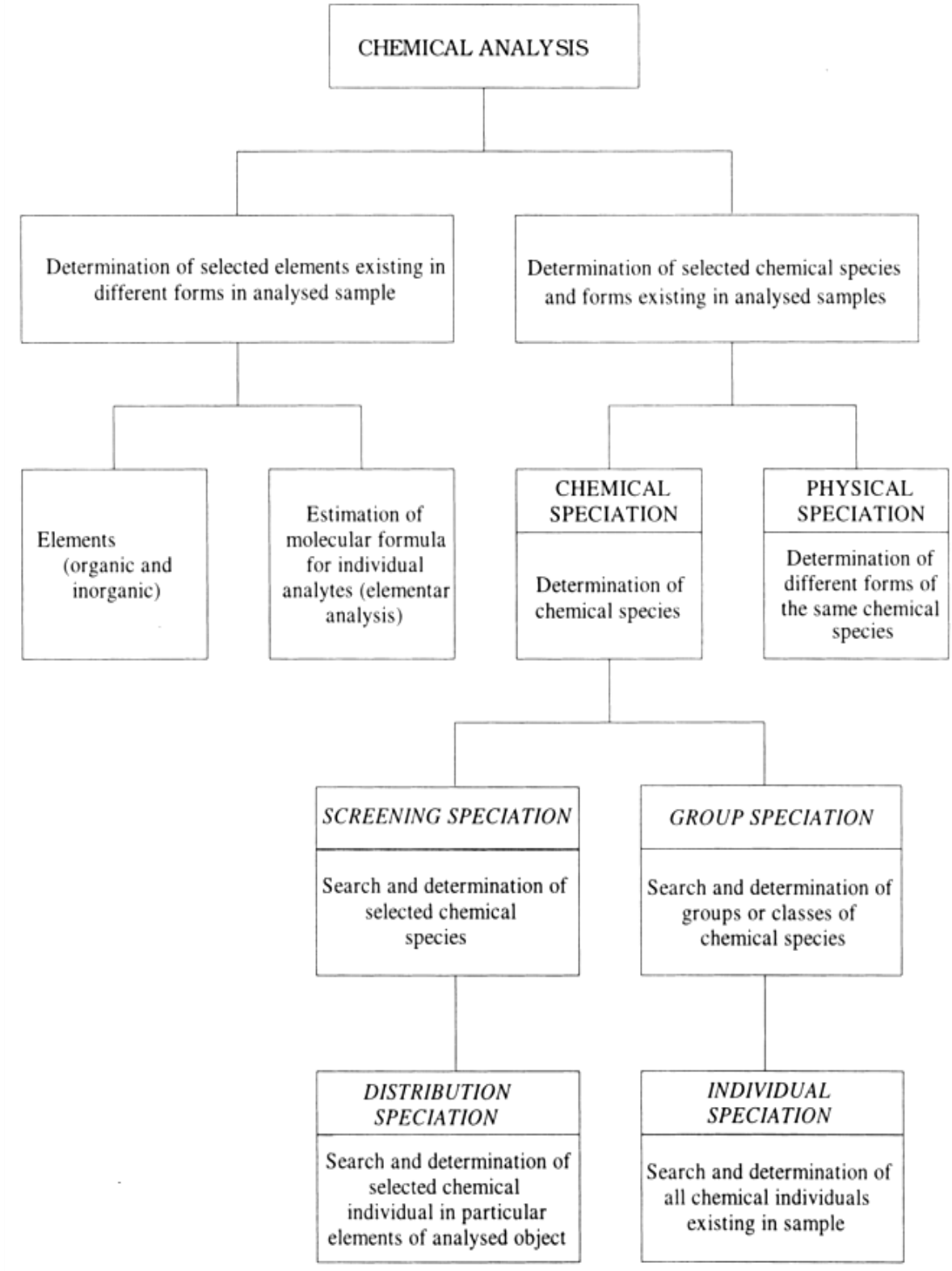

Figure 1.1. Description of the different types of speciation analysis performed in analytical chemistry.

1.2. The aim of the thesis

The aim of this thesis is a speciation study of metal cations (M^{n+}, for n = 2, 3) in the presence of ligands (L^{z-}) of different nature and fields of application, in ionic medium NaCl, the main inorganic component of mostly natural[6,7] and biological fluids.[8]

The first step of the work was a potentiometric study in aqueous solution of the M^{n+}/L^{z-} interactions, choosing as ligands three commercially available molecules such as Gantrez® AN169 (GTZ^{4-}), citric acid (Cit^{3-}) and orthosilicic acid ($H_2SiO_4^{2-}$).

Gantrez® AN169, a synthetic copolymer,[9] and citric acid are O-donor organic ligands and were chosen for their wide industrial use and for the well-known role of the citric acid in biological field.[10] The orthosilicic acid instead is an inorganic compound and the main form of bioavailable silica for humans and animals.[11]

The interactions of Gantrez® AN169 with bivalent (Mg^{2+}, Zn^{2+}, Sn^{2+}) and trivalent (Al^{3+}) metal cations and between citric acid and Al^{3+} were studied in different conditions of ionic strength (I) and temperature (T). The Al^{3+}/orthosilicic acid system was investigated only at variable ionic strength.

The speciation study in all case took into account the acid – base properties of each ligand (reactions of protonation) and metal cations (reactions of hydrolysis).

Furthermore, for all the metal – ligand systems the stability constants dependence on ionic strength and temperature was investigated and modeled by a modified Debye-Hückel equation.

The second step of the work was a spectrophotometric and spectrofluorimetric study of the acid – base behavior in aqueous solution of eight 3-hydroxy-4-pyridinones, ligands used in the field of chelating therapy with the aim of detoxification from hard metal cations.[12]

Four of these compounds were synthesized during a period of six months of research abroad under the supervision of the Prof. Maria Amélia Santos, at the Centro de Química Estrutural of the Instituto Superior Técnico (Universidade de Lisboa). Two products are monosubstituted 3-hydroxy-4-pyridinone derivatives of aspartic anhydride while the other two compounds are disubstituted derivatives of diethylenetriaminepentaacetic bisanhydride (DTPA bisanhydride) and of nitrilotriacetic acid (NTA), respectively.

The binding ability of all these compounds towards the Al^{3+} was studied by carrying out either spectrophotometric or potentiometric experiments at I = 0.15 mol L^{-1} in $NaCl_{(aq)}$ and T = 298.15 K.

In the case of the disubstituted 3-hydroxy-4-pyridinone derivatives, spectrophotometric measurements in the same experimental conditions were also performed to investigate their speciation in aqueous solution in the presence of bivalent metal cations such as Ca^{2+}, Cu^{2+} and Zn^{2+}.

Finally, the sequestering ability of all the ligands studied during the work presented in this thesis towards the chosen metal cations was investigated with the calculation of the $pL_{0.5,}$ an empirical parameter already proposed by the research group,[13] which represents the total concentration of ligand necessary to sequester 50% of a given ion present in trace (10^{-12} mol L^{-1}) in solution.

Chapter 2

The ligands

2.1. Gantrez® AN169

The Gantrez® (GTZ) compounds are a family of synthetic copolymers of methyl vinyl ether (MVE) and maleic anhydride (MA) having several applications in industrial (textiles, paper, adhesives, coatings), cosmetics, pharmaceutical and oral care product fields.[14]
Figure 2.1 represents the possible different classes of Gantrez® copolymers.

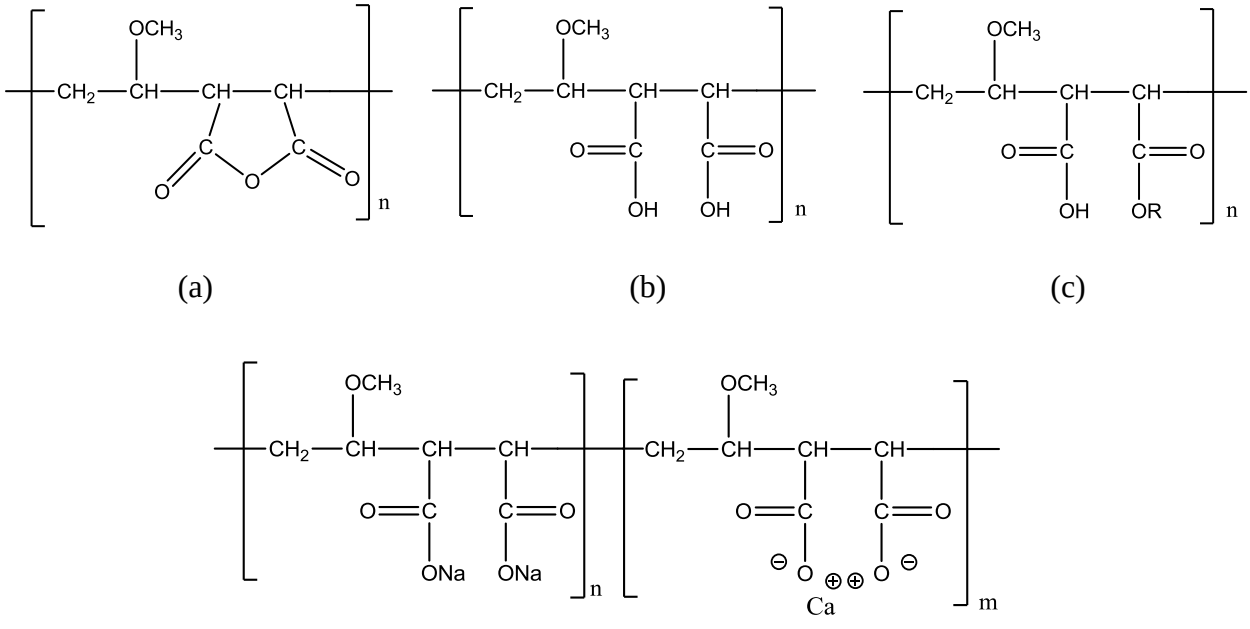

(a) (b) (c)

(d)

Figure 2.1. Different classes of Gantrez® copolymers: Gantrez® AN (a), Gantrez® S (b), Gantrez® ES (c), Gantrez® MS (d).

On the base of their structure, Gantrez® compounds can be classified in:

- Gantrez® AN copolymers, which are characterized by outstanding physical properties such as the ability to form protective films and to be good adhesive agents, thickening in organic and aqueous systems and moisture resistance.[15] Four types of this material are commercially available, characterized by different molecular weights and viscosities,[9] as reported in Table 2.1.

Table 2.1. Different grades of Gantrez® AN

Grade	Molecular weight / kDa	Specific viscosity
Gantrez® AN119	200	0.1 - 0.5
Gantrez® AN139	1000	1.0 - 1.5
Gantrez® AN149	1250	1.5 - 2.5
Gantrez® AN169	2000	2.6 - 3.5

Gantrez® AN compounds present an anhydride functional group; in water they can hydrolyze slowly in the corresponding dicarboxylic acid, the Gantrez® S, according to the reaction reported in Figure 2.2.

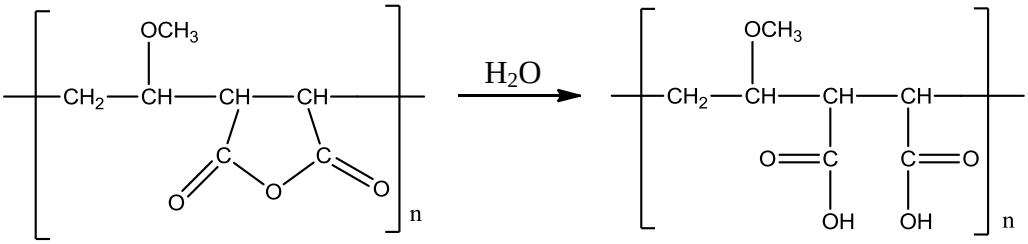

Figure 2.2. Hydrolysis of Gantrez® AN to Gantrez® S.

This class of compounds has many applications, such as: calcium encrustation inhibitors in laundry detergents, acid layers in diffusion transfer film to neutralize alkaline developers and dyes, intermediates in adhesive applications and liquid laundry detergent stabilizers, metal sequestrants, anionic polyacids.

- Gantrez® S copolymers, which contain carboxylic groups and derive from the hydrolysis of Gantrez® AN. They are water-soluble, giving clear and tacky films. In term of applications, it is possible to find these compounds as calcium encrustation inhibitors in laundry detergents, dispersant aids, aluminum surface conditioning, diagnostic test strips, base-activated adhesives for peel-apart instant film.

- Gantrez® ES copolymers, that derive from Gantrez® AN119 copolymer and present carboxylic and ester groups. Their films are flexible, clear and glossy and the water resistance is higher than for Gantrez® S. They are used for pH-dependent soluble films for enteric coatings and as pigment dispersants in cosmetics.

- Gantrez® MS copolymers, mixed salts of sodium and calcium that are soluble in water and are used as biadhesives and coatings.[9]

2.2. Citric acid

Citric acid or 2-hydroxy-1,2,3-propane tricarboxylic acid (Figure 2.3) is a natural organic acid, whose name derives from the Latin "citrus", the citron tree.[16]

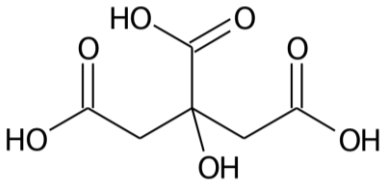

Figure 2.3. Structure of the citric acid.

It is naturally present in citrus fruits, strawberries, blueberries, raspberries, gooseberries, black currant, pineapple, tamarind, vegetables, tomatoes, lettuce but also in wine, vinegar and milk.[17, 18]

This acid was isolated for the first time in 1784 from lemon juice by the Swedish chemist Scheele, while in 1834 the German chemist Liebig understood that citric acid was an hydroxycarboxylic acid.[19] In 1815 Parkes wrote: "*There is a peculiar acid in the juice of lemons, citrons, limes and a variety of other fruits, different in some of its properties from all others, and known to chemist by the name of citric acid*".[20]

Citric acid was produced for a long time by extraction from lemons and limes which came from Sicily and South Italy. Until 1919, Italy became the world market leader but this monopoly had as consequence an increase of prices. Therefore, the scientific research tried to find different sources to produce citric acid.

The first step was the synthesis of this molecule performed by Grimoux and Adams,[21] starting first from glycerol and later from dichloroacetone (i) for reaction with hydrogen cyanide and hydrochloric acid to obtain dichloroacetonic acid (ii) and converting it in the presence of

potassium cyanide into dicyanoacetonid acid (iii), that for hydrolysis gave citric acid (iv) as product. The general reaction is reported in Figure 2.4.

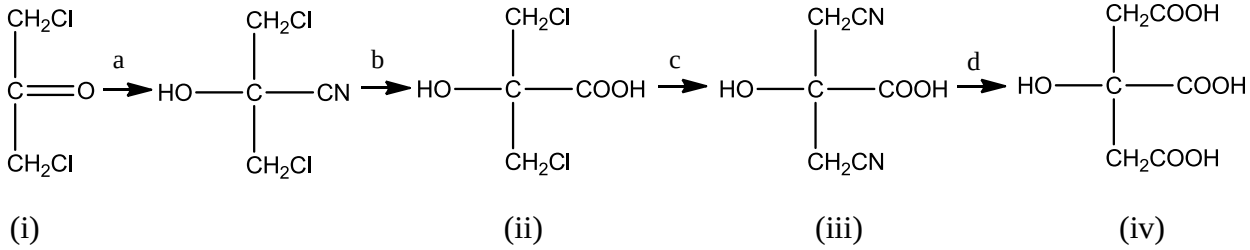

(i) (ii) (iii) (iv)

Figure 2.4. Synthesis of citric acid by Grimoux and Adams procedure[21]: a) HCN; b) HCl; c) KCN; d) H_2O.

Unfortunately, this method was not cheap and it was also uncompetitive and unsuitable, so the microbiological approach, remembering the very good results obtained by Pasteur pioneering studies about fermentation with the use of fungi and bacteria, was considered a possible good way. In 1893 Whermer demonstrated that *Citromyces* (nowadays called *Penicilium*) could accumulate citric acid in a culture medium which contained inorganic salts and sugars.[16] This process did not led to a commercial production but to the research of other organisms able to do this type of work. Many organisms were found with the aim of producing citric acid, such as *Aspergillus niger, Aspergillus awamori, Aspergillus nidulans, Aspergillus luchensis, Aspergillus phoenicus, Aspergillus flavus, Arcemonium species, Botrytis species, Eupenicillium, Talaromyces, Trichoderma viride, Ustulina vulgaris*. Moreover, in 1917 Curie found that some strains of *Aspergillus niger* were able to grow in a medium containing sugars and little amounts of inorganic salts, at low pH values (*e.g.* pH ~ 2.5 - 3.5): throughout their growth, these organisms excreted large amounts of citric acid, so this process established the basis for the industrial production.[19, 22]

From the biochemical point of view, the citric acid cycle, or Krebs cycle, is the central part of the cellular respiration that occurs into the mitochondria in the eukaryotes, in the cytoplasm for prokaryote organisms. It is also called tricarboxylic acids (TCA) cycle because some intermediates involved into the mechanisms own three carboxylic groups.

The Krebs cycle is a metabolic process of amphibolic nature for its role either in catabolism or in the anabolism.[10] It has a chief importance because it is used by the aerobic organisms to produce energy through the oxidation of acetyl-CoA derived from carbohydrates, fats and proteins in CO_2, 25 molecules of ATP (adenosine triphosphate), four molecules of NADH

(reduced nicotinamide adenine dinucleotide) and one of $FADH_2$ (two times reduced flavine adenine dinucleotide).[23, 24]

A schematic representation of the citric acid cycle is reported in Figure 2.5.

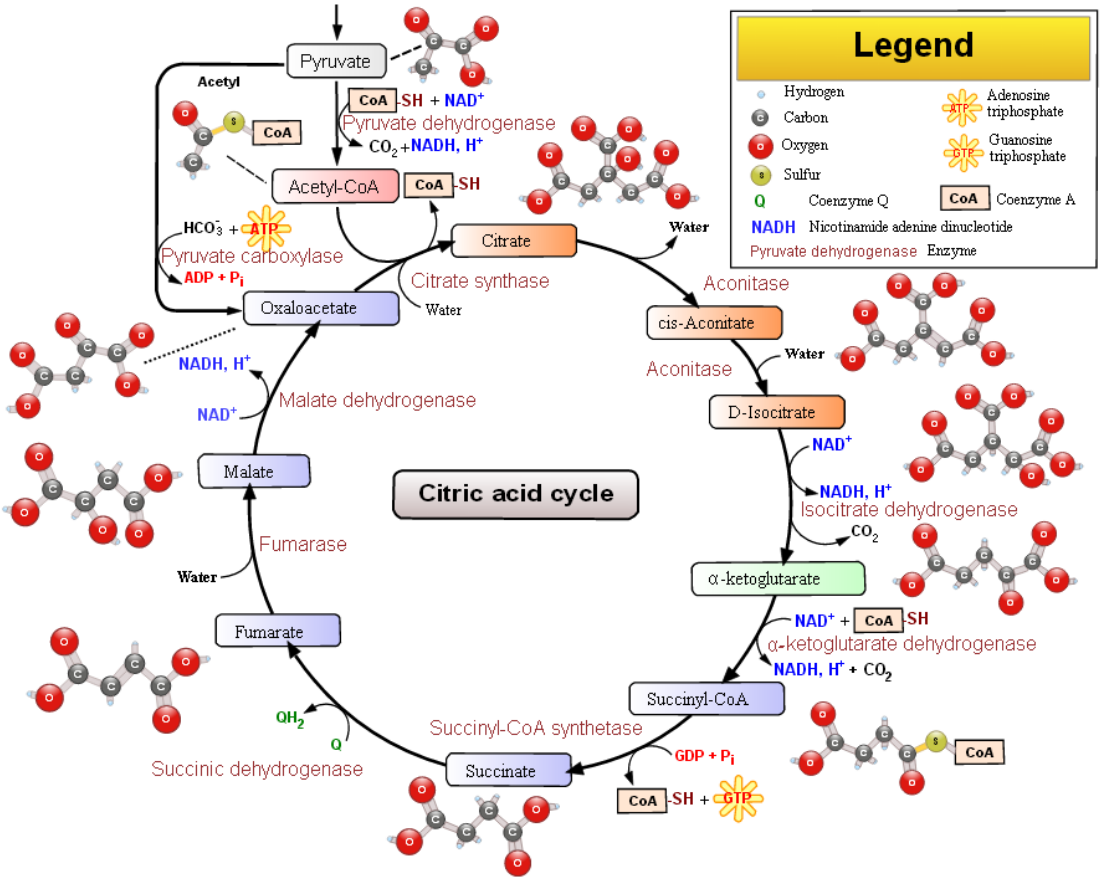

Figure 2.5. Krebs cycle representation.

The citric acid has antioxidant properties by fighting the production of free radicals responsible for cell aging.

Citric acid is also a good chelating agent, capable of binding heavy metals toxic for the human body come from the environment. Furthermore, the tendency of this ligand to form complexes with metal cations such as copper, iron, manganese, calcium and magnesium is the reason why it is used as sequestering agent in industrial processes and as anticoagulant blood preservative.

It participates to the process of absorption of iron, very important in particular for patients with Fe deficiency.

Other functions of the citric acid are depurative, because it interferes with the formation of kidney stones and uric acid, stabilizing the skeletal system and antibacterial.

The main applications of this compound are the following:

- food, such as in juices and fruit nectars, lemonades, instant soups, frozen fish, jams, creams, oils and vegetable and animal fats emulsified, chocolate, cocoa, baked goods, food for infants and raw meat.[17-19] Thanks to its antioxidant properties, citric acid is an efficient food preservative and an acidity regulator. In a lot of labels of foods, it is easy to find it with the acronym E330, as reported in Figure 2.6;

Figure 2.6. Label of an extract of coconut containing citric acid as acidity regulator.

- pharmaceutical, as blood anticoagulant, in the preparation of compresses and effervescent products and for the diuresis;
- cosmetic, in anti-aging creams because of its detergenting and purifying properties;
- cleaning and home care products, with a cleaning and descaling action comparable to the other detergents commonly used;
- agriculture, in herbicide products to prevent weeds;
- industry, for example in the field of polymerization because of citric acid sequestering properties.

2.3. Orthosilicic acid

Silicon (Si) is the second most abundant element on the earth's crust with a percentage of 27.2%, besides oxygen (45.5%).[11, 25] Silicon is present in foods derived from plants such as white wheat flour, cereals, oats, polished rice and barley, but also in beverages like drinking and mineral waters and in beer. Conversely, the amount of this element in animal food and in dairy products is lower than in vegetable foodstuffs.

In the human body, the highest silicon concentration can be found in hair and nails, in connective tissues (*e.g.* aorta), in the tracheas, in the bone and in the skin.[11, 26-28]

Moreover it is present in blood in levels that are similar to physiologically essential element such as iron, copper and zinc and it can be excreted in urine in comparable orders of magnitude than calcium.[29]

The silicon would be linked to collagen synthesis and ageing of skin[30], bone mineralization and osteoporosis[31], Alzheimer disease[32-34], atherosclerosis[35, 36] and other type of disorders.

Because of its chemical and physical properties, as for example to be a semiconductor, the spread of these elements in the field of scientific research and technical application is growing.

From the chemical point of view, silica or silicon dioxide (SiO_2) is one of the most studied chemical molecule and the main Si-containing inorganic substance. Most of the SiO_2 in the aqueous systems and oceans is present in the form of orthosilicic acid, whose structure is represented in Figure 2.7. The formula of this compound can be written either as $Si(OH)_4$, the most correct form to represent the nature of the molecule, or H_4SiO_4, to underline its capacity to lose H^+ ions and its behavior as an acid.[37]

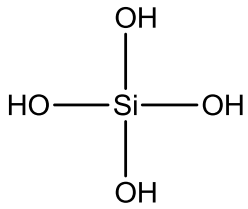

Figure 2.7. Structure of the orthosilicic acid.

It is a weak acid, not soluble in water (a white gelatinous mass) and in mineral acids but only in hydrofluoric acid and in alkaline compounds.

In contact with air it can lose very slowly a molecule of water, and the product of the reaction represented in eq. (2.1), is the metasilicic acid (H_2SiO_3). Its structure is reported in Figure 2.8.

$$H_4SiO_4 \xrightarrow[-H_2O]{} H_2SiO_3 \qquad (2.1)$$

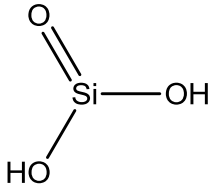

Figure 2.8. Structure of metasilicic acid (H_2SiO_3).

The orthosilicic acid can have also the tendency to give reactions of polymerization with the formation of polysilicic acids. Some example of these polymeric compounds are the disilicic (*e.g.* $H_6Si_2O_7$) and the trisilicic ($H_4Si_3O_8$) acids. The orthosilicic acid is the major form of bioavailable silicon for humans and animals.[11] The most important sources able to release orthosilicic acid in biologically helpful form of silicium are colloidal silicic acid (gel of silica in the hydrated form), silica gel (amorphous SiO_2) and zeolites. The zeolites are a class of microporous alluminosilicates with ion exchange properties, particularly diffused in biology and medicine,[38] like in the examples of applications reported in Figure 2.9, and in the fields of production of commercial adsorbents and catalysts.

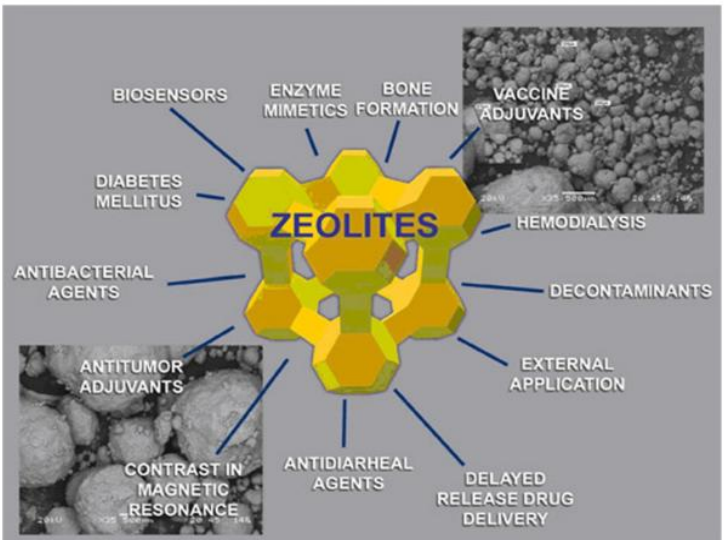

Figure 2.9. Biomedical applications of zeolites.

The general formula of zeolites is $(M^{n+})_{x/n}[(AlO_2)_x(SiO_2)_y] \bullet mH_2O$, where M is a metal ion with a positive charge like sodium (Na^+), potassium (K^+), magnesium (Mg^{2+}) or calcium (Ca^{2+}). Usually the metal cation is trapped in cage or tunnel cavities and Figure 2.10 is just a representation of the molecular structure of the zeolites.

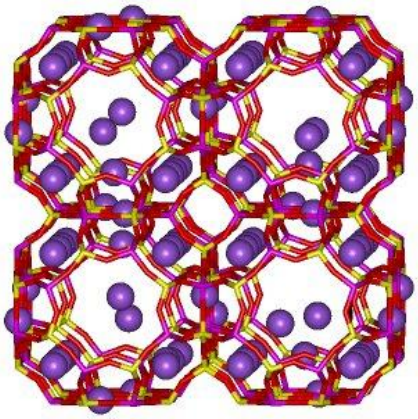

Figure 2.10. Representation of the zeolites with the metal cations into the cavities.

2.4. 3-Hydroxy-4-Pyridinones

The treatment of diseases related to the accumulation of hard metal ions in the body is based on the chelating therapy. This approach consists in the administration of chelators to the patients, to help the sequestration of the metal ion (*e.g.* Fe^{3+}, Al^{3+}) and their systemic excretion.[12] From the diet, the environment or other external sources the heavy metals can go into the human body, reach the blood and the human organs, and compete with other metals for vital functions.

For a long time the Deferoxamine (DFO or Desferal®), whose structure is represented in Figure 2.11, was used as chelator for the treatment of iron overload.[39]

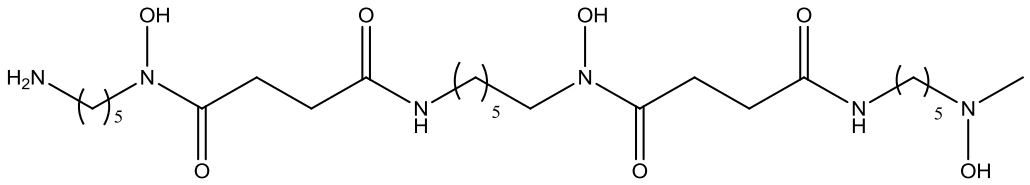

Figure 2.11. Structure of Deferoxamine (DFO or Desferal®).

It is a microbial trishydroxamic acid able to form with Fe^{3+}, as hexadentate ligand, a metal – ligand complex, as shown in Figure 2.12, with a high stability from the thermodynamic point of view ($\log K_{ML}$ = 30.6)[40]. It presents many undesired effects, hydrophilic character, oral inactivity, toxicity and it is very expensive.[41]

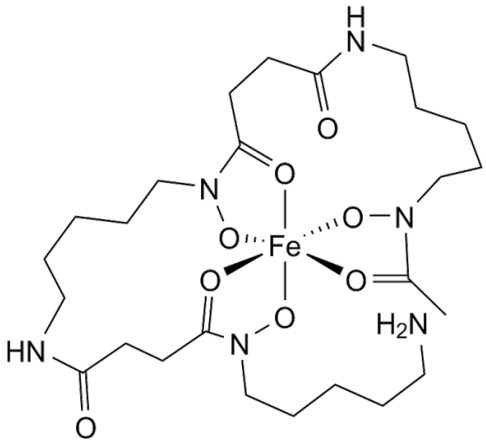

Figure 2.12. Structure of Fe-Deferoxamine complex with stoichiometry 1:1.

To avoid that the patients would have all these kinds of problems, the scientific research developed the use of a new class of chelating agents: the family of 3-hydroxy-4-pyridinones

(also called 3,4-hydroxypyridinones, 3-hydroxypiridin-4-ones, or 3,4-HPs), derived of 1,2-dimethyl-3-hydroxy-4-pyridinone, commercially known as Deferiprone (DFP) or Ferriprox®, and approved as orally drug for the treatment of patients affected by iron overload.[12, 39]
The structure of the DFP is reported in Figure 2.13.

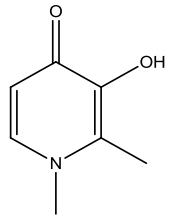

Figure 2.13. Structure of 1,2-dimethyl-3-hydroxy-4-pyridinone (Deferiprone).

The 3,4-hydroxypyridinones are a class of bidentate compounds, characterized by an aromatoid N-heterocycle with hydroxyl and ketone groups in ortho position. Conversely to the DFO, they are economically convenient, can be effective in all biological conditions and do not cause problems of toxicity and oral activity.[42, 43]
They can be synthesized from a simple and natural compound the 3-hydroxy-2-methyl-4*H*-pyran-4-one (maltol), according to the scheme of reaction shown in Figure 2.14.

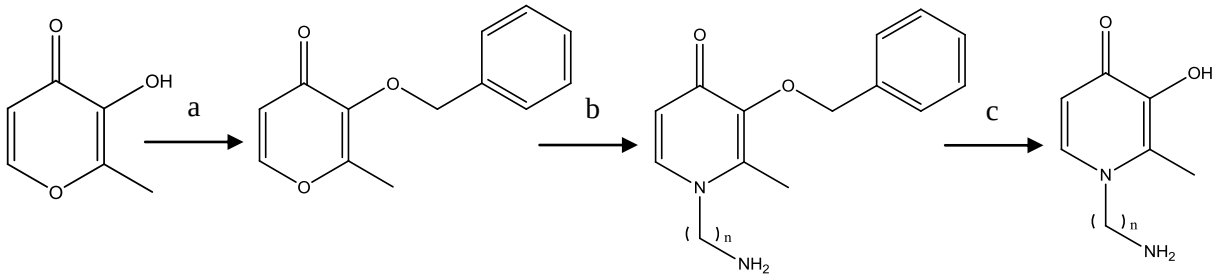

maltol protected maltol protected 3,4-HP 3,4-HP

Figure 2.14. General scheme for the synthesis of a generic 3-hydroxy-4-pyridinone:
a) BnCl, NaOH, MeOH / H_2O, reflux T = 348 K, 20 hours; b) primary amine, NaOH, EtOH / H_2O, reflux T = 348 K, 20 hours; c) H_2, Pd/C, MeOH, p = 4.5 atm, 4 hours.

The first step of the synthesis is a reaction of protection of the –OH group with a benzyl group, according to the mechanism of Williamson synthesis of ethers starting from alcohols [44, 45] (Figure 2.15).

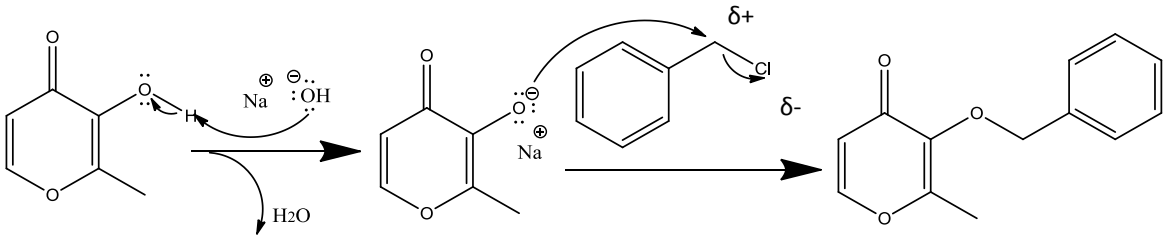

Figure 2.15. Mechanism of protection of –OH group of maltol.

The second step involves a double Michael-type addition of a primary amine on ether, with opening and closure of the heterocyclic ring, according to the procedure by Harris et al.,[46, 47] (Figure 2.16).

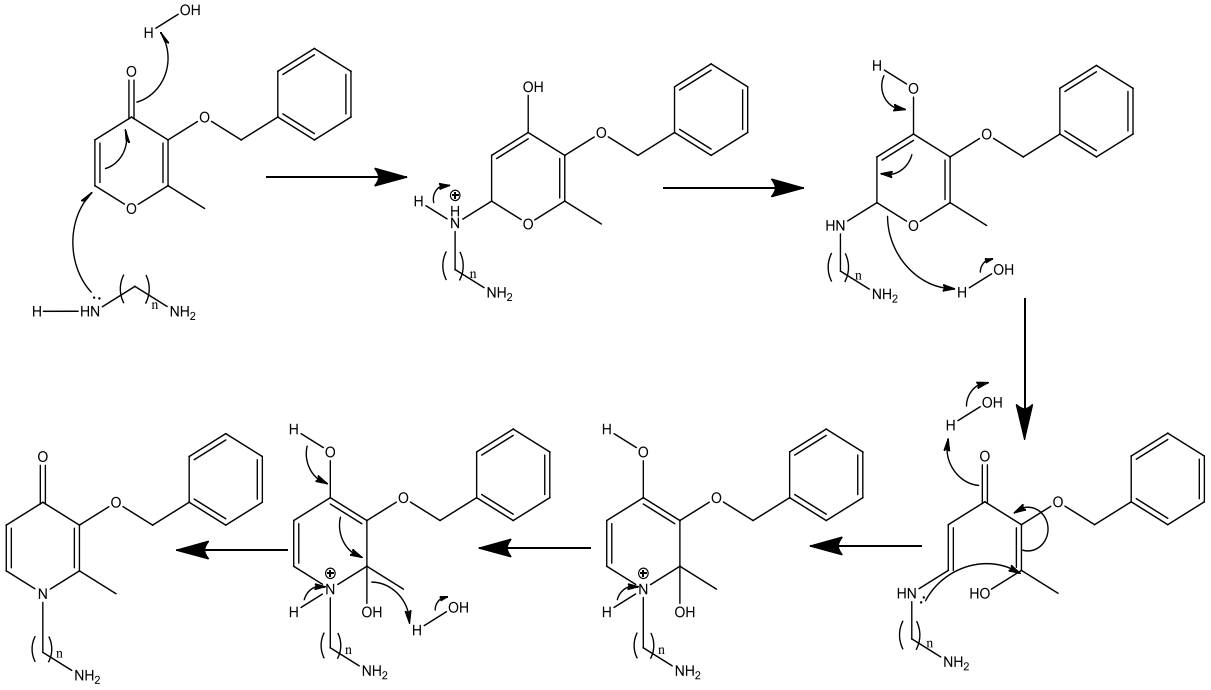

Figure 2.16. Mechanism of synthesis of protected 3,4-hydroxypyridinones from protected maltol.

The last step of reaction is the deprotection of the hydroxyl group of the protected 3,4-hydroxypyridinone with a hydrogenation catalyzed by 10% Pd/C.

The 3,4-hydroxypyridinones can be extrafunctionalized [39, 48-50] to improve their interaction with biological sites through reactions of coupling by condensation with anhydrides or carboxylic acids, sometimes catalyzed by a coupling agent, the n-propylphosphonic anhydride (T3P or 2,4,6-tripropyl-1,3,5,2,4,6-trioxatriphosphinane-2,4,6-trioxide, Figure 2.17) in the presence of base, with the formation of new amide bonds. [51-53]

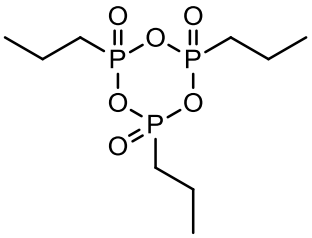

Figure 2.17. Structure of n-propylphosphonic anhydride.

Figure 2.18 represents the T3P catalyzed mechanism, in which the base deprotonates a carboxylic acid and the carboxylate anion attacks the T3P.

The amine, the 3-hydroxy-4-pyridinone, attacks the T3P-carboxylic acid intermediate and the free T3P part is obtained by a workup in an aqueous solution.

Finally, a second equivalent binds the proton in excess and forms the amide.

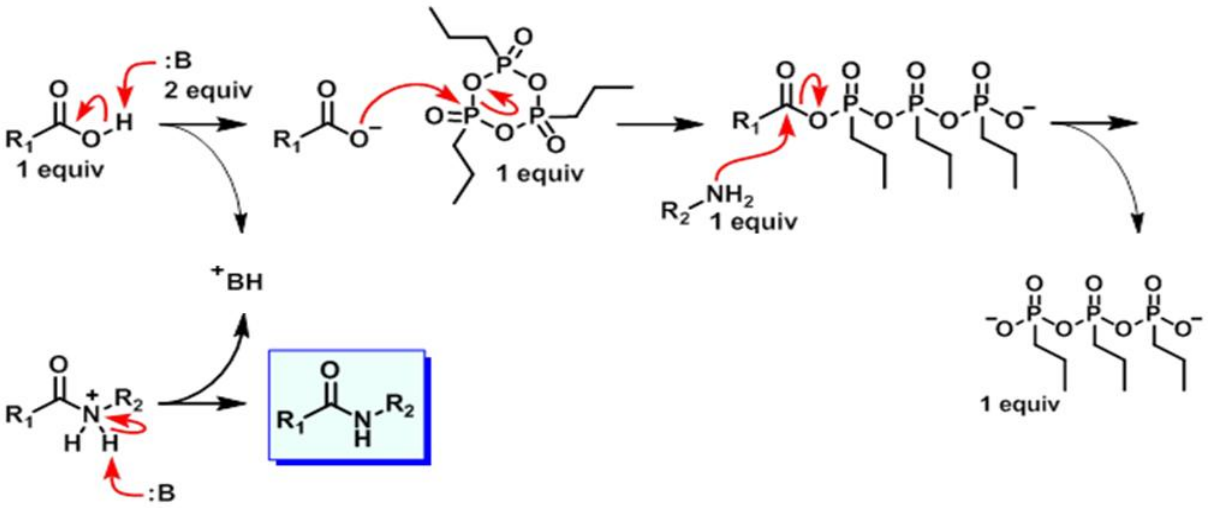

Figure 2.18. Mechanism of synthesis of an amide through a T3P catalyzed mechanism.

Chapter 3

The metal cations

3.1. Calcium

Calcium is a silvery – white metal, ductile and malleable. It represents the fifth most abundant element in environment and in the human body and constitutes the 3.63% of the earth's crust. The name of this element derives from the Latin "calx", meaning lime.

From the historical point of view, calcium was discovered in 1808 independently by Sir Davy and by Berzelius and Pontin while in 1898 Moissan was the first person to produce the pure metal.[54]

Calcium is present with a percentage of 1% in about 700 minerals of magmatic, sedimentary and metamorphic type, more than 3.63% in magmatic rocks like granites, basalts and gneisses. Soil contains a variable concentration of calcium, depending on their geological origin. The amount of this metal on grass and other plants used for the nutrition of the animals such as goats, cows and sheeps is between 1.2 and 17 g kg^{-1} dry weight.[55] The oceans contain an average amount of calcium of about 390 mg kg^{-1}, but it could arrive also to 440 mg kg^{-1} in some areas. Since the seawater contains a big concentration of Ca, the living organisms do not have problems to accumulate this metal in sufficient amount. An adult man owns in total about 1000 g of calcium distributed in the bone (99%), in the muscle tissue (0.3%), in plasma, in the extracellular fluid and in other cells (0.7%). The calcium in the plasma is represented by free calcium ions (50%), bound to the protein (40%) and complexed with anions (10%).[54]

The content of calcium that from outside arrives to the human body comes from food, mainly from milk and derivative products such as yogurt and cheese. Other sources are fruits (*e.g.* kiwi, orange), vegetables such as in lettuce, broccoli and dried beans, cocoa, tea, chocolate,

bread and cakes, spices, baby and infants food, meat, offal, eggs, fish (*e.g.* anchovies, octopus, squid, shrimp) and tinned fish, beverages and in drinking and mineral water.[55, 56] For snacks, walnuts, pistachios, peanuts and hazelnuts can give a sufficient amount of calcium. For vegan people the soy-based products, such as tofu or soymilk, are excellent for the content of this metal.

Calcium has several roles in the human body, such as:

- formation of the structures of bones, nails and teeth, together with iron, magnesium and phosphorous;
- activation of enzymes and other molecules in the processes of blood clotting;
- contraction of the muscles and the heart, thanks to the bonding of calcium with actin and myosin;
- participation to the cellular communication, working as intracellular second messenger.

The Recommended Daily Allowance (RDA) of calcium is 700 mg for children (1-3 years), 1000 mg (4- 8 years), 1300 mg for adolescents, 1000 mg for young adults, 1200 mg for women over 51 and 1200 mg for men and women over 70. Calcium used clinically is prescribed as a dietary supplement in the form of pills, or like calcium-fortified juices (easier to take, more digestible). They can be used, for example, for the treatment of diseases due to calcium malabsorption, (*e.g.* hypoparathyroidism, malabsorptive bowel disease) and in the case of arising of the osteoporosis.[57] This latter pathology is characterized by symptoms such as muscular and skeletal pain, ache at the ends of the fingers, forearm and lower back, cramps, weakness and bone fragility, especially in women. In rapidly growing children, the calcium deficiency may provoke rickets. Low concentrations of this metal in the intestine, because of a not correct dietary, is suspected to be associated with the increased risk of kidney stones and colon cancer.[58] This aspect could be due to the decreased binding and increased absorption of oxalic acid, the main constituent of kidney stones and of carcinogens such as bile acids.[57]

Other problems linked to the deficiency of calcium are imbalances in the correct activity of thyroid, liver and kidneys and also insomnia and tachycardia.

The decrease of the concentration of calcium ions in the plasma leads to an increase of neuromuscular excitability and a syndrome called tetania.[59] The opposite condition, and so the

increase of the total blood calcium, causes symptoms such as anorexia, nausea, constipation and depression.

3.2. Magnesium

Magnesium is a metal of the second group of the periodic table and it is one of the essential elements for the correct functions and for the health of human body.

Already in ancient times, the use of this metal in the form of magnesium-rich mineral waters had developed, but only in the seventeenth century it was discovered that the magnesium sulfate, called Epsom salt in Anglo-Saxon countries, was a cathartic agent in mineral waters. Three centuries later Willstätter and Stoll demonstrated that magnesium was the main constituent of chlorophyll molecules. In 1926 Leroy described the importance of this metal in animals, while Kruse and coworkers[60] induced deficiency of magnesium in rats. In 1934 the first studies about depletion of Mg in humans were published.[61] Moreover, during the 1950s different pathologies were presented to the scientific community as consequence of deficiency of magnesium in the human body.[62]

Mg is the eighth most abundant terrestrial element and constitutes 2% of the Earth's crust. It is presents in nature in more than 60 minerals such as dolomite, brucite, olivite, magnesite and olivine while in seawater it is the third element in term of concentration.[63]

An adult man owns about 1 mol, namely 24 g of magnesium, distributed in: bone (60 – 65%), muscles (27%), other cells (6 – 7%), extracellular (< 1%), erythrocytes, serum (55% free, 13% complexed with citrate, phosphate, etc., 32% bound, primarily to albumin), mononuclear blood cells, cerebrospinal fluid (55% free, 45% complexed), sweat, secretions.[64]

The highest magnesium content comes from food. Leafy green vegetables, dried fruit (*e.g.* nuts, hazelnuts, almonds), legumes, mushrooms, cereals, pumpkin seeds, soybeans, bananas, artichokes, dates, avocados, dried figs, rice and also cocoa and fondant chocolate are good examples of foodstuffs containing this element. Conversely, the amount of magnesium in foods of animal origin (*e.g.* fish, eggs, meat, milk) is lower than in vegetables.

Magnesium plays a chief role in all the living systems; in plants, for example, this element gives its contribution to the function of chlorophyll. In the human body it is involved in the action of a huge number of enzymes either as part of the enzyme complex or as allosteric activator.[65]

The enzyme systems activated by Mg are the alkaline phosphatases, the peptidases, the enolase and the thiamine pyrophosphate as a cofactor.[66, 67]

Magnesium has many therapeutic properties, which can bring benefits to the human body, such as:

- it is indicated for the treatment of states of depression, anxiety and nervousness because an increase of these symptoms is linked to a higher consumption of this element;

- the assumption of magnesium regulates digestion and intestinal functions in case of constipation and diarrhea, it relieves any inflammation and has a mild laxative effect;

- it has energizing properties to combat mental and physical fatigue;

- this metal can help women during the menstrual period to reduce the states of irritability, mood swings and water retention;

- Mg can have purifying effects on the skin and for this reason it is used for the treatment of the phenomenon of acne;

- it prevents the states of osteoporosis by helping the bones to fix calcium and phosphorus and acting on osteoblasts, the cells that are responsible for building bones;

- this element acts on the muscular system as it helps the prevention of the onset of cramps, fatigue and contractures.

The supply of little dietary amounts of magnesium can induce Mg deficiency in humans and animals, like it was found for example in the case of experiments performed on developing rats.[68] In humans magnesium deficiency occurs with:

- very low dietary magnesium intake for prolonged periods or low dietary magnesium intake combined with pregnancy or lactation, increased losses via sweat for the athletes;

- low or normal magnesium intake combined with increased urinary losses due to magnesium wasting genetic disorders, diabetes, alcohol abuse, diuretics, aminoglycoside antibiotics, cisplatin, cyclosporine;

- low or normal magnesium intake combined with reduced intestinal absorption because of not correct absorption syndromes, short bowel syndrome, laxative abuse, Crohn's disease, parathyroid diseases.

The symptoms of deficiency of magnesium can be: neuromuscular hyperexcitability, cardiac arrhythmias, increase of muscle tension and stress susceptibility, muscle cramps, headaches, irritability, mental confusion and dizziness.[63]

3.3. Zinc

Zinc is a transition metal and an essential trace element for the life. Its name comes from the German "zinc", derived from the Persian word "sing", meaning stone.

Hystorically, Zn was used by the Romans in the time of Augustus emperor to produce brass, but only from the 1374, it was recognized in India as a new metal. The waste from a zinc smelter at Zawar, in Rajasthan, testifies to the large scale with which it was refined during the period between 1100 and 1500. In the 17th century from India zinc manufacture moved to China, while in 1743 the first European zinc smelter was established at Bristol in the United Kingdom. In 1745 an East India Company ship sank off the coast of Sweden: it was carrying a cargo of Chinese zinc and the analysis of recovered ingots showed them to be almost the pure metal. In 1668 the Flemish metallurgist Moras de Respour, reported the extraction of metallic Zn from ZnO.

The abundance of this metal in the Earth's crust is about 70 g ton^{-1}.[69] Zinc is a chalcophilic element, together with copper and lead and a trace constituent of most rocks. The amount of Zn in soils and rocks is, for example, 10 – 30 mg kg^{-1} in sand, 50 mg kg^{-1} in granitic rocks, 95 mg kg^{-1} in basalt.[70, 71] Sphalerite (zinc blende, ZnS) is the main ore mineral and the principal source for Zn production, while the main impurities in zinc ores are iron (1 – 14%), cadmium (0.1 – 0.6%) and lead (0.1 – 2%), changing on the base of the location of the deposit. In waters the amount of this metal depends from factors such as biological and physical - chemical conditions, from the seasonal variations and also from the nature and the age of the geological formations through which the water flows.[69] The ocean waters contain a concentration of zinc between 0.002 and 0.1 μg kg^{-1}, with higher amounts at bigger depth and a lower ones in the surface.[72] The fresh waters, in particular from rivers, if contaminated by wastewater, can contain big amount of this metal, while in drinking waters its concentration is lower than 0.2 mg L^{-1}. Anthropogenic sources of zinc can be the following: mining, zinc and

metal production facilities, corrosion of galvanized structures, coal and fuel combustion, waste disposal and incineration, use of fertilizers and agrochemicals which containing Zn, zinc smelters.

Furthermore, the level of the metal in rural areas are lower than in industrial zones. As an example, it was found that the concentrations of Zn in European rural areas is between 0.4 and 300 ng m^{-3} while in the urban zones the range is 10 – 2400 ng m^{-3}.[73]

In plants the concentration of zinc depends by their vegetation state and by the geological origin of the material for soil formation. The age of the plants is also important because the amount of the metal decreases with increasing the lifetime of the plant.[74] In animals Zn is present in sea fish and mollusks with an average concentration of about 25 mg kg^{-1}, in crustaceans between 7 and 50 mg kg^{-1}. In mammals, the bones contain 75- 170 mg kg^{-1} of zinc, while the white muscle tissue about 240 mg kg^{-1}.[69] In the human body this metal is found in all the tissues and all the body fluids. In an adult man the amount of zinc in the body is in the range 1.5 – 3 g distributed in the muscles (~ 60%), bones (~ 30%), skin and hair (~ 6%), liver (~ 5%), gastrointestinal tract and pancreas (~ 3%), other organs (≤ 1%).[75]

In foodstuffs this metal is present in the following categories:

- meat, such as beef (64 mg kg^{-1}), mutton (31 mg kg^{-1}), lamb (53 mg kg^{-1}), pork (19 mg kg^{-1}, liver 90 mg kg^{-1}), chicken (8.5 mg kg^{-1}, eggs 15 mg kg^{-1});

- fish and seafood, in sea fish (10 mg kg^{-1}), oysters (average 1430 mg kg^{-1}, maximum 2000 mg kg^{-1}) and shrimps (23 mg kg^{-1});

- cereals and cereal products, like rice (5 mg kg^{-1}), rye (13 mg kg^{-1}), wheat bread (5 mg kg^{-1}), corn flakes (3 mg kg^{-1}), pasta (16 mg kg^{-1});

- dairy products, in butter (2.3 mg kg^{-1}), cow's milk (3.8 mg kg^{-1}), cheese (35 mg kg^{-1});

- fruits, such as apple (1.2 mg kg^{-1}), banana (2.8 mg kg^{-1}), exotic fruits (9 mg kg^{-1}) and nuts (34 mg kg^{-1});

- vegetables, in cabbage (8 mg kg^{-1}), potatoes (2.9 mg kg^{-1}), carrots (20 mg kg^{-1}), tomatos (2.4 mg kg^{-1}), beans (40 mg kg^{-1}).[76]

Zinc has also several properties in the human body, such as:

- regulation of immune functions through the activation of T lymphocytes (T cells), which help the body to control and regulate the immune responses and to attack infected or cancerous cells;[77]

- wound healing, in particular leg ulcer healing, improving the re-epithelialization, decreasing inflammation and bacterial growth;[78]

- help for the protection of the skin and muscles from premature aging and antioxidant function against the action of free radicals;[79]

- fight against diseases such as eczema and acne;

- increase of the production of insulin level, the hormone responsible for reducing blood glucose and the excess of fat in the human body;

- correct functionality of male and female reproductive system, together with the use by the patient of folic acid, and fight against the infertility;

- important role for the proper growth and development of human body;

- help for problems of memory and learning;

- treatment of the common cold, reducing the episodes to more than the 40%;[80]

The deficiency of zinc can be due to different factors such as a not adequate diet, gastrointestinal problems like ulcerative colitis, Crohn's disease, short bowel syndrome, chronic liver or chronic kidney disease, alcoholism which provoke a decrease of Zn absorption and favors the increase of the urinary metal excretion, sickle cell disease, diabetes, pregnancy and breast-feeding.

The symptoms could be anorexia, lethargy, diarrhea, delayed bone maturation, impaired immune function and susceptibility to infections and, in severe cases, also delayed sexual maturation, impotence, alopecia, dermatitis, intellectual disability, impaired nerve conduction and nerve damages, weight loss, impaired taste, smell and wound healing.[81] Conversely, an excess of zinc can be toxic for human body. The acute toxicity, with an amount of zinc of 200 mg for day, can cause abdominal pain, nausea, vomiting and diarrhea, gastric irritation, headache, irritability, lethargy, anemia and dizziness. The chronic toxicity, with an amount of

zinc of 50 – 150 mg for day, could lead to problems such as disturbances of copper metabolism, reduced levels of high-density lipoproteins, dysfunctions of the cardiac functions and the proper operation of pancreatic enzymes amylase and lipase.[82]

3.4. Tin

Tin is a silvery – white, soft and malleable metal and it is the 24th element as abundance on the Earth's crust,[83] representing 2 – 3 ppm compared with 94 ppm for zinc, 63 ppm for copper and 12 ppm for lead. Its name derives from the Latin "stannum" and it is one of the first metals to be discovered. Since ancient times tin was used intensively for its effect as copper binder, of which greatly increases the hardness and for the mechanical qualities of forming the alloy known as bronze, in use from the 3500 B.C. The mining activities probably started in Cornwall and at Dartmoor in classical period and these regions developed an intense trade with the civilized areas of the Mediterranean Sea. The use of the pure metal was not spread in the field of metallurgy before the 600 B.C. In 1900, Malaysia became the producer of the half of all the world's tin; the extraction began there in 1853 after that Britain abolished the tax on this metal.

It is a versatile metal and its compounds can be divided in two categories:

- metal and inorganic tin salts, with oxidation number of tin +2, in the stannous form, and +4, in the stannic form;

- organotin compounds, with one to four atoms of carbon directly bound to the Sn atom, giving the general formula R_nSnX_{4-n}, where R is an alkyl or phenyl group and X an ionic species in the form of chloride, fluoride, oxide, hydroxide, carboxylate or thiolate.[84]

Tin is present in a small amount in silicate rocks, like in the ore cassiterite (SnO_2) which has the main commercial importance, and in sulfur-complex salts such as stannite (Cu_2FeSnS_4), cilindrite, frankeite, canfieldite and teallite. Nowadays, the principal tin-producing countries are Malaysia for the 40%, Bolivia, Thailand and Indonesia. The world-wide production of this metal from SnO_2 mining resources is in the range 150000 – 200000 tons per year.[85]

Focusing on the inorganic tin, it can be released to the environment mostly from anthropogenic sources, such as smelting and refining processes, industrial uses of Sn, waste incineration and burning of fossil fuels produce gases, dusts and fumes containing this metal.[86] As an example, the air concentrations of tin in US industrialized cities is more than

0.8 μg m^{-3}. [87] Furthermore, the wind may transfer Sn particles over long distances before their deposition, that depends from the type of emitting source, physical form and properties (*e.g.* size, density), physical or chemical changes that could happen during the transport, adsorption processes and meteorological conditions.[88] In waters, inorganic tin can exist in both its oxidation states under environmental conditions. [87] In fresh waters the concentration of tin is about 1 ng L^{-1} in the Great Lakes of North America but it can reach 1 μg L^{-1} in polluted areas. Large rivers contain Sn for less than 10 ng L^{-1}, while in ocean it varies between few pg kg^{-1} offshore and few ng inshore kg^{-1}. [85] In fresh snow from the French Alps collected at different altitudes the range of inorganic tin goes from 0.16 to 0.44 μg L^{-1}. [89] In a lot of sediments collected from Canadian waterways the concentrations of Sn ranged up to 8 mg kg^{-1} dry weight in coastal areas and up to 15.5 mg kg^{-1} in rivers and lakes, [90] while in Antarctic sediments it was 2.1 and 5.1 mg kg^{-1} dry weight for the fractions < 2 mm and < 63 μm, respectively. [91] Tin concentrations in soil are low, with the exception of areas where tin-containing minerals are present.

This metal can also be bioaccumulated by plants, animals and humans. Indeed, marine macroalgae bioconcentrate tin from seawater with concentrations of 0.5 - 101 mg kg^{-1} dry weight.[92] In muscle and liver of juvenile Japanese squids the inorganic metal reaches maximum 0.13 mg kg^{-1} dry weight[93], more than 0.9 mg kg^{-1} dry weight in fishes from the Great Lakes in North America. [90]

Tin concentrations in the feathers of seabirds from the North Pacific[94] and water birds from the coast of Namibia [95] are in the range 0.2 - 15.2 mg kg^{-1} dry weight. In striped dolphins from the Mediterranean Sea the amounts of Sn for kg dry weight are 0.4 mg in lung tissue, 1.3 mg in liver [96] and less than 0.4 mg kg^{-1} dry weight in the livers of Antarctic fur seals. [97]

The bioaccumulation of inorganic tin on humans could be mostly due to the use of canned foods because of the dissolution of the tin coating or tin plate.[87]

Acidic foods are more aggressive to the tin coating in metal cans; oxidizing agents, such as nitrates, iron salts, copper salts and sulfur, accelerate detinning, while sugars and gelatin can reduce the dissolution rate. [98] In vegetables, fruits and fruit juices, nuts, dairy products, meat, fish, poultry, eggs, beverages and other foods not packaged in metal cans the concentration of Sn are lower than 2 mg kg^{-1}, pasta and bread between 0.003 and 0.03 mg kg^{-1}. Besides the packaging of food products and beverages, inorganic tin is used for holding paints, motor oil, disinfectants, polishes and in the pharmaceutical industry in the fields of dentary, veterinary medicine, radiopharmacology and chemotherapy.

The occupational exposure limit of inorganic tin compounds is 2 mg m^{-3}. [87] The intoxication by Sn can occur through three types of routes: inhalation, ingestion and skin. The first way of intoxication can cause diseases such as:

- syndrome of metal fume fever, due to the breathing of tin oxide fumes;
- the stannosis, a benign pneumoconiosis that could arise for exposure to tin oxide fumes and dusts;
- bronchial syndrome, with symptoms such as wheezing, shortness of breath, cough and thoracic pain, like in the case of workers in a bottle-factory exposed to a stannous chloride solution;
- hemolysis, due to the action of tetrahydrogenated tin (SnH_4) which is a hemolytic poison.

The accidental ingestion of inorganic tin compounds may cause a gastrointestinal syndrome characterized by nausea, vomiting and loose stools. Furthermore, also the irritation of the skin or the eyes could occur for Sn intoxication.

3.5. Copper

Copper, whose name derives from the Latin "cuprum", meaning "from the island of Cyprus", is a heavy metal belonging to the series of transition metals in the periodic table and to the group of the essential elements for the human species.

Copper is man's oldest metal, dating back more than 10000 years. A copper pendant, dated to about 8700 B.C., was discovered in that area that now is northern Iraq. The Egyptians used the ankh symbol to denote copper in their system of hieroglyphs and it represented the eternal life. Researchers believe that the regular use of copper for a whole period, called the "Copper Age", prior to its substitution by bronze, an alloy of copper and tin, in West Asia and Europe, during the "Bronze Age", occurred between 3500 to 2500 B.C. Other alloys of copper are those with zinc (brass), nickel (money metal), aluminium, gold, lead, cadmium, chromium, beryllium, silicon and phosphorous.[99]

Copper is one of the oldest metals known to civilization. Its uses and contributions continue to grow. It is distributed ubiquitously in the Earth's crust and in sea water in concentration of about 20 mg kg^{-1} and 3 μg kg^{-1} respectively.[99, 100] This metal occurs naturally in minerals such

as cuprite (Cu_2O), malachite ($Cu_2CO_3 \cdot Cu(OH)_2$), azurite ($2Cu_2CO_3 \cdot Cu(OH)_2$), bornite (Cu_3FeS_4), chalcopyrite ($CuFeS_2$), chalcocite (Cu_2S). Sediments are good reservoir of copper; in particular, it was found that its background levels in marine sediments are in the range 16 – 5000 mg kg^{-1} dry weight.[101]

The Recommended Daily Allowance (RDA) of copper is at 1.2 mg in adult men, while for lactating women is 1.5 mg.

Among foods rich of copper there are liver, integral cereals, almonds, green leafy vegetables, shellfish, crustaceans, kidneys, nuts, molasses, cauliflower, avocados, viscera, eggs, poultry and dried legumes (especially soybeans). It is also found in beer, in copper pots, in pasteurized milk and in the insecticides. Drinking water may be one of the main sources of copper because it is levied during its passage through copper pipes.

Copper has many important roles in the human body. A summary of these functions is reported below:

- brain and nervous system: it favors the normal development of the brain and nervous system. Copper plays an important role in the production and maintenance of myelin, the substance that insulates nervous cells to ensure a proper transmission of the nervous signals. It participates also to the synthesis of neurotransmitters, which allow the communication between the nervous cells;

- immune system: maintaining a fair level of white blood cells; a big amount of them are phagocytes that engulf and destroy the invading microorganisms;

- blood and blood vessels: this metal acts as a cofactor for an enzyme important for the blood clotting. Blood vessels are surrounded and protected by connective tissue and the copper contributes to support its elasticity, in particular for the aorta and small arteries;

- heart: copper is essential for the synthesis of collagen located in the connective tissue, the principal support and body connection tissue. It is also necessary to maintain the tone and muscle functions and plays a vital role at heart level;

- iron transport: Cu has a fundamental role in the conversion of iron in ferric form (Fe^{3+}) and participates to the iron transport in the body;

- skin: the collagen is the protein mostly present in the skin and it is important for maintaining its elasticity. Copper participates, as cofactor for the tyrosinase enzyme, to the synthesis of melanin that pigment the skin;

- cells: the generation of cellular energy in the form of ATP into the mitochondria depends on the involvement of an enzyme containing copper.

This metal can be bioaccumulated by living organisms like microorganisms, plants and animals from the environment (water, air, soil, sediment, diet).

For example, fishes tend to accumulate copper from their aquatic environment and it leads to an increase of its concentration,[102] in particular in organs like the gills[103] and the liver.[104] In terrestrial mammals and humans, copper is absorbed mostly from the food. The accumulation of this metal in the gastrointestinal tract occurs mainly in the duodenum and in the ilenum[105] and only a portion is excreted through the feces. Cu absorbed in the endothelial cells can be sequestered by an intracellular copper-binding protein like the metallothionein. When Cu(II) arrives in the hepatocytes, it is initially reduced and complexed by glutathione, before of the binding and the induction of liver metallothionein. Copper ions are exported from the liver cells by a P-type copper translocase.[106] A mutation of this gene is responsible of the Wilson's disease, clinically characterized by hepatic and neurological manifestations.[107]

The deficiency of this metal in human body is not common and would not occur if it is present in the daily diet with a concentration $\geq$ 2 mg. Secondary copper deficiency can be caused by severe malabsorption or in the genetic disorder of the transport and utilization of this metal in the case of the Menkes' disease.[99, 108]

Conversely, an excess of Cu in the body can cause an excessive stimulation of the nervous system and problems related to the organs where it mainly tends to accumulate, as liver, brain and reproductive organs. The most common symptoms are states of chronic anxiety, bipolar disorder, depression, schizophrenia, hyperactivity, learning disabilities, Tourette syndrome, sexually problems, hypothyroidism and hair loss.

The toxicity of the metal can develop when an excess of copper causes reactions, such as:

- structural damages of essential metal binding sites by displacement of metals;

- functional impairment by binding of Cu to sites in macromolecules like DNA or enzymes and in those containing thiolic, carboxylate, or imidazole groups; this aspect

may lead to protein damage or oxidative DNA changes with various functional changes; [109]

- cellular damages because of the production of oxyradicals by the Fenton reaction: [110]

$$Cu^{+} + H_2O_2 \rightarrow Cu^{2+} + OH^{*} + OH^{-} \quad (3.1)$$

The excessive production of radicals causes oxidation and reduction chain reactions, the so-called oxidative stress, that can lead to the loss of cellular integrity. The causes of these damages include increased cytosolic calcium levels, ATP depletion, thiol oxidation, lipid peroxidation, DNA damage and critical problems to organelles like the mitochondria and the lysosomes.[99]

3.6. Aluminium

Aluminium is the third most abundant element on the terrestrial planet. It constitutes the 8.8% of the Earth's crust and it is not an essential metal for human life. Its name derives from "alum", an aluminum sulfate used since ancient times for the preparation of dyes and medicines.

It is a small hard metal cation (Al^{3+}), a Lewis acid, which prefers to coordinate small hard Lewis bases (OH^-, COO^-, RO^-, ROH, PO_4^{3-}, SO_4^{2-}), amines as part of multidentate systems and amino - carboxylic ligands. Its preferred coordination number is 6, to form complexes with octahedral geometry.[111]

From the historical point of view, in 1807 the English chemist Sir Davy suggested that the alum was the salt of an unknown metal that he named "alumium", later called "aluminium". The attempt by Davy to obtain the aluminium through a process of electrolysis of a solution of Al_2O_3 and potassium carbonate did not give positive results. Only in 1825 the Danish physicist Oersted was able to produce some aluminum drops, by heating an amalgam of potassium and aluminum. In 1854, the Frenchman Deville developed a complex thermo-chemical process which allowed a limited industrial production of this metal. This process, diffused throughout all the Europe, was extremely expensive and aluminium had a price higher than gold. Only in 1886 the American Hall and the young French scientist Heroult, discovered simultaneously, but in an independent way, the first process of electrolytic fusion for the production of aluminum from alumina. Their method allowed the production of high quantities of low cost Al and it is still today the system used for the production of this metal.

In 1888 the Austrian Bayer patented the technique for the extraction of aluminum oxide from bauxite.

Because of its reactivity, only the isotope ^{27}Al is natural and stable, aluminium never occurs in nature as free metal, but it is combined with other elements such as oxygen, silicon and fluorine. It is present in the form of aluminium silicates in igneous minerals (*e.g.* feldspar, clays, mica), oxides and hydroxides in soils and rocks. Above pH ~ 5.5 in soils this metal occurs as insoluble aluminium hydroxide, also called gibbsite, and as aluminohydroxosilicate (*e.g.* kaolinite, vermiculite, montmorillonite).[111] The contribution of aluminium from natural sources exceeds the 13% the amount from anthropogenic sources[112] with most Al released into the atmosphere. In natural waters this metal derives from weathering of minerals and rocks. Non-polluted seawaters are characterized by a concentration of aluminium in the range 0.1 – 20 μg L^{-1}.[113] In the rivers the amount of the metal varies and it is dependent on pH, with significant concentrations at pH < 5. Moreover, the complexation with humic and fulvic acids happens at pH values between 3 and 6 with the formation of soluble and insoluble complexes. At pH ~ 6 – 9 the hydroxyaluminium complexes are predominant. Concerning drinking water, tap water contains a wide range of aluminium concentration.[114] The treatment of water with salts of this metal generally increases the total Al amount.[115]

Usually aluminium does not bioaccumulate up the food chain because of its toxicity to several aquatic organisms.[116] There are about 25 plant families with members that strongly bioaccumulate Al in their leaves, with concentrations of more than 1000 mg kg^{-1},[117] as well as also subtropical woody plants, algae, bryophytes and aquatic mosses.[111]

Aluminium is present in foodstuffs either as a natural component of food materials or as an additive. In foods, this metal can be found in cereals, vegetables (*e.g.* mushrooms, spinach, radish and lettuce), beverages (fruit juices, drinks, tea and coffee), cocoa and baby foods.

The Al content in cola and non-cola soft drinks and beers from lacquered aluminium cans is higher than in beverages contained in plastic or glass bottles.[118]

Moreover, the migration of substances from the container of aluminium to the food is about null, with the use of water or sunflower oil. The use of salt or of acid substances, such as vinegar and tomato, contributes to increase the migration of the metal to the foods. Aluminium is also added to refrigerated and frozen dough and baked goods, cocoa mixes, cake and pancake/waffle mixes, self rising flours and baking powder. Some examples of additives are the leavening agent acidic sodium aluminum phosphate (acronym E541) and nondairy creamers as sodium silicoaluminate (acronym E554).[119]

The use of aluminium is spread also in the field of industry (textile, sugar refining, glass, water purification, ceramics, wood preservatives) and for the preparation of cosmetics such as deodorants and make up products. In medicine Al is a component of several antiacids, antibiotics, buffered aspirin products and antiperspirants. This metal is also present in acne cleaning preparations, in dental rinses and in toothpastes for the treatment of dentinal hypersensitivity, in products for dermatitis as astringents, in first aid antibiotics and antiseptics, in antidiarrheal products and as antibacterial to treat athlete's foot.[120]

From the diet, the environment or the drugs, aluminium can reach the blood passing through the gastrointestinal tract, and from there goes into the human bones, brain, lungs, kidneys, brain, liver and thyroid. The symptoms of Al overload could be learning disabilities, confusion, disorientation, memory loss, intestinal colic, headaches, heartburn and colitis, anemia, tooth decay, hypoparathyroidism, kidney disorders, liver disorders and osteomalacia.

This metal is a neuro-toxic element but the link between the aluminium and the arise of brain diseases, such as dialysis encephalopathy, amyotrophic lateral sclerosis, Parkinson dementia, Alzheimer's disease and multiple sclerosis, is still controversial.[121-123]

Chapter 4

Experimental section

4.1. Potentiometry

The potentiometry is an analytical technique that allows to measure the difference of electrochemical potential between two electrodes of a galvanic cell in absence of current. Figure 4.1 shows a scheme of a typical potentiometric system, which consists of a thermostatted cell, two electrodes (one reference and one indicator), a stirrer, a thermostat and a potentiometer.

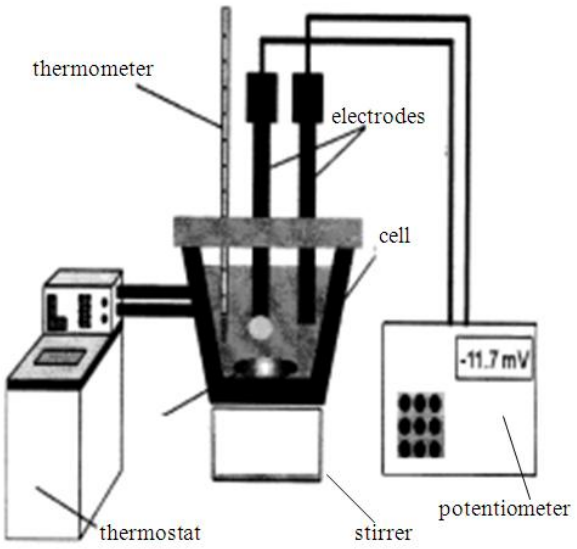

Figure 4.1 Potentiometric equipment.

The reference electrode has a known potential, constant in the time and independent by the composition of the solution containing the analyte in which it is immersed; the indicator or

work electrode responds in a quick and reproducible way to the change of the activity of the analyte. The potentiometric measurements of this study were performed using a glass electrode, represented in Figure 4.2. It is an ion-selective electrode that responds selectively to a single species in solution, the H^+ ions, and so it is used for pH measurement in solution.

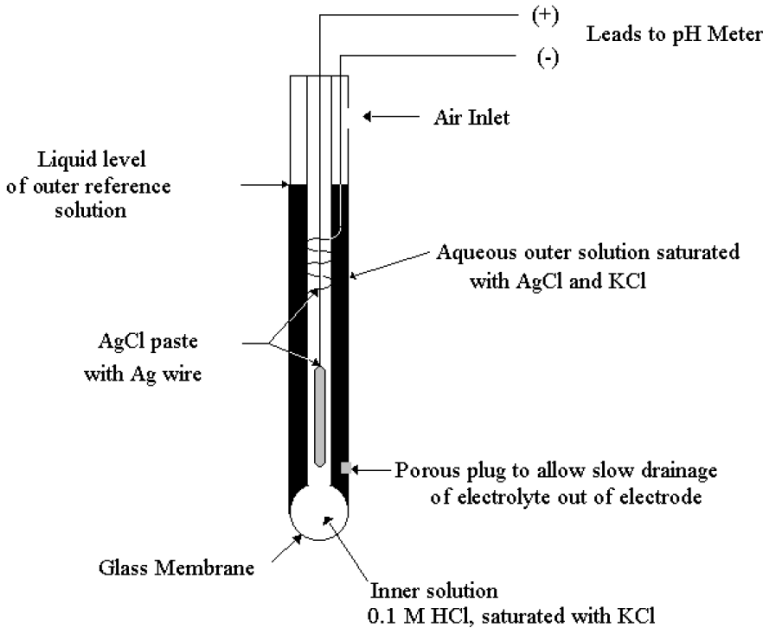

Figure 4.2. Glass electrode used for the potentiometric titrations.

This type of electrode is characterized by a thin glass membrane that separates the sample from the internal solution containing the H^+ ion to be determined at a defined and constant activity. The difference of potential across the membrane is dependent by the difference of activity between the ion in the internal solution of the electrode and in the sample.[124]
The glass electrode potential is described by the Nernst equation, expressed by eq. (4.1):

$$E = E^{\circ\prime} - (0.05916)\log\frac{a_{H^+}(\text{int})}{a_{H^+}(\text{ext})} \qquad (4.1)$$

where $E^{0,}$ includes, in addition to the standard potential E^0, also the asymmetry potential and the junction potential. The asymmetry potential is due to the imperfections of the surface of the membrane and this aspect can be corrected by calibrating the potential of the electrode with known pH solutions. The junction potential is present at the interface between the salt bridge and the cell and it is due to the different of mobility of ions in solution, namely at their unequal spread from each side of the junction surface, which causes a charge separation and therefore the potential.[125]

4.1.1. Potentiometric apparatus and procedures

Potentiometric measurements were carried out by using a Metrohm model 809 Titrando, a potentiometer connected to an automatic burette, and equipped with a combined glass electrode (Ross type 8102, from Thermo-Orion). The apparatus, represented in Figure 4.3, was linked to a PC and automatic titrations were performed using the MetrohmTiAMO 1.2 software to control titrant delivery, data acquisition and to check for e.m.f. stability. Estimated accuracy was ±0.15 mV and ±0.003 mL for e.m.f. and titrant volume readings, respectively.

Figure 4.3. Metrohm model 809 Titrando and the apparatus for potentiometric measurements.

Potentiometric titrations were performed at different conditions of temperature ($283.15 \leq T / K \leq 310.15$) and ionic strength ($0.10 \leq I$ / mol $L^{-1} \leq 1.0$) in ionic medium NaCl.

The measurements were performed in thermostatted cells under magnetic stirring and bubbling purified presaturated $N_{2(g)}$ through the solution to exclude $O_{2(g)}$ and $CO_{2(g)}$ inside.

For each experiment, independent titrations of strong acid with standard base solutions were performed, at the same experimental conditions of ionic medium, ionic strength (I) and temperature (T) of the investigated systems, to determine the value of electrode potential (E^0), the acidic junction potential ($Ej = ja[H^+]$), and the ionic product of water (K_w). The pH scale used was the free scale and $pH \equiv -\log[H^+]$, where $[H^+]$ is the free proton concentration. For each titration, 80 – 100 data points were collected, and the equilibrium state during titrations was checked by adopting precautions, such as to check the necessary time to reach equilibrium and performing back titrations.

During a strong acid – strong base titration, the graph obtained is a sigmoid curve from which, through the method of the first derivative or even the method of the second derivative, more precise than the graphical extrapolation methods, it is possible to calculate the equivalence point.

In Figure 4.4 some examples of an acid-base titration curve, the curve obtained by the methods of the first and the second derivative, respectively, are shown.

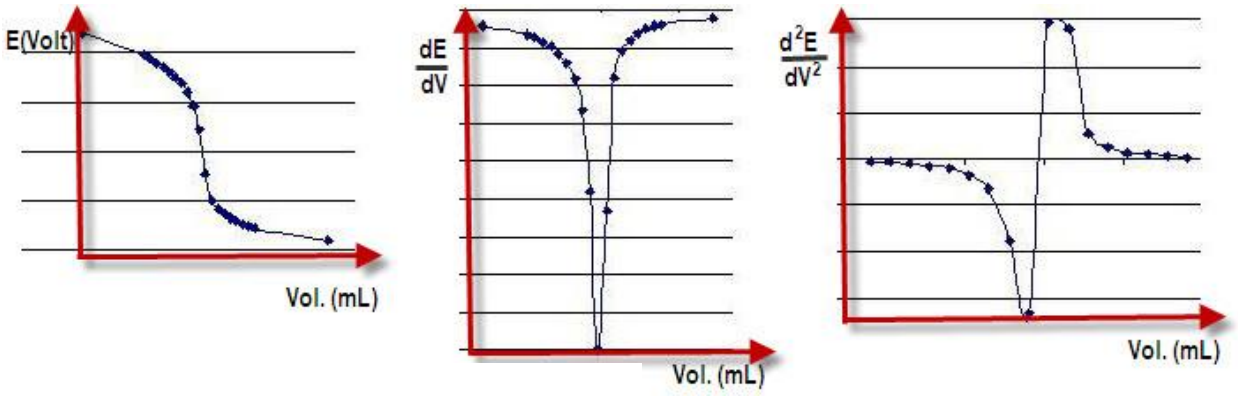

(a) (b) (c)

Figure 4.4. Representations of the titration curves: E *vs*. V (a),
dE / dV *vs.* V (b) in the first derived method
and d^2E / dV^2 *vs.* V (c) in the second derivative method.

In the case of the systems investigated, the titration curves were more complicated than for a strong acid – strong base reaction, and they were characterized by the presence of more flex points because of the presence of different protonable sites.

4.2. UV-Vis Spectrophotometry

The spectrophotometric methods are based on the measurements of the intensity of an electromagnetic radiation absorbed by a molecule.

Electromagnetic radiation is a form of energy whose behavior is described by the properties of both waves and particles. The optical properties of electromagnetic radiation are better explained considering it as a wave. While the interactions between an electromagnetic radiation and the matter, are better described treating the light as a particle or a photon. Electromagnetic radiation consists of oscillating electric and magnetic fields that propagate through space along a linear path and with a constant velocity. The oscillations in the electric and magnetic fields are perpendicular to each other, and to the direction of the wave propagation.

Every wave is described by parameters such as an amplitude A, a wavelength λ, a frequency ν and a velocity of propagation v.

The energy E associated to a wave is proportional to its frequency, according to Planck law:

$$E = h\nu \qquad (4.2)$$

where

h is the Planck constant and its value is $6.63 \cdot 10^{-34}$ J s.

The range of all the electromagnetic radiations constitutes the electromagnetic spectrum, represented in Figure 4.5.

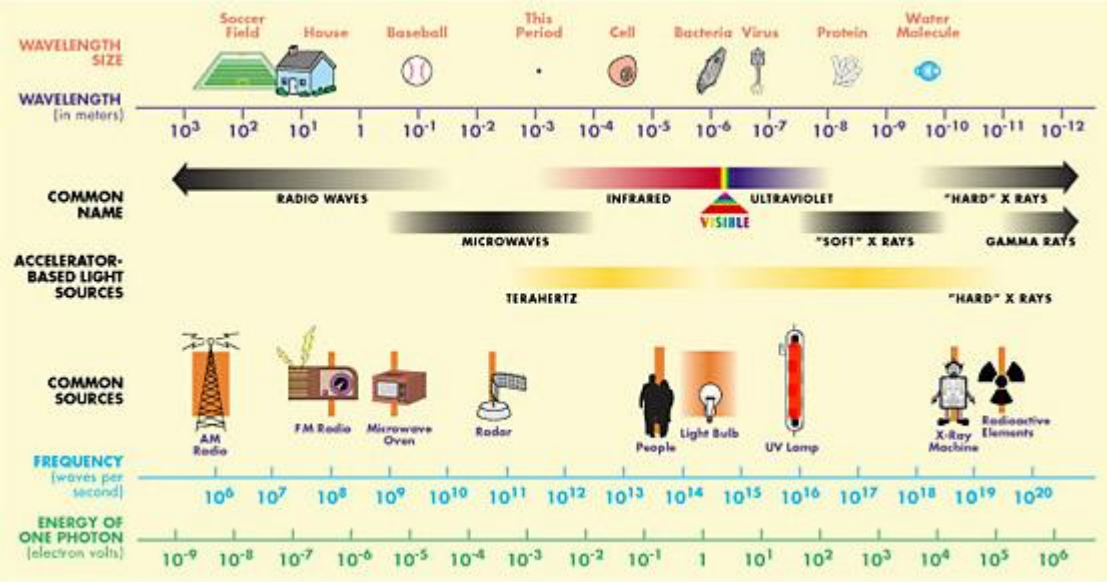

Figure 4.5. Electromagnetic spectrum.

The total energy associated to a molecule is given by the sum of the electronic energy, which is associated to the electrons in the external orbitals, of the vibrational energy, linked to the interatomic vibrations and, finally, of the rotational energy associated to the rotations of the molecule around its centre of gravity, according to eq. (4.3):

$$E = E_{electronic} + E_{vibrational} + E_{rotational} \quad (4.3)$$

At room temperature, most molecules (M) are in their ground state, the level at minimum energy. If M absorbs a radiation of energy E, it can undergo transitions towards excited states characterized by higher energy and this process is called absorption:

$$M + h\nu \rightarrow M^* \quad (4.4)$$

In the case of the UV-Vis radiations, the possible transitions can involve:

- π, σ and n electrons, as shown in Figure 4.6, in the case of mostly organic molecules and some inorganic anion;

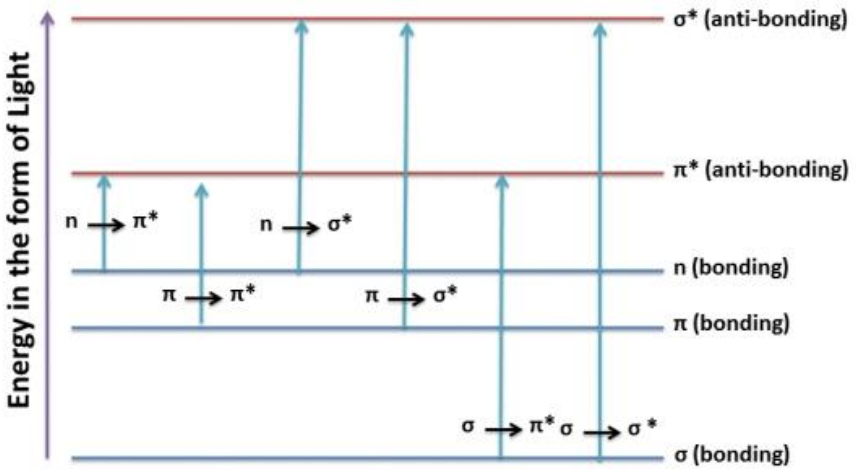

Figure 4.6. Possible electronic transitions involving π, σ and n electrons.

- d and f electrons, in particular in the case of transition metals;
- charge transfer complexes, with electron transfer between a donor and an acceptor.

The functional groups that absorb the ultraviolet and visible radiations are called chromophores, like for example C=C, C≡C, C=O, N=O, C-X (with X = Br, I).

If an UV-Vis radiation of intensity I_0 strikes an absorbent material perpendicular to the surface, an attenuation of the trasmitted radiation will be evidenced and its intensity will become I. Quantitatively, this aspect can be described by the transmittance T and the absorbance A. The equations (4.5) and (4.6) describe the transmittance and absorbance, respectively:

$$T = I / I_0 \tag{4.5}$$

and

$$A = - \log T = - \log I / I_0 \tag{4.6}$$

The absorbance, according to the Lambert Beer law, eq. (4.7), is proportional to the concentration, of the analyte with a concentration *c* (mol L^{-1}), contained in a cell of thickness b (cm):

$$A = \varepsilon \, b \, c \tag{4.7}$$

where

ε is the molar absorbance or molar absorptivity (mol^{-1} L cm^{-1}), it represents the value of absorbance measured if the optical path and the concentration of the analyte are unitary and depends on the wavelength, the solvent and the type of chemical species which absorbs.
During a titration, the chromophores could produce a bathochromic shift (or red shift), that is shift of the maximum of absorption towards higher wavelengths and lower energy. Differently, an hypsocromic shift (or blue shift) occurs when the maximum of absorption shifts towards lower λ and higher energy. Furthermore, an effect that produces a variation of the ε is defined hyperchromic or hypochromic, depending on whether the change is positive or negative.

4.2.1. Spectrophotometric apparatus and procedures

The spectrophotometric measurements were performed using a Varian Cary 50 UV–Vis spectrophotometer, shown in Figure 4.7, equipped with an optic fiber probe with a fixed 1 cm path length.

Figure 4.7. Varian Cary 50 UV–Vis spectrophotometer and the apparatus used for the experiments.

The spectrophotometer was connected to a PC and the acquisition of the couple of data absorbance (A) *vs.* wavelength (λ / nm) was realized by the Varian Cary WinUV (version 3.00) software; at the same time, also the measurement of pH values was carried out. The titrant was delivered in the measurement cell by means of a Metrohm 665 automatic burette, and the homogeneity of the solutions during the titration was ensured by a stirring bar. Before each experiment, $N_{2(g)}$ was bubbled in the solutions for at least 5 minutes in order to exclude the presence of $CO_{2(g)}$ and $O_{2(g)}$.

4.3. Spectrofluorimetry

The lifetime of a M* molecule which arrived to excited state because of a phenomenon of excitation are in the range 10^{-6} - 10^{-14} s, after which the species spontaneously relaxes and returns to the ground state, yielding energy (E) in different forms (photon or heat), according to the following reaction reported by eq. (4.8):

$$M^* \rightarrow M + E \qquad (4.8)$$

There are different emissive phenomena, represented in Figure 4.8, such as:

- fluorescence, the process in which the molecules are involved in vertical transitions from the excited state to the ground state with emission of a photon, maintaining the multiplicity of singlet state, namely the electrons are spin paired;

- phosphorescence, where for heavy atoms molecule it is possible a transition with different multiplicity from singlet to triplet state, where the electrons are spin unpaired. This type of transition would be prohibited for the change of the orientation, so it needs a big amount of energy to take place and the necessary time is higher than for the fluorescence;

- vibrational relaxation, in which M* reaches the lower vibrational level of an electronic state after the transfer of the excess of vibrational energy to the molecules of solvent. This process occurs in less than 10^{-15} seconds;

- internal conversion, a not radiative relaxation with the transfer between the lower vibrational level of an electronic state and the lower vibrational state of another electronic state having lower energy. This process occurs in 10^{-6} - 10^{-9} seconds;

- intersystem crossing, which is the analogue of the internal conversion but with a variation of multiplicity.

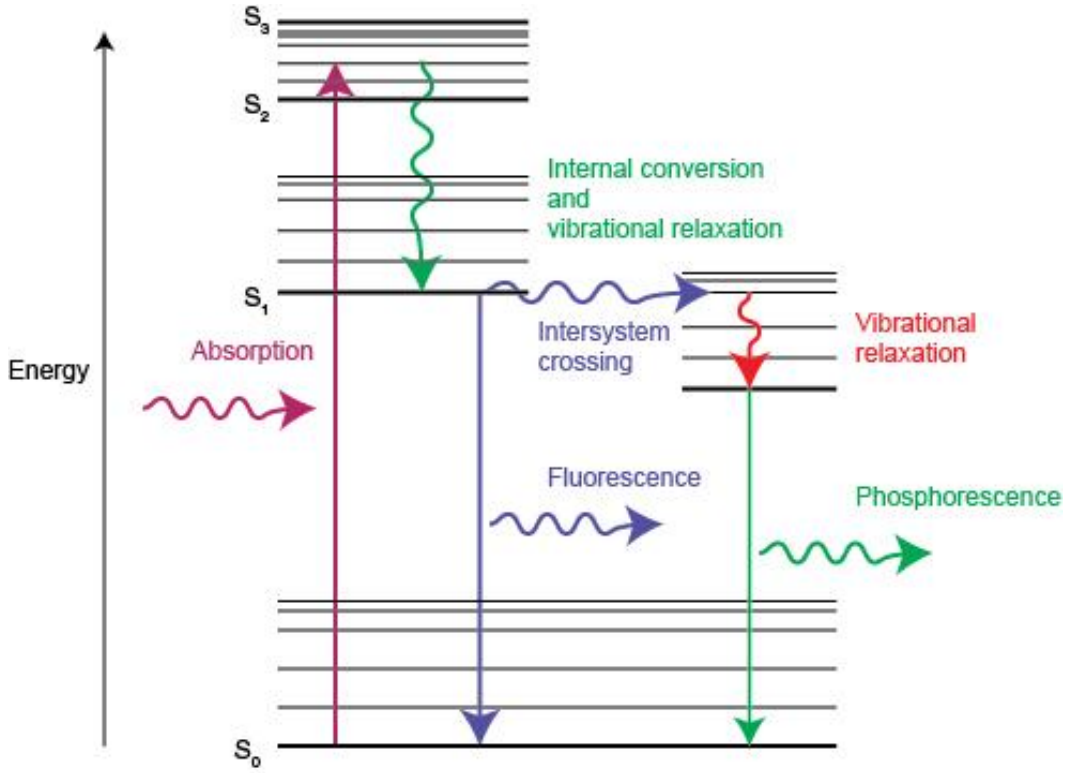

Figure 4.8. Excitation and emission processes.

From the instrumental point of view, the spectrofluorimeters and the fluorimeters are used for the experimental measurements if the selectors of wavelengths are monochromators and filters, respectively.

In Figure 4.9 a block diagram of these type of instruments is represented.

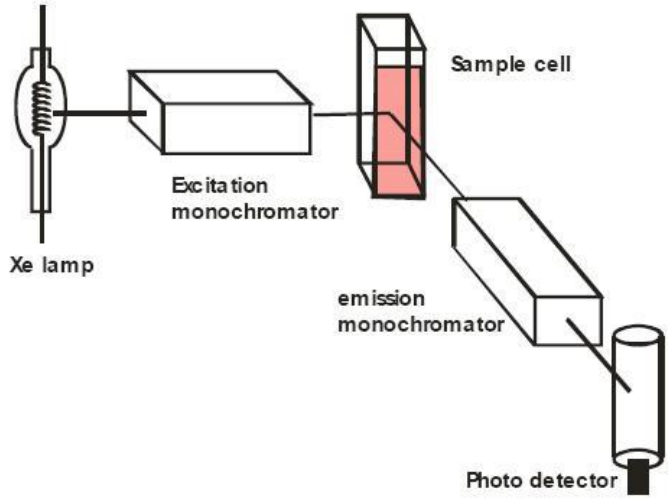

Figure 4.9. Block diagram of a spectrofluorimeter.

The fluorescent radiation is observed at 90° versus the excitation beams because in this direction there is a lower dispersion of the signal and a higher intensity of emission.

From the quantitative analysis point of view, the intensity of the fluorescent radiation is proportional to the concentration *c* of the analyte, according to eq. (4.9):

$$I = k\,c \qquad (4.9)$$

where k is the proportionality constant.

4.3.1. Spectrofluometric apparatus and procedures

A FluoroMax-4 spectrofluorometer by Horiba Jobin-Yvon, represented in Figure 4.10, equipped with F-3006 Autotitration Injector with two Hamilton Syringes (mods. Gastight 1725 and 1001 TLLX, 250 μL and 1 mL capacity, respectively), was used to carry out the measurements.

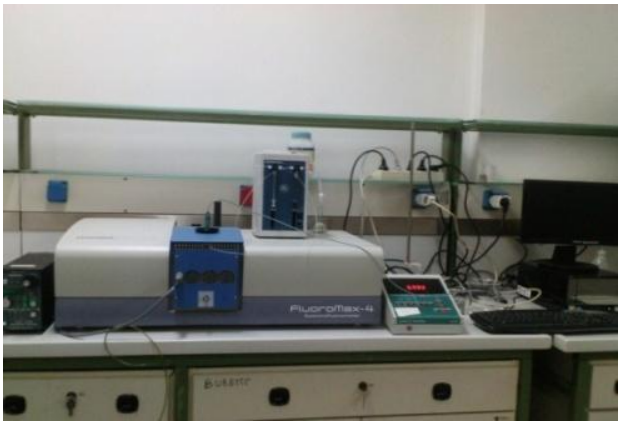

Figure 4.10. FluoroMax-4 spectrofluorimeter and apparatus used for the measurements.

The resolutions of wavelength selectors and titrant additions were 0.3 nm and 0.25 μL, respectively. The spectrofluorometer was equipped with a Peltier Sample Cooler (mod. F-3004) controlled by a Peltier Thermoelectric Temperature Controller model LFI-3751 (5 A - 40 W). The whole system was controlled by the FluorEssence 2.1 software by Horiba Jobin-Yvon. The titrations were carried out in a Hellma type 101-OS precision cell (Light Path 10 mm), with a magnetic stirrer, an ISE-H^+ combined microelectrode (model biotrode 6.0224.100 purchased from Metrohm) and the anti-diffusion burette tip was inserted. The burette tip and the electrode were positioned to not interfere with the light beam. The automatic acquisition of data, in term of fluorescence intensity *vs.* volume in μL of titrant was performed using the same FluorEssence 2.1 software. All the experimental conditions were determined through preliminary evaluations in which several parameters, such as equilibration time, scan rate, scan range and integration time, excitation and emission wavelengths, were systematically changed to select the values giving the best signal/noise ratio.

4.4. Chemicals

Gantrez® AN169 and citric acid were used without further purification and their purity, checked alkalimetrically, was found to be > 99%. A standard solution of silicium (Fluka) in 2% NaOH, prepared from sodium hydroxide TraceSELECT® and water TraceSELECT® Ultra, was used as source of orthosilicic acid.

Hydrochloric acid and sodium hydroxide solutions were prepared by diluting concentrated ampoules (Riedel-deHäen) and were standardized against sodium carbonate and potassium hydrogen phthalate, respectively.

NaOH solutions were preserved from atmospheric CO_2 by means of soda lime traps. The solutions of calcium, magnesium, tin, zinc, copper and aluminium were prepared by weighing the corresponding salts (Fluka products: $CaCl_2$ dihydrate, $MgCl_2$ hexahydrate, $SnCl_2$ dihydrate, $ZnCl_2$, $CuCl_2$ dihydrate, $AlCl_3$ hexahydrate), without further purification. Their purity was checked by titrations with EDTA standard solutions[126] and was always ≥ 98%, while for the products synthesized at the University of Lisbon it was verified through ^1H NMR measurements.

NaCl aqueous solutions were prepared by weighing the pure salt (Fluka), previously dried in an oven at T = 383.15 K for at least 2 hours. All the solutions were prepared with analytical grade water (R = 18 MΩ cm^{-1}) using grade A glassware.

4.5 Computer programs

The experimental data were elaborated using different computer programs, with the aim to obtain all the thermodynamic parameters necessary to model the behavior of the analytes and the corresponding parameters for the dependence on the ionic strength and temperature.

The computer programs used were the following:

1. STACO [127] and BSTAC [128]: both of them use the non linear least square minimization method and allow the refinement of all the analytical parameters of a potentiometric titration at constant or different ionic strength. These programs consider also the variation of the ionic strength during a titration and allow the refinement of the stoichiometric and thermodynamic equilibrium constants. Furthermore, they can refine parameters of the dependence of stability constants on ionic strength using the Debye-Hückel equation. Concerning the refinement procedure, STACO program minimizes

the error squares on volumes, while BSTAC does the same operation on the e.m.f. readings:

$$U_V = \sum_n w_n (v_n^{\exp} - v_n^{calc})^2 \qquad \text{(STACO)} \qquad (4.10)$$

$$U_E = \sum_n w_n (E_n^{\exp} - E_n^{calc})^2 \qquad \text{(BSTAC)} \qquad (4.11)$$

where:

$$w_n = 1/\sigma_n^2 \qquad (4.12)$$

$$\sigma_n^2 = \sigma_V^2 + (\delta v_i / \delta E_i)^2 \sigma_E^2 \qquad \text{(STACO)} \qquad (4.13)$$

$$\sigma_n^2 = \sigma_E^2 + (\delta E_i / \delta v_i)^2 \sigma_v^2 \qquad \text{(BSTAC)} \qquad (4.14)$$

2. Alternatively $w_n = 1$, usually this last assumption is made when using STACO, because the partial derivative in eq. (4.13) is null. For both programs, it is possible to perform two refinements processes, the first one with weight=1, and the second one by eq. (4.12), where σ is taken from the first refinement cycle. The possibility to perform two cycles allows the operator to give minor weight, in the second cycle, to the data points affected by higher errors (σ).

3. ESAB2M (Equilibria in Solution, Acid Base titrations, program n° 2) [129]: it uses the non linear least square minimization method; it can refine the stoichiometric protonation constants and the analytical parameters of an acid - base system. It is often used to calculate the purity of the reagents. In an acid - base titration, the mass balance equations can be solved to obtain an explicit function of the titrant concentration and number of protons bound to it. By minimizing the squares sum of the residuals on the volume (analogously to STACO), it is possible to refine all the parameters involved in the titration, such as the analytical concentrations of reagents, the standard electrode potential E^0, K_w, liquid junction potential coefficient j_a and the protonation constants.
Another possibility is to minimize the squares sum of the residuals on the e.m.f. readings. Analogously to BSTAC and STACO, the weight can be calculated by variance propagation as reported in the eqs. (4.13 - 4.14). Usually, by using ESAB2M, the minimization of the eq. (4.10), as objective function, is faster. The algorithm used

for the refinement is the Gauss-Newton one, with the Levenberg-Marquardt as protection algorithm from divergence. Although ESAB2M, BSTAC and STACO can appear identical, they have different options. ESAB2M can be used in the case of the refinement of acid-base titrations or when dealing with a single titration; whilst the other two programs are preferred when dealing with more than acid – base or complex formation titration at different ionic strength, since ESAB2M does not take into account the ionic strength variation.

4. LIANA (Linear and Nonlinear Analysis) [130]: this is a very flexible computer program, written in Pascal code, used for general fitting and optimization of experimental data, with some peculiarities that make it suitable for application to chemical sciences:
   a) it can be used for the calculation of the parameter of linear and non linear equations;
   b) the equations can be written by operator;
   c) the equation can be splitted into several partial equations;
   d) several equations can be written in the same input and the parameters can be present in several equations;
   e) it is possible to give different weights to different variables and multivariables fitting can be solved;
   f) some graphics can be displayed for a more rapid evaluation of the results.

5. ES4ECI [128] and HySS [131]: these programs are useful for the calculation of the formation percentage of the species in a multicomponent solution. The programs allow to draw, from stability constants and analytical concentrations of the components, the speciation diagrams.

6. HYPERQUAD [132]: this programs allows to analyze the experimental data obtained from different analytical techniques (potentiometry, UV-Vis spectrophotometry, spectrofluorimetry) and to determine the speciation model, the formation constants and the distribution of the species. The advantage of this program compared to BSTAC and STACO, is that it allows to treat simultaneously the potentiometric and spectrophotometric data. The program Hyperquad 2008 can calculate the values of the molar absorbances of each species, to know the absorption spectra and the analytical concentrations of the reagents and to identify the speciation model that best fits the

experimental data. The spectra are obtained through deconvolution procedures for each species in solution (molar extinction coefficients, ε/mol^{-1} L cm^{-1}, versus wavelength, λ/nm), assuming the additivity of absorbances in the concentration range investigated (Beer-Lambert law). At this point, the experimental spectra are again reconstructed from those calculated using the concentration of the species calculated according to their distribution. This program, however, does not take into account the shape of the possible curves, as well as the nature of the electronic transitions.

4.6 Models for the dependence on ionic strength and temperature of thermodynamic parameters

4.6.1. Equilibrium constants

The protonation constants of all the ligands (L^{z-}) considered in this thesis, they are given according to the following equilibria:

$$H^+ + H_{(r-1)}L^{(z-(r-1))} = H_rL^{(z-r)} \qquad K_r^H \qquad (4.15)$$

and

$$rH^+ + L^{z-} = H_rL^{(z-r)} \qquad \beta_r^H \qquad (4.16)$$

where r represents the r-th protonation step and z is the charge of the different ligands.
The metal hydrolysis reactions are given as follows:

$$pM^{n+} + rH_2O = M_p(OH)_r^{(pn-r)} + rH^+ \qquad \beta_r^{OH} \qquad (4.17)$$

During the calculations of the formation constants of the metal-ligand species, the hydrolysis of the single metal cation, at the experimental conditions of ionic medium, ionic strength and temperature, was taken into account. In some cases, at the experimental conditions, in the distribution diagrams it has been evidenced that the hydrolytic species did not form, therefore they were neglected.
The reactions of formation of the species are expressed by equation:

$$pM^{n+} + rOH^- = M_p(OH)_r^{(pn-r)} \qquad \beta^*_{pr} \qquad (4.18)$$

The formation constants for the metal–ligand complexes investigated, refer to the following equilibria:

$$pM^{n+} + H_rL_q^{(qz-r)} = M_pL_qH_r^{(pn+r-qz)} \qquad K_{pqr} \qquad (4.19)$$

or

$$pM^{n+} + qL^{z-} + rH^{+} = M_pL_qH_r^{(pn+r-qz)} \qquad \beta_{pqr} \qquad (4.20)$$

The hydrolytic mixed species are described as follows:

$$M_p(OH)_r^{(pn-r)} + qL^{z-} = M_pL_q(OH)_r^{(pn-r-qz)} \qquad K_{pqr}^{OH} \qquad (4.21)$$

or

$$pM^{n+} + rH_2O + qL^{z-} = M_pL_q(OH)_r^{(pn-r-qz)} \qquad \beta_{pqr}^{OH} \qquad (4.22)$$

Along the text, that charges of the species determined are mostly omitted for simplicity, unless otherwise specified.

4.6.2. Dependence on ionic strength of the thermodynamic parameters

The necessity to perform experimental measurements at different ionic strengths is due to the fact that the thermodynamic parameters such as the protonation and hydrolysis constants as well as the stability constants of the metal – ligand complexes are related to the activity coefficient of the species which are present in solution. It depends on the ionic strength, temperature, pressure, chemical characteristics of the species and properties of the solvent.
The activity coefficient is related to the ionic strength through the Limited Debye – Hückel theory, based on the description of the different physical-chemical interactions between the ions and of their interactions with the molecules of the solvent. This theory takes into account only the electrostatic interactions between ions of opposite charge and the ions are considered as point charges. The Limited Debye – Hückel law, valid for solution with $0 \leq I$ / mol kg$^{-1} \leq 0.001$, is:

$$\log \gamma_i = -A\,|z^+ z^-|\,\sqrt{I} \qquad (4.23)$$

where
γ_i = activity coefficient of the i-th ion;
z = charge of the ion;
A = constant dependent from temperature and solvent (in water at T = 298.15 K, A = 0.51);
I = ionic strength in the molal scale.

In a successive elaboration of the law, Debye and Hückel considered the ions of finite dimensions and interacting with each other at distances not lower than the sum of their radii.

The Extended Debye – Hückel law, valid for solutions characterized by $0.001 \leq I$ / mol $kg^{-1} \leq 0.01$, is:

$$\log \gamma_i = (-A\,|z^+ z^-|\,\sqrt{I}) / (1+å\,B\,\sqrt{I}) \qquad (4.24)$$

where

B = constant dependent from temperature, pressure and dielectric constant of the solvent (in water at T = 298.15 K, B = 0.32);

å = the maximum distance of approach between oppositely charged ions expressed in Angstrom (Å).

For ionic strength values up to 0.2 mol kg^{-1}, the Extended Debye – Hückel law is substituted by the Davies equation,[133] eq. (4.25). It is more suitable and takes into account only the charge of the ions and not their individual features.

$$\log \gamma_i = -0.51\,z^2\,((\sqrt{I} / (1+\sqrt{I}) - 0.3I) \qquad (4.25)$$

Many different approaches were proposed to model the dependence of the equilibrium constants on ionic strength and to extend its validity at higher values of ionic strength, typical of a lot of natural fluids. The extended Debye - Hückel equation, implemented by a term L(I), is:

$$\log \gamma_i = (-A\,|z^+ z^-|\,\sqrt{I}) / (1+å\,B\,\sqrt{I}) + L(I) \qquad (4.26)$$

where

L(I) represents the specific short range interactions.

A modified model, was proposed by the research group, eq. (4.27), was proposed by the research group[134] in which this thesis was developed:

$$\log K_i = \log {}^{T}K_i - z^*\,DH + C\,I + D\,I^{3/2} + E\,I^2 \qquad (4.27)$$

where

K_i = equilibrium constant of the i-th species at an I value;

${}^{T}K_i$ = thermodynamic equilibrium constant of the i-th species at infinite dilution;

$z^* = \Sigma\,(z)^2_{reactants} - \Sigma\,(z)^2_{products}$

$DH = 0.51\,(\sqrt{I} / (1+1.5\sqrt{I}))$;

$C = (c_o\,p^* + c_1\,z^*)$;

$D = (d_o\ p^* + d_1\ z^*)$;

$E = (e_o\ p^* + e_1\ z^*)$;

c_o , c_1, d_o, d_1, e_o, e_1 = empirical parameters for the dependence on ionic strength;

$p^* = \Sigma\ (p)^2_{reactants} - \Sigma\ (p)^2_{products}$ (p = stoichiometric coefficients).

The empirical parameters C, D and E can be considered constants, or independent of the stoichiometry of the complex considered. When $I >> 1$ mol L^{-1}, it is necessary to use one or both the terms D $I^{3/2}$ and E I^2. Furthermore, the use of one or more linear terms depends also on the supporting electrolyte. For $I \leq 1$ mol L^{-1} only one term (C I) in NaCl aqueous solutions has been used, while for tetraethyl ammonium iodide (Et_4NI) aqueous solutions it has been necessary to fit the data with two empirical parameters, C and D. Moreover, the eq. (4.27) can be used with both molar and molal concentration scales.

4.6.3. Dependence on temperature of the thermodynamic parameters

Formation constants at different temperatures allowed to calculate the enthalpy values by applying the Van't Hoff equation, assuming that the contribution of ΔCp in a small temperature range, as in our case 283.15-318.15 K, is negligible:

$$\log K_T = \log K_\theta + (\Delta H_\theta / 2.303R)\ (1/\theta - 1/T) \qquad (4.28)$$

where

θ = reference temperature (298.15 K);

T = temperature in Kelvin;

ΔH_θ = enthalpy change at reference temperature;

R = 8.314 J K^{-1} mol^{-1} and is the universal gas constant.

The dependence on ionic strength of the enthalpy changes was modeled by a modified Debye - Hückel type equation:

$$\Delta H = (\Delta H^0 - z^*\ 1.5\sqrt{I} / (1 + 1.5\sqrt{I}) + C_T \cdot I) \cdot 52.23 \qquad (4.29)$$

where

ΔH^0 = enthalpy change at infinite dilution;

C_T = dependence parameter on ionic strength of the enthalpy changes;

52.23 = 1/(R ln10) in kJ mol^{-1}.

It is necessary to consider that the enthalpy changes here mentioned, is not really the state function, inasmuch the concentration scale used was the molar one, therefore it was obtained a gradient of the temperature.

Furthermore, the Gibbs free energy can be calculated from the equilibrium constants as reported by eq. (4.30):

$$\Delta G = -RT \ln K \qquad (4.30)$$

From the knowledge of the enthalpy changes and the Gibbs free energy, the $T\Delta S$ values can be calculated in the same experimental conditions:

$$T\Delta S = \Delta H - \Delta G \qquad (4.31)$$

The knowledge of the parameters for the dependence on ionic strength and temperature gives a complete thermodynamic picture of these systems, whose equilibrium constants can therefore be predicted for any experimental condition.

Chapter 5

M^{n+} / Gantrez® AN169 systems

5.1. Acid – base properties of the ligand and of the metal cations

The metal - ligand interactions can be investigated only if the acid-base behavior of the ligand and of the metal cations are already known.

The protonation constants of Gantrez® AN169 were already studied in different conditions of temperature, ionic strength and ionic medium by the research group in which this thesis was elaborated.

The protonation constants of the ligand were determined from potentiometric ISE H^+ data using the "Diprotic-like model". [135] This model consider the polyelectrolyte as low molecular weight carboxylic compound and the acid – base properties of each monomeric unit are described by two protonation constants.

In the case of the Gantrez® AN169 two monomeric units were considered and the ligand was assimilable to a tetraprotic acid (H_4(*GTZ*)).

The results obtained, still unpublished, are in agreement with those achieved in the past for other similar polyelectrolytes.[136]

The protonation constants used for the study of the binding ability of Gantrez® AN169 towards the metal cations are reported in Table 5.1.

Table 5.1. Protonation constants[a)] of Gantrez® AN169 in $NaCl_{(aq)}$ at different conditions of ionic strength and temperature

T / K	I / mol L^{-1}	H(*GTZ*)	H_2(*GTZ*)	H_3(*GTZ*)	H_4(*GTZ*)
283.15	0.10	8.12	14.69	18.58	22.28
	0.25	7.94	14.22	18.22	21.55
	0.50	7.68	13.92	17.80	21.04
	1.00	7.43	13.63	17.43	20.53
298.15	0.10	8.21	14.87	19.00	22.38
	0.25	7.94	14.37	18.32	21.62
	0.50	7.71	14.03	17.86	21.06
	1.00	7.46	13.70	17.45	20.51
318.15	0.10	8.31	15.09	19.17	22.50
	0.25	8.01	14.54	18.44	21.68
	0.50	7.75	14.16	17.93	21.09
	1.00	7.49	13.79	17.46	20.49

[a)] $\log\beta_r$ refers to eq. (4.18).

The hydrolysis of Mg^{2+}, Sn^{2+}, Zn^{2+}, Al^{3+} and, in some case, the formation of scarcely soluble species, was already known and available in literature. [83, 137, 138-140]

5.2. Stability of M^{n+}/Gantrez® AN169 complexes

5.2.1. Experimental details

Potentiometric measurements (ISE-H^+) in $NaCl_{(aq)}$ and at different conditions of ionic strength ($0.10 \leq I$ / mol $L^{-1} \leq 1.00$) and temperature ($283.15 \leq T$ / K ≤ 318.15) were carried out to study the interaction between Gantrez® AN169 and bivalent (Mg^{2+}, Zn^{2+}, Sn^{2+}) and trivalent (Al^{3+}) metal cations. In Table 5.2 the experimental condition for all the M^{n+}/Gantrez® AN169 systems are reported.

Potentiometric data allowed the determination of the formation constants of different complex species between Gantrez® AN169 and the four metal ions, namely $M_pL_qH_r$.

The binding ability of the Gantrez® AN169 towards metal cations was not known, so it has not been possible to perform some comparisons with literature data.

Table 5.2. Experimental conditions for the M^{n+}/Gantrez® AN169 measurements at $0.10 \leq I$ / mol $L^{-1} \leq 1.00$ in $NaCl_{(aq)}$ and $283.15 \leq T$ / K ≤ 318.15

System	pH	c_L / mol L^{-1}	c_M/ mol L^{-1}
Mg^{2+}/GTZ^{4-}	2.0 – 8.0	0.002 - 0.004	0.002 - 0.004
Sn^{2+}/GTZ^{4-}	2.0 – 5.8	0.0005 - 0.001	0.001 - 0.002
Zn^{2+}/GTZ^{4-}	2.0 – 7.0	0.002 - 0.004	0.002 - 0.004
Al^{3+}/GTZ^{4-}	2.0 – 8.0	0.001 - 0.002	0.002 - 0.004

5.2.2. Mg^{2+}/Gantrez® AN169 and Sn^{2+}/Gantrez® systems

The study on the Mg^{2+}/GTZ^{4-} and Sn^{2+}/GTZ^{4-} systems at the experimental conditions already reported in Table 5.2 allowed in both cases the determination of only one species $M_2(GTZ)_{(aq)}$. The Mg^{2+}/GTZ^{4-} system was studied in the pH range 2.0 – 8.0 and precipitate did not occur during the experimental measurements.

In the case of Sn^{2+}/GTZ^{4-} system, the hydrolytic behavior of the metal cation, the formation of the scarcely soluble species $Sn(OH)_{2(s)}$ and the complexes $SnCl_i$ (SnCl, $SnCl_2$, $SnCl_3$ and SnCl(OH))[83] influenced strongly the speciation. Measurements were performed in the pH range 2.0 – 5.8, to avoid sparingly soluble species $Sn(OH)_{2(s)}$.

The stability constants of the species refer to the following equilibria:

$$2Mg^{2+} + (GTZ)^{4-} = Mg_2(GTZ)^0 \qquad \beta_{210} \qquad (5.1)$$

and

$$2Sn^{2+} + (GTZ)^{4-} = Sn_2(GTZ)^0 \qquad \beta_{210} \qquad (5.2)$$

The experimental formation constants determined for both the systems by BSTAC and STACO computer programs, at $0.10 \leq I$ / mol $L^{-1} \leq 1.00$ in $NaCl_{(aq)}$ and $283.15 \leq T$ / K $\leq$ 318.15, are reported in Tables 5.3 and 5.4.

In general, it was found that the stability constant values decrease with increasing the ionic strenght and increase by increasing the temperature.

Table 5.3. Experimental stability constants[a)] of $Mg_2(GTZ)_{(aq)}$ species at $0.10 \leq I$ / mol $L^{-1} \leq 1.00$ in $NaCl_{(aq)}$ and $283.15 \leq T$ / K ≤ 318.15

T / K	I / mol L^{-1}	$\log\beta_{210}$
283.15	0.103	6.703±0.009[b)]
	0.244	5.96±0.01
	0.488	5.40 ±0.02
	0.933	4.94±0.02
298.15	0.110	7.17±0.02
	0.263	6.14±0.01
	0.477	5.15±0.09
	0.982	5.74±0.03
318.15	0.106	7.64±0.02
	0.255	6.46±0.02
	0.490	6.15±0.02
	0.940	5.37±0.02

[a)] $\log\beta_{pqr}$ refers to eq. (5.1); [b)] ±Std. Deviation.

Table 5.4. Experimental stability constants[a)] of $Sn_2(GTZ)_{(aq)}$ species at $0.10 \leq I$ / mol $L^{-1} \leq 1.00$ in $NaCl_{(aq)}$ and $283.15 \leq T$ / K ≤ 318.15

T / K	I / mol L^{-1}	$\log\beta_{210}$
283.15	0.097	20.40±0.19[b)]
	0.248	19.15±0.05
	0.481	18.42 ±0.02
	0.959	18.01±0.01
298.15	0.098	21.70±0.06
	0.251	20.52±0.01
	0.494	18.75±0.04
	0.984	17.95±0.04
318.15	0.100	21.88±0.03
	0.252	20.48±0.07
	0.490	21.66±0.02
	0.963	18.52±0.04

[a)] $\log\beta_{pqr}$ refers to eq. (5.2); [b)] ±Std. Deviation.

The effect of ionic strenght on the stability constants of Mg^{2+}/GTZ^{4-} system can be observed analyzing the speciation diagram reported in Figure 5.1 at I = 0.110 mol L^{-1} and I = 0.982 mol L^{-1} in $NaCl_{(aq)}$ and T = 298.15 K.

In both cases, the free metal cation is present in solution until pH ~ 4.7 and pH ~ 5.5, respectively, probably because the ligand is still protonated, therefore not binding the metal. The formation of the $Mg_2(GTZ)_{(aq)}$ species starts at pH ~ 5 and its percentage decreases with increasing the ionic strength.

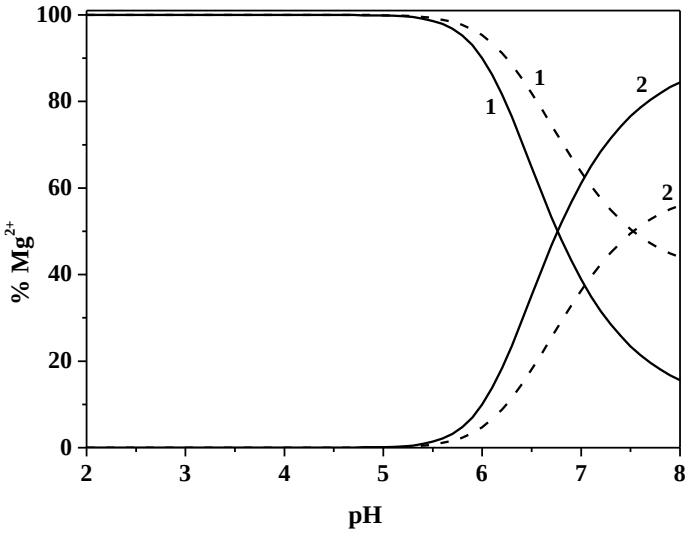

Figure 5.1. Speciation diagram of Mg^{2+}/GTZ^{4-} species at I = 0.110 mol L^{-1} (solid line) and I = 0.982 mol L^{-1} (dashed line) in $NaCl_{(aq)}$ and at T = 298.15 K. $c_{Mg^{2+}}$ = 0.001 mol L^{-1}; $c_{GTZ^{4-}}$ = 0.003 mol L^{-1}. Species: 1. free Mg^{2+}; 2. $Mg_2(GTZ)_{(aq)}$.

In the case of Sn^{2+}/GTZ^{4-} system, at I = 0.098 mol L^{-1} in $NaCl_{(aq)}$ and T = 298.15 K, the polynuclear $Sn_2(GTZ)_{(aq)}$ species, is present at maximum of percentage in all the pH ranges investigated and hinders the hydrolysis of the metal cation, in fact the hydrolytic Sn(OH) and $Sn(OH)_{2(aq)}$ species have very low percentages, in both cases less than the 10%, hampering furthermore the formation of scarcely soluble $Sn(OH)_{2(s)}$ species.

5.2.3. Zn^{2+}/Gantrez® AN169 system

The study on the Zn^{2+}/GTZ^{4-} system allowed the determination of three species, namely $Zn(GTZ)H_2$, $Zn(GTZ)$ and $Zn_2(GTZ)_{(aq)}$, in the pH range 2.0 – 8.0. The stability constants of the complexes refer to the following equilibria:

$$pZn^{2+} + q(GTZ)^{4-} + rH^{+} = Zn_p(GTZ)_qH_r^{(2p+r-4q)} \qquad \beta_{pqr} \qquad (5.3)$$

In Table 5.5, the experimental stability constants for the interaction between Zn^{2+} and GTZ^{4-} at different ionic strengths and temperatures are reported.

From the analysis of the data it was possible to note that the values obtained, in the most of the cases, increase with increasing the temperature and they have on opposite trend increasing the ionic strength.

To better appreciate the effect of ionic strength on the stability constants, Figure 5.2. can be observed, where the speciation diagram of the of Zn^{2+}/GTZ^{4-} complex at I = 0.111 mol L^{-1} and I = 0.961 mol L^{-1} in $NaCl_{(aq)}$ and T = 298.15 K is reported.

Table 5.5. Experimental stability constants[a)] of Zn^{2+}/GTZ^{4-} system at $0.10 \leq I$ / mol $L^{-1} \leq 1.00$ in $NaCl_{(aq)}$ and $283.15 \leq T$ / K ≤ 318.15

T / K	I / mol L^{-1}	$\log\beta_{112}$	$\log\beta_{110}$	$\log\beta_{210}$
283.15	0.104	16.35±0.02[b)]	5.71±0.03	8.91±0.09
	0.252	16.52±0.06	5.21±0.04	8.28±0.06
	0.485	15.86±0.05	4.96 ±0.02	7.19±0.08
	0.998	15.45±0.02	4.744±0.006	6.19±0.10
298.15	0.111	17.44±0.07	6.30±0.04	9.51±0.07
	0.261	16.35±0.07	5.75±0.03	8.30±0.09
	0.491	16.46±0.07	5.81±0.02	7.40±0.15
	0.961	15.82±0.04	5.27±0.02	6.21±0.07
318.15	0.106	17.15±0.10	6.80±0.04	9.77±0.06
	0.254	16.53±0.02	6.25±0.04	8.38±0.05
	0.490	16.42±0.02	5.86±0.01	8.07±0.05
	0.940	16.20±0.02	5.62±0.01	6.72±0.06

[a)] $\log\beta_{pqr}$ refers to eq. (5.3); [b)] ±Std. Deviation.

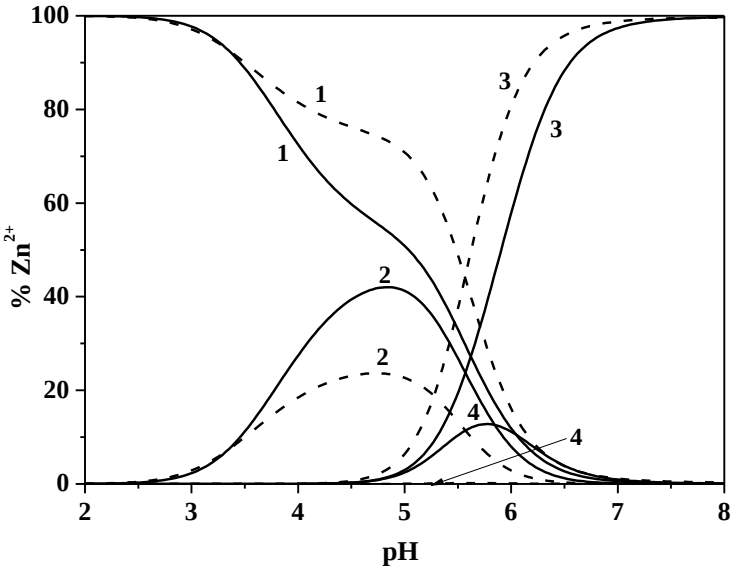

Figure 5.2. Speciation diagram of Zn^{2+}/GTZ^{4-} complexes at I = 0.111 mol L^{-1} (solid line) and I 0.961 mol L^{-1} (dashed line) in $NaCl_{(aq)}$ and T = 298.15 K. $c_{Zn^{2+}}$ = 0.001 mol L^{-1}; $c_{GTZ^{4-}}$ = 0.004 mol L^{-1}. Species: 1. free Zn^{2+}; 2. Zn(*GTZ*)H_2; 3. Zn(*GTZ*); 4. Zn_2(*GTZ*)$_{(aq)}$.

Figure 5.2 shows the speciation diagrams of Zn^{2+}/GTZ^{4-} complexes at I = 0.111 mol L^{-1} and I = 0.961 mol L^{-1} in $NaCl_{(aq)}$ and T = 298.15 K. In both cases, the free metal cation is present in solution at pH ~ 2 and the ligand is still protonated. The formation percentages of the Zn(*GTZ*)H_2 and Zn_2(*GTZ*) species decrease increasing the ionic strength, probably because the competition between the zinc and the sodium from the ionic medium in binding the ligand. The Zn(*GTZ*) start to form at pH ~ 4.3 at I = 0.111 mol L^{-1} and pH ~ 4.5 at I = 0.961mol L^{-1} and achieves the maximum of formation percentage at pH ~ 8.

5.2.5. Al^{3+}/Gantrez® AN169 complexes

The study of speciation of the Al^{3+} in the presence of the Gantrez® AN169 at $0.10 \leq I$ / mol $L^{-1} \leq 1.00$ in $NaCl_{(aq)}$ and $283.15 \leq T$ / K ≤ 318.15 led to the determination of four species, Al(*GTZ*)$H_{(aq)}$, Al(*GTZ*), Al(*GTZ*)$(OH)_2$ and Al_2(*GTZ*)$_2(OH)_2$, in the pH range 2.0 – 8.0.
The stability constants of the complexes refer to the following equilibria:

$$pAl^{3+} + q(GTZ)^{4-} + rH^{+} = Al_p(GTZ)_qH_r^{(3p+r-4q)} \qquad \beta_{pqr} \qquad (5.4)$$

In Table 5.6 the experimental stability constants of the Al^{3+}/GTZ^{4-} species at different ionic strengths and temperatures are reported.

As for the M^{2+}/ GTZ^{4-} systems, also in the case of aluminium complexes the stability constant values decrease with increasing the ionic strength and increase increasing the temperature.

Figure 5.3 can be useful to understand the distribution of the different Al^{3+}/GTZ^{4-} species at different conditions of ionic strength (I = 0.099 and 0.973 mol L^{-1}) in $NaCl_{(aq)}$ and T = 298.15 K. The complex species are uniformly distributed in all the pH range investigated.

The formation of the $Al(OH)_{3(s)}$ species was not observed experimentally, because of its slow kinetics.[141]

Considering the solubility product of this scarcely soluble species in the calculations, it should start to form at pH ~ 5.5 at I = 0.973 mol L^{-1}, corresponding to the shaded zone in Figure 5.3, hindering the formation of th $Al(GTZ)(OH)_2$ species. Differently, at lower ionic strength, the formation of the $Al(OH)_{3(s)}$ species occurs at more alkaline pH values.

Table 5.6. Experimental stability constants[a)] of Al^{3+}/GTZ^{4-} complexes at $0.10 \leq I$ / mol $L^{-1} \leq 1.00$ in $NaCl_{(aq)}$ and $283.15 \leq T$ / K ≤ 318.15

T / K	I / mol L^{-1}	$\log\beta_{111}$	$\log\beta_{110}$	$\log\beta_{11\text{-}2}$	$\log\beta_{22\text{-}2}$
283.15	0.099	15.31±0.01[b)]	10.85±0.02	-3.75±0.02	12.07±0.04
	0.251	14.10±0.01	9.85±0.01	-4.22±0.01	10.33±0.02
	0.489	13.59±0.03	9.15±0.04	-4.63±0.04	9.48±0.08
	0.958	12.35±0.01	8.345±0.005	-4.866±0.007	9.48±0.08
298.15	0.099	16.05±0.03	11.23±0.04	-3.20±0.09	13.05±0.10
	0.251	14.89±0.02	10.35±0.02	-3.59±0.02	11.35±0.03
	0.484	14.19±0.03	10.19±0.03	-3.75±0.04	11.68±0.06
	0.973	13.27±0.01	9.22±0.01	-3.80±0.01	10.33±0.02
318.15	0.101	16.98±0.02	12.04±0.03	-2.13±0.06	14.27±0.05
	0.244	16.28±0.06	12.07±0.05	-2.79±0.10	14.25±0.09
	0.489	15.08±0.01	10.92±0.04	-2.81±0.10	13.02±0.08
	0.965	14.58±0.03	10.36±0.06	-2.93±0.09	11.99±0.10

[a)] $\log\beta_{pqr}$ refers to eq. (5.4); [b)] ±Std. Deviation.

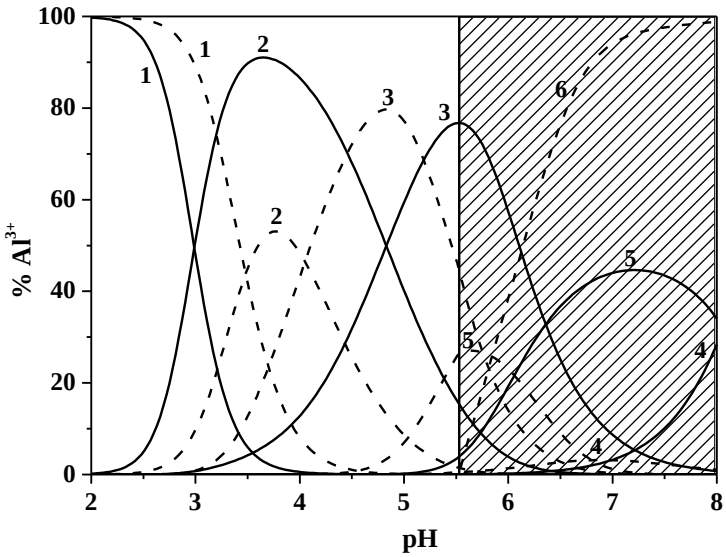

Figure 5.3. Speciation diagram of Al^{3+}/GTZ^{4-} complexes at I = 0.099 mol L^{-1} (solid line) and I = 0.973 mol L^{-1} (dashed line) in $NaCl_{(aq)}$ and T = 298.15 K. $c_{Al^{3+}}$ = 0.0015 mol L^{-1}; $c_{GTZ^{4-}}$ = 0.004 mol L^{-1}. Species: 1. free Al^{3+}; 2. Al(*GTZ*)$H_{(aq)}$; 3. Al(*GTZ*); 4. Al(*GTZ*)$(OH)_2$; 5. $Al_2(GTZ)_2(OH)_2$; 6. $Al(OH)_{3(s)}$.

5.2.6. Dependence on ionic strength and temperature of the stability constants

The dependence on ionic strength and on temperature of the formation constants of M^{n+}/GTZ^{4-} systems was modeled by the eqs. (4.27 - 4.31) and the thermodynamic parameters, such as the formation constants at infinite dilution, the empirical parameters C, ΔH, C_T, are reported in Table 5.7, together with the overall free energy and the entropy changes determined by taking into account the stability constants obtained from potentiometric measurements. As already said, the knowledge of these parameters gives a complete thermodynamic picture of these systems, whose equilibrium constants can therefore be predicted for any experimental condition.

From the enthalpy changes obtained, it was evidenced that all the reactions are endothermic, and the entropic contribution can be considered the driving force for the stability of the complexes.

Table 5.7. Formation constants[a)] at infinite dilution and dependence parameters on ionic strength and temperature of M^{n+}/GTZ^{4-} complexes in molar concentration scale at T = 298.15 K

	$\log^T\beta$	z*	C[b)]	ΔH[c)]	C_T[d)]	ΔG[c), e)]	$T\Delta S$[c), f)]
$Mg_2(GTZ)_{(aq)}$	9.69±0.02[g)]	24	0.34±0.05	58.8±2.4	-0.28±0.21	-55.3±0.1	114.2±2.4
$Sn_2(GTZ)_{(aq)}$	23.34±0.18	24	2.61±0.06	82.2±10.2	0.55±0.30	-133.4±1.0	215.5±10.2
$Zn(GTZ)H_2$	18.96±0.04	22	1.55±0.06	50.5±5.4	-0.41±0.31	-108.0±0.2	158.7±5.4
$Zn(GTZ)$	7.88±0.03	16	0.66±0.04	61.6±3.7	-0.78±0.33	-79.9±0.2	106.6±3.7
$Zn_2(GTZ)_{(aq)}$	12.03±0.04	24	-0.93±0.08	55.6±4.6	-0.91±0.40	10.0±0.1	124.3±4.6
$Al(GTZ)H_{(aq)}$	18.92±0.03	26	0.40±0.09	88.2±3.1	-2.06±0.20	-108.0±0.2	196.2±3.1
$Al(GTZ)$	13.99±0.06	24	0.66±0.08	89.4±2.6	-2.06±0.20	-79.9±0.2	169.2±2.6
$Al(GTZ)(OH)_2$	-1.75±0.02	14	0.93±0.05	73.7±2.0	-2.06±0.20	10.0±0.1	63.7±2.0
$Al_2(GTZ)_2(OH)_2$	16.51±0.04	32	0.71±0.09	162.0±3.7	-2.06±0.20	-94.2±0.2	256.2±3.7

[a)] $\log\beta_{pqr}$ refer to eq. (5.1-5.4); [b)] eq. (4.27); [c)] in kJ mol^{-1}, [d)] eq. (4.29); [e)] eq. (4.30); [f)] eq. (4.31); [g)]±Std. Deviation.

Chapter 6

Al^{3+} / Citric acid interactions

6.1. Acid – base properties of the ligand and of the metal cation

The acid – base properties of the citric acid were previously investigated in $NaCl_{(aq)}$ and the data at different conditions of temperature, ionic strength and supporting electrolyte are reported in literature. [142, 143]

In Table 6.1. the protonation constants, in the experimental conditions of the systems here studied, are reported.

Table 6.1. Overall protonation constants[a)] of citric acid in $NaCl_{(aq)}$ at different conditions of ionic strength and temperature

T / K	I / mol L^{-1}	H(*Cit*)	H_2(*Cit*)	H_3(*Cit*)
283.15	0.249	5.44	9.71	12.63
298.15	0.249	5.42	9.62	12.49
	0.956	5.22	9.29	12.03
318.15	0.249	5.45	9.61	12.41

[a)] $\log\beta_r$ refer to of eq. (4.16).

The hydrolysis of the metal cation was already studied in different experimental conditions and several data were published in the literature. [138-140]

6.2. Stability of Al^{3+}/Cit^{3-} complexes

6.2.1. Experimental details

The study on the stability of the Al^{3+}/Cit^{3-} complexes was carried out by performing potentiometric measurements in $NaCl_{(aq)}$ I = 0.25 and 1.00 mol L^{-1} at T = 298.15 K and at different T values and I = 0.25 mol L^{-1}, respectively. The measurements were performed at different concentrations of metal cation ($0.001 \leq c_{Al^{3+}}$ / mol $L^{-1} \leq 0.002$) and ligand ($0.002 \leq c_L$ / mol $L^{-1} \leq 0.004$), in the pH range 2.0 – 7.0.

6.2.2. Formation constants of Al^{3+}/Cit^{3-} complexes

The treatment of the experimental data with BSTAC and STACO computer programs led to the determination of five species, namely Al(*Cit*)H, $Al(Cit)_{(aq)}$, Al(*Cit*)OH, $Al(Cit)_2$ and $Al_3(Cit)_3(OH)_4$, evidencing the tendency of the metal cation to form polynuclear species. The speciation model chosen, was considered the best possible one based on criteria such as simplicity, probability, formation percentage of species, statistical parameters and literature comparison.

The stability constant values, reported in Table 6.2, refer to the following equilibrium:

$$pAl^{3+} + q(Cit)^{3-} + rH^{+} = Al_p(Cit)_qH_r^{(3p+r-3q)} \qquad \beta_{pqr} \qquad (6.1)$$

Table 6.2. Experimental stability constants[a)] of Al^{3+}/Cit^{3-} complexes in $NaCl_{(aq)}$

T / K	I / mol L^{-1}	$\log\beta_{111}$	$\log\beta_{110}$	$\log\beta_{11-1}$	$\log\beta_{120}$	$\log\beta_{33-4}$
283.15	0.249	9.55±0.05[b)]	7.19±0.02	2.66±0.04	11.40±0.04	7.75±0.20
298.15	0.249	9.91±0.05	7.57±0.02	3.81±0.04	12.12±0.04	11.68±0.12
	0.956	9.32±0.01	6.554±0.002	3.167±0.003	10.85±0.02	10.24±0.03
318.15	0.249	9.93±0.17	7.82±0.03	4.44±0.05	12.74±0.05	16.08±0.09

[a)] $\log\beta_{pqr}$ refer to equilibria of eq. (6.1); [b)] ±Std. Deviation.

From the comparison of the stability constants obtained for the Al^{3+}/Cit^{3-} species at the different conditions, it was possible to note that the values decrease with increasing the ionic strength while increase with increasing the temperature.

The effect of ionic strenght on the stability constants can is shown in the speciation diagram of Al^{3+}/Cit^{3-} complexes reported in Figure 6.1 at I = 0.249 mol L^{-1} and I = 0.956 mol L^{-1} in $NaCl_{(aq)}$ and T = 298.15 K.

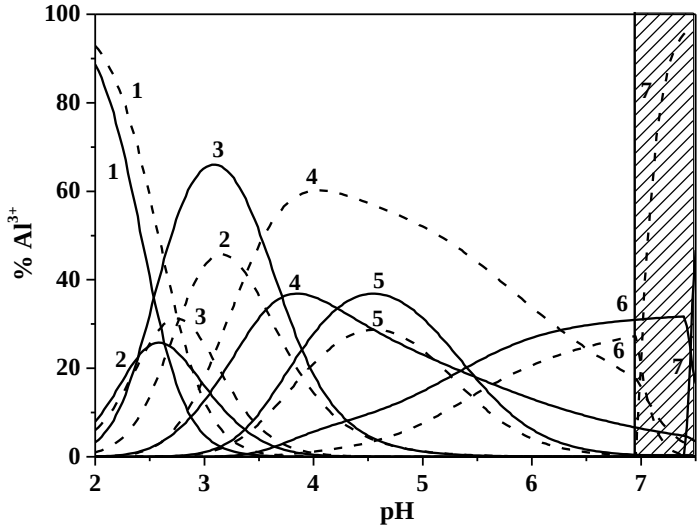

Figure 6.1. Speciation diagrams of Al^{3+}/Cit^{3-} complexes at I = 0.249 mol L^{-1} (solid line) and I = 0.956 mol L^{-1} (dashed line) in $NaCl_{(aq)}$ T = 298.15 K. $c_{Al^{3+}}$ = 0.001 mol L^{-1}; $c_{Cit^{3-}}$ = 0.004 mol L^{-1}. Species: 1. free Al^{3+}; 2. Al(*Cit*)H; 3. Al(*Cit*)$_{(aq)}$; 4. Al(*Cit*)OH; 5. Al(*Cit*)$_2$; 6. $Al_3(Cit)_3(OH)_4$; 7. $Al(OH)_{3(s)}$.

The percentages of the complexes, distributed in all the pH range investigated, exceed the 30%. The formation of the $Al(OH)_{3(s)}$ species was not observed experimentally, because of its slow kinetics.[141]

Considering in the calculations the solubility product of this scarcely soluble species, it should start to form at pH ~ 6.9 at I = 0.956 mol L^{-1}, corresponding to the shaded zone in Figure 6.1. Differently, at lower ionic strength, the formation of the $Al(OH)_{3(s)}$ species occurs from pH ~ 7.9.

In the past, several studies on the Al^{3+}/Cit^{3-} system were performed by different authors, such as Ohman et al. [141, 144], Gregor et al. [145] and Lakatos et al. [146], using different experimental conditions and techniques (*e.g.* NMR).

The speciation model and the stability constant values proposed in this thesis are in good agreement with those of the authors. For example, Lakatos et al. and Gregor et al. reported for the Al(*Cit*)$_{(aq)}$ species at T = 298.15 K and I = 0.10 and 0.20 mol L^{-1} in $KCl_{(aq)}$, a $\log\beta_{110}$ =

7.85±0.05 and 8.35±0.23, respectively, which are in accordance with the value here listed, $\log\beta_{110}$ = 7.57±0.02 at T = 298.15 K and I = 0.249 mol L^{-1} in $NaCl_{(aq)}$.

A $\log\beta_{110}$ = 7.15±0.01 obtained at the same temperature and at I = 0.60 mol L^{-1} in $NaCl_{(aq)}$ was reported by Ohman et al., which follows the trend of the values listed in the present thesis, as shown in Figure 6.2.

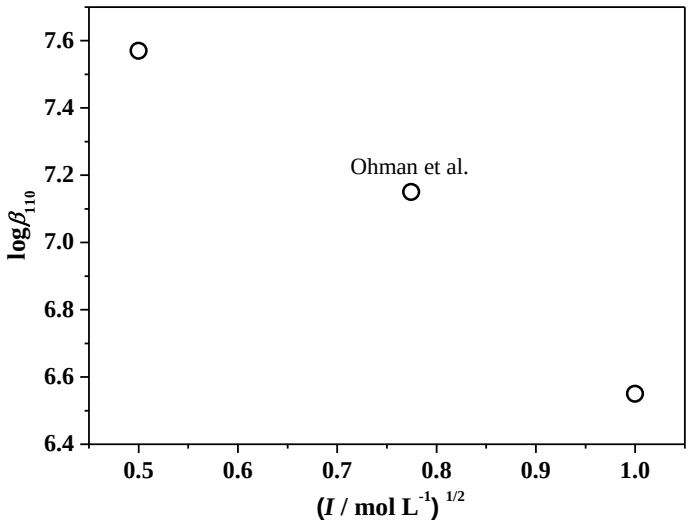

Figure 6.2. Experimental $\log\beta_{110}$ values and Ohman data[141] *vs.* (I / mol L^{-1})$^{1/2}$

Ohman et al. and Wiese and Veith[147] considered also the formation of mixed hydroxo species, such as the $Al(Cit)_2(OH)_2$ and the polynuclear $Al_3(Cit)_3(OH)_7$ and $Al_{10}(Cit)_6(OH)_{15}$ species, which can form at quite high concentrations of both ligand and metal cation, not determined in the speciation model reported in this thesis.

6.2.3. Dependence on ionic strength and temperature of the stability constants

The dependence on ionic strength and on temperature of the formation constants of the Al^{3+}/Cit^{3-} complexes was modeled by the eqs. (4.27 - 4.31) and the obtained thermodynamic parameters are reported in Tables 6.3 and 6.4.

Table 6.3. Formation constants[a)] at infinite dilution of Al^{3+}/Cit^{3-} complexes at infinite dilution and in molar concentration scale

	$\log^{T}\beta$	z*	C[b)]
Al(*Cit*)H	12.59±0.02[c)]	18	0.80±0.05
$Al(Cit)_{(aq)}$	10.16±0.01	18	0.66±0.04
Al(*Cit*)OH	6.41±0.01	16	0.46±0.03
$Al(Cit)_2$	14.77±0.02	18	0.80±0.05
$Al_3(Cit)_3(OH)_4$	18.21±0.06	34	1.13±0.08

[a)] $\log\beta_{pqr}$ refers to of eq. (6.1); [b)] eq. (4.27); [c)]±Std. Deviation.

Using the dependence parameter values on ionic strength of eq. (4.27), the stability constant of the $Al(Cit)_{(aq)}$ species was recalculated at Ohman experimental condition, I = 0.60 mol L^{-1}. The calculated value is $\log\beta_{110}$ = 7.32 against $\log\beta_{110}$ = 7.15 reported by the author.
The analysis of the stability constants at different T and I = 0.249 mol L^{-1} in $NaCl_{(aq)}$, showed that all the reactions are endothermic, and the entropic contribution can be considered the driving force for the stability of the complexes.

Table 6.4. Dependence parameter on temperature of the stability constants of Al^{3+}/Cit^{3-} complexes at I = 0.249 mol L^{-1} in $NaCl_{(aq)}$ and T = 298.15 K

	Al(*Cit*)H	$Al(Cit)_{(aq)}$	Al(*Cit*)OH	$Al(Cit)_2$	$Al_3(Cit)_3(OH)_4$
$\Delta H^{a), b)}$	18.1±4.0[c)]	30.7±2.8	86.6±5.4	65.7±3.0	414.8±3.9
$\Delta G^{a), d)}$	-55.8±0.3	-42.8±0.3	-20.3±0.4	-68.7±0.3	-65.9±0.3
$T\Delta S^{a), e)}$	73.9±4.0	73.5±2.8	106.9±5.4	134.4±3.0	480.7±3.9

[a)] in kJ mol^{-1}; [b)] eq. (4.28); [c)] ±Std. Deviation; [d)] eq. (4.30); [e)] eq. (4.31).

Chapter 7

Al^{3+} / Orthosilicic acid system

7.1. Study of $Al^{3+}/(H_2SiO_4)^{2-}$ interactions

The $Al^{3+}/(H_2SiO_4)^{2-}$ interactions were studied in NaCl aqueous solutions at I = 0.10 and 1.00 mol L^{-1} at T = 298.15±0.15 K, by potentiometric measurements at different concentrations of Al^{3+} ($0.0005 \leq c_{Al^{3+}}$ / mol $L^{-1} \leq 0.0009$) and ligand ($0.0018 \leq c_{H_2SiO_4^{2-}}$/ mol $L^{-1} \leq 0.003$).

The acid – base behavior of the orthosilicic acid was previously investigated in $NaCl_{(aq)}$ at different ionic strengths and at T = 298.15 K was already known,[140] and the values, at the same ionic strengths of the metal – ligand interactions, are reported in Table 7.1.

Table 7.1. Protonation constants[a)] of orthosilicic acid at different ionic strengths in $NaCl_{(aq)}$ and at T = 298.15 K

I / mol L^{-1}	$\log\beta_1^H$	$\log\beta_2^H$ ($\log K_2^H$)
0.139	12.86	22.45 (9.59)[b)]
1.018	12.63	22.08 (9.45)

[a)] $\log \beta_r^H$ refers eq. (4.16); [b)] $\log K_r^H$ refers to eq. (4.15).

As regards the hydrolysis of the metal cation, as already written in the previous chapters, several data are reported in the literature.[138-140]

The potentiometric data, carried out in the pH range 2.0 - 4.5, were analyzed by the computer programs BSTAC and STACO. The stability constants of only one complex species, the protonated $[AlH(H_2SiO_4)]^{2+}$ was possible to refine.

The overall and stepwise stability constants of the $[AlH(H_2SiO_4)]^{2+}$ species at different ionic strengths in $NaCl_{(aq)}$ are reported in Table 7.2, according to the following equilibria:

$$Al^{3+} + H(H_2SiO_4)^- = [AlH(H_2SiO_4)]^{2+} \qquad K_{111} \qquad (7.1)$$

and

$$Al^{3+} + (H_2SiO_4)^{2-} + H^+ = [AlH(H_2SiO_4)]^{2+} \qquad \beta_{111} \qquad (7.2)$$

Table 7.2. Overall[a] and stepwise[b] formation constants of the complex $[AlH(H_2SiO_4)]^{2+}$ at two different ionic strengths in $NaCl_{(aq)}$ and at T = 298.15 K

I / mol L^{-1}	$\log\beta_{111}$	$\log K_{111}$
0.139	20.39±0.05[c]	7.43
1.018	19.22±0.13	6.58

[a] $\log\beta_{111}$ refers to equilibrium (eq. 7.2); [b] $\log K_{111}$ refers to equilibrium (eq. 7.1);[c] ± Std. deviation.

The formation constant values for the species decreases by increasing the ionic strength.

In Figure 7.1, the speciation diagram at the two different ionic strength values, reported in Figure 7.1, it is possible to note that at I = 0.139 mol L^{-1}, $[AlH(H_2SiO_4)]^{2+}$species does not exceed a percentage of 18% at pH ~ 4. In correspondence of this pH value, the precipitation of the $Al(OH)_{3(s)}$ species occurs, but it was not observed experimentally: it was due to its slow kinetics.[141]

At I = 1.018 mol L^{-1}, the formation of $[AlH(H_2SiO_4)]^{2+}$ species reaches less than 10% at pH ~ 4.3 and meanwhile the sparingly soluble species starts to precipitate. In both experimental conditions of ionic strength the low formation percentage of the protonated species is due to the fact that the ligand is still protonated in the pH range of the measurements and at pH ~ 4.1 the formation of the sparingly soluble $Al(OH)_{3(s)}$ started, corresponding to the shaded zone in Figure 7.1, avoiding the possibility to investigate higher pH range.

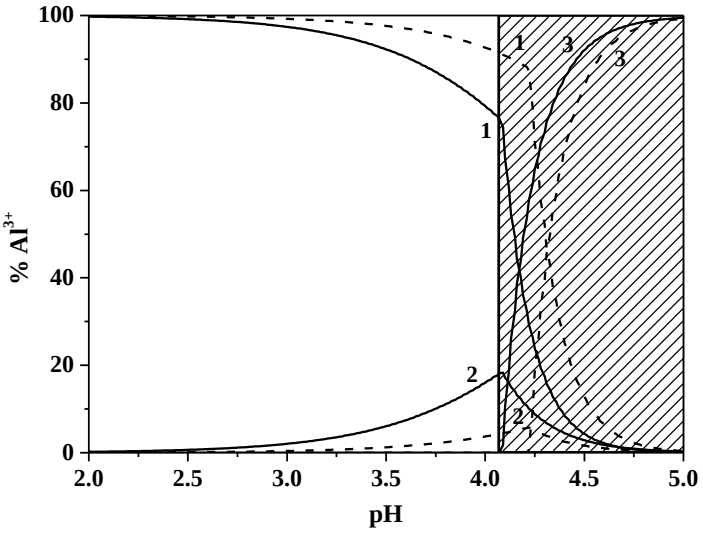

Figure 7.1.Speciation diagram of $Al^{3+}/H_2SiO_4^{2-}$ system in $NaCl_{(aq)}$ at T = 298.15 K and I = 0.139 mol L^{-1} (solid lines) and I = 1.018 mol L^{-1} (dashed lines).

Concentrations: $c_{Al^{3+}}$ = 0.0008 mol L^{-1}, $c_{H_2SiO_4^{2-}}$= 0.003 mol L^{-1}.

Species: 1. free Al^{3+}; 2. $AlH(H_2SiO_4)$; 3. $Al(OH)_{3(s)}$.

Spadini et al.[148] reported the results of some potentiometric studies carried out at T = 298.15 K and I = 0.60 mol L^{-1} in $NaCl_{(aq)}$ at different concentration ratios of ligand ($0.0003 \leq c_{H_2SiO_4^{2-}}$ / mol $L^{-1} \leq 0.0025$) and metal cation ($0.0005 \leq c_{Al^{3+}}$ / mol $L^{-1} \leq 0.0026$), in the pH range 2.0 - 4.2.

The author determined, at that experimental conditions, the formation of the $[AlH(H_2SiO_4)]^{2+}$ species with $\log K_{111}$ = 6.72, which follows the trend of the formation constant values reported in the present thesis, obtained in the same conditions of temperature and ionic medium but at different ionic strengths (0.139, 1.018 mol L^{-1}), as evidenced in Figure 7.2.

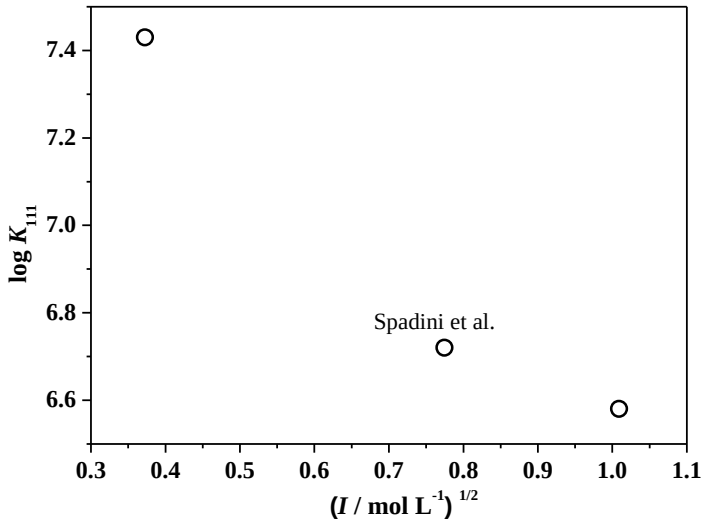

Figure 7.2. Experimental logK_{111} values and Spadini data[148] *vs.* (I / mol L^{-1})$^{1/2}$

7.2. Dependence on ionic strength of the stability constants

The dependence on ionic strength of the formation constant of the protonated species $[AlH(H_2SiO_4)]^{2+}$ species was modeled by a Debye-Hückel type equation (eq. 4.27), neglecting the contribution of the terms D $I^{3/2}$ and E I^2. The analysis of the experimental data at different ionic strengths by LIANA computer program allowed the simultaneous refinement of both the stability constants of the species at infinite dilution ($\log^T\beta$) and the empirical parameter C for the dependence on ionic strength. The values are reported in Table 7.3.

Table 7.3. Stability constant of $[AlH(H_2SiO_4)]^{2+}$species at infinite dilution and empirical parameter for dependence on ionic strength in $NaCl_{(aq)}$, according to eq. (4.27)

Species	$\log^T\beta_{111}$ [a)]	z^*	C
$[AlH(H_2SiO_4)]^{2+}$	21.52±0.06[b)]	10	-0.11±0.15[b)]

[a)] $\log^T\beta_{111}$ refers to eq. (7.2); [b)] ± Std. Deviation.

Using the dependence parameter values on ionic strength of eq. (4.27), the stability constant of the $[AlH(H_2SiO_4)]^{2+}$ species was recalculated at Spadini experimental condition, I = 0.60 mol L^{-1}. The calculated value is logK_{111} = 6.92 against logK_{111} = 6.72 reported by the author.

Chapter 8

Synthesis of 3-Hydroxy-4-Pyridinones

8.1. General Information

The synthesis and characterization of 3-hydroxy-4-pyridinones was performed during a period of six months of research abroad under the supervision of Prof. Maria Amélia Santos, at the Centro de Química Estrutural of the Instituto Superior Técnico (Universidade de Lisboa).

All the reagents used for the synthesis were of the highest available purity and were all purchased from Sigma-Aldrich and its various brands. The solvents, if necessary, were dried according to standard methods.[149]

The reactions were TLC controlled and the most common used mobile phases were: S1 (Dichloromethane (DCM)-MeOH 9.5:0.5), S2 (DCM-MeOH-NH_4OH 8.5:1:0.5), S3 (DCM-MeOH-NH_4OH 8:2:0.5), S4 (DCM-MeOH-NH_4OH 7:3:0.5) solvents mixtures. Moreover, ferric chloride (for checking the presence of -OH groups), ninhydrine (for amino groups) and Dragensdorf (if quaternary nitrogen groups were present) assays were carried out. The measurement of the melting points of each compound was realized using a Leica Galen III hot stage apparatus and are uncorrected.

^{1}H and ^{13}C NMR experiments were performed in deuterated solvents (D_2O, Methanol-d_4, DMSO-d_6), whose peaks in the spectra were assigned according to the literature data.[150] Bruker AVANCE III 300MHz and Bruker AVANCE III 400 MHz spectrometers were used

for all NMR measurements. IR spectra were carried out on a Bruker, Vertex 700 spectrometer.

The schemes of the reactions of synthesis of the compounds are reported in Paragraph 8.2.

8.2. Schemes of reactions

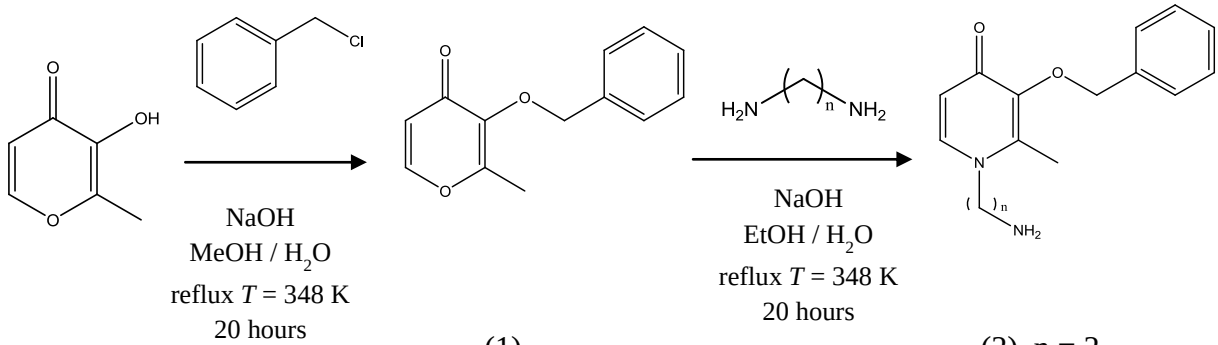

(1) (2) n = 2 (3) n = 3

Figure 8.1. Synthesis of protected maltol (1) and of the protected 3,4-hydroxypyridinones, with ethyl (n = 2) and propyl (n = 3) alkyl chain.

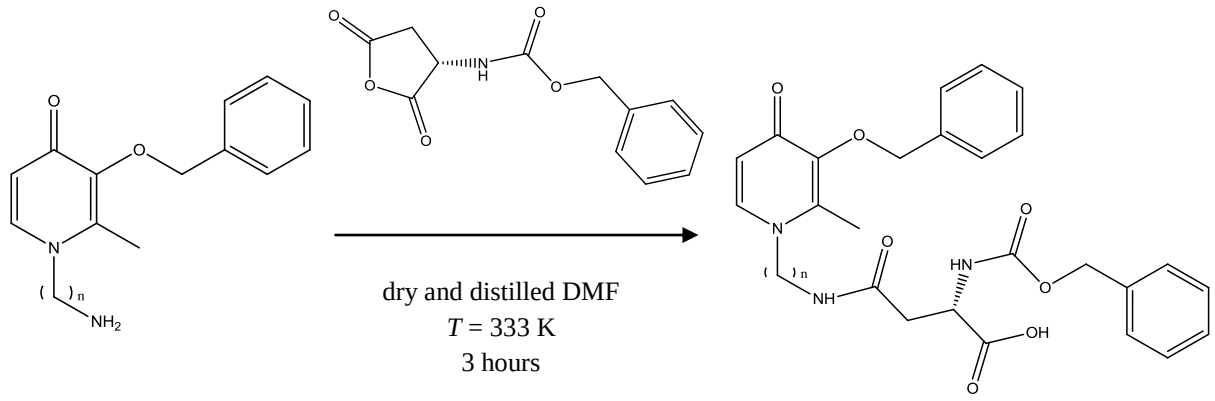

(2), (3)

(4) n = 2
(6) n = 3

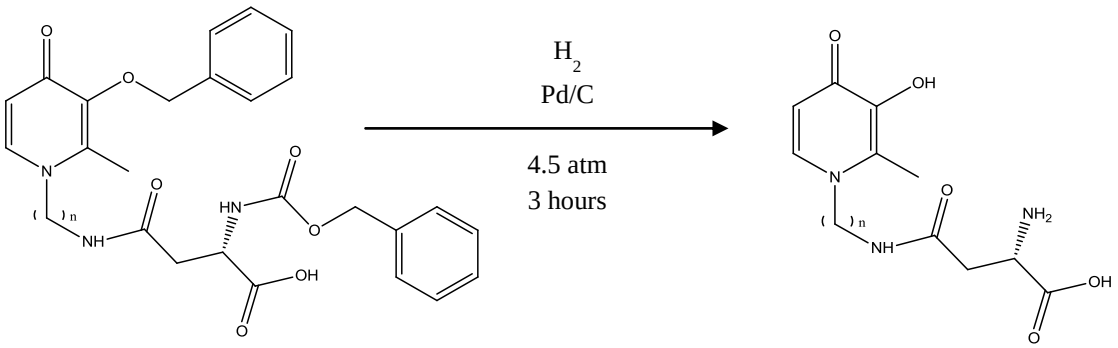

(4) n = 2
(6) n = 3

(5) n = 2
(7) n = 3

Figure 8.2. Synthesis of N-Z-L-aspartic anhydride derivatives (5, 7 products) and catalytic hydrogenation to remove the protecting groups.

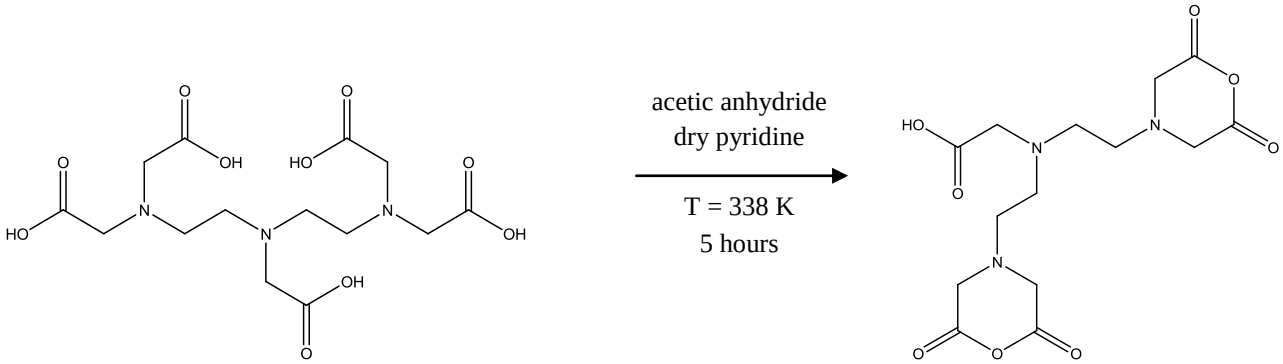

Figure 8.3. Synthesis of DTPA bisanhydride from DTPA.[151]

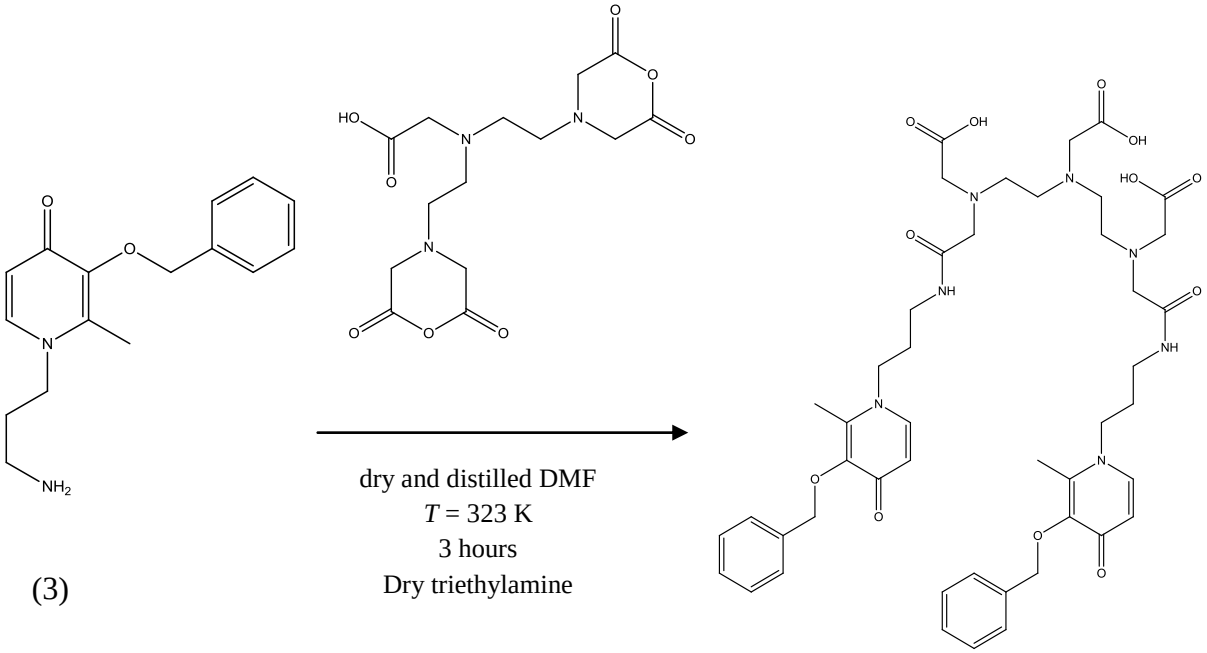

(3)

(8)

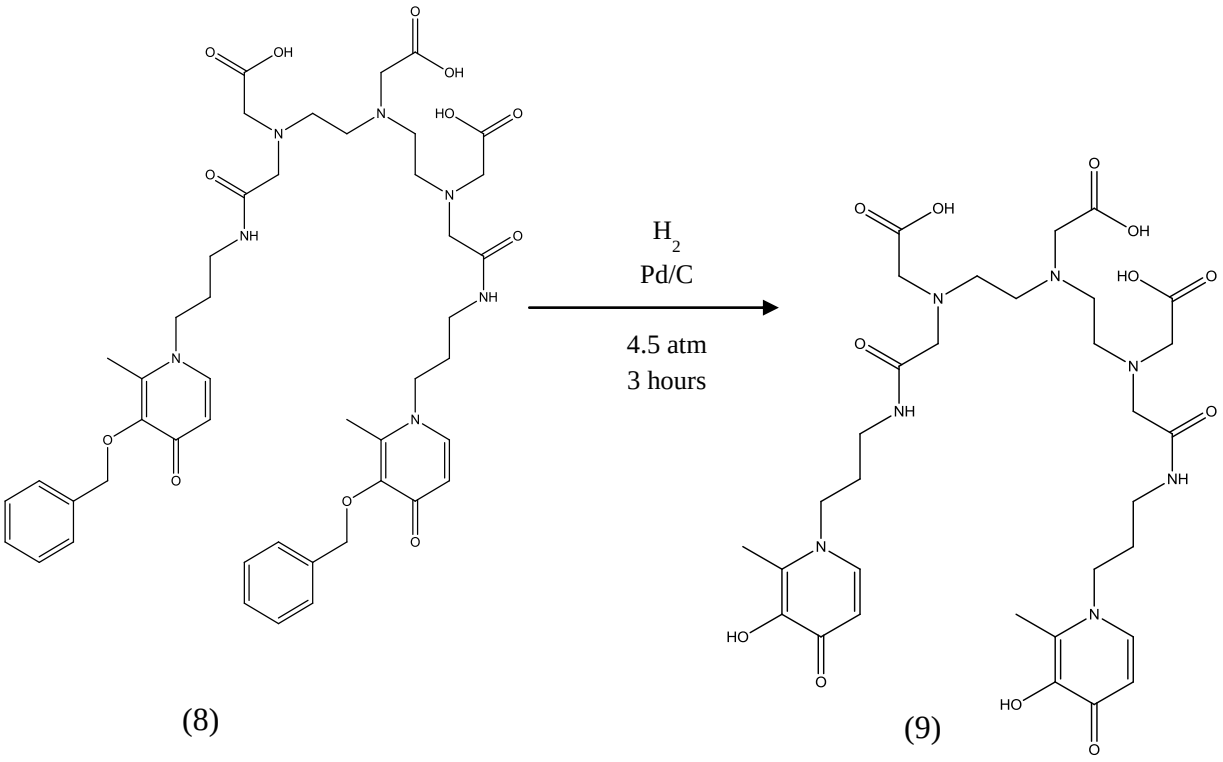

(8) (9)

Figure 8.4. Synthesis of 3-hydroxy-4-pyridinone - DTPA derivative and hydrogenation to eliminate the protecting groups.

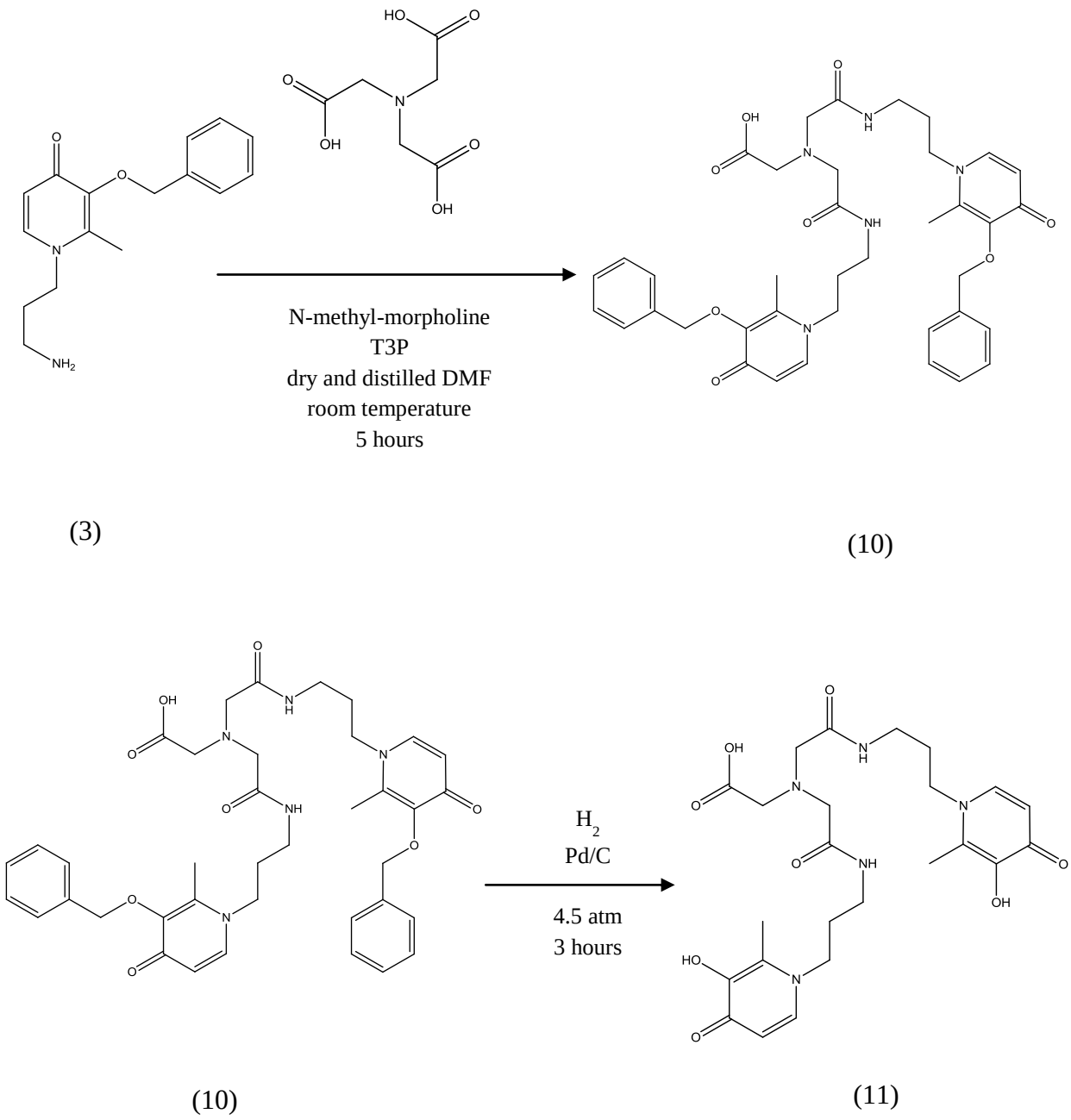

Figure 8.5. Synthesis of 3-hydroxy-4-pyridinone - NTA derivative through the T3P catalyzed method of coupling.

8.3. Synthesis of protected 3,4-Hydroxypyridinones

3-benzyloxy-2-methyl-4-pyrone (1)

3-Hydroxy-2-methyl-4-pyrone (20.07 g, 159.15 mmol) was dissolved in 200 mL of methanol and ca. 10% more of the equivalent amount of sodium hydroxide (6.98 g, 174.50 mmol) in 22 mL of water was added to this mixture, followed, dropwise, by benzyl chloride (16.50 mL, 142.75 mol), according to the mechanism reported in Figure 2.15. The reaction mixture was heated to reflux at T = 348 K for 20 hours. The solvent was evaporated under reduced pressure and the remaining orange oil was dissolved in dichloromethane (80 mL) and washed with 5% (w/v) of NaOH aqueous solution (3 x 30 mL) and with water (2 x 30 mL). The organic phase was dried over anhydrous sodium sulfate and filtered. The solvent was evaporated by using a rotavapor and dried in vacuum to give a pale yellow oil product (32.93 g, η = 95%). TLCs were performed in S1 mixture. ^{1}H NMR (400 MHz, Methanol-d_4), δ(ppm): 7.82 (1H, d, J = 8 Hz, 6-**H**Py), 7.33 (5H, s, Ph), 6.35 (1H, d, J = 8 Hz, 5-**H**Py), 5.03 (2H, s, C**H$_2$**Ph), 2.05 (3H, s, C**H$_3$**). ^{13}C NMR (400 MHz, Methanol-d_4), δ(ppm): 175.81, 160.98, 155.05, 143.49, 136.81, 128.76, 128.19, 128.18, 116.22, 73.37, 13.67. *m/z* (ESI-MS) = 217 (M+1).

3'-(aminoethyl)-3-benzyloxy-2-methyl-4-pyridinone (2)

3-benzyloxy-2-methyl-4-pyrone (20.18 g, 93.35 mol) was dissolved in a EtOH/H_2O mixture (6/8 mL) and added dropwise to a mixture constituted by ethylenediamine (6.90 mL, 102.66 mol) in 37 mL of ethanol and 24 mL of water and 8.5 mL of a NaOH aqueous solution (c_{NaOH} = 2 mol L^{-1}). This reaction mixture was left under reflux at T = 348 K for 20 hours. After cooling, 2 M HCl aqueous solution was added until pH ~ 1 and the ethanol was evaporated. To the remaining solution, water was added (50 mL) and an extraction with diethyl ether (4 x 50 mL) followed. The aqueous phase was alkalinized with 10 M NaOH aqueous solution until about pH ~ 12 and extracted with dichloromethane (3 x 50 mL). The organic phase was dried over anhydrous sodium sulfate and filtered and the solvent evaporated to dryness. To this dried residue, 3 mL of EtOH were added and the solution was acidified until pH ~ 2 with HCl-saturated EtOH that gave a white precipitate that was recrystallized from ethanol-acetonitrile to give a pure product as the corresponding hydrochloride salt (4.40 g, η = 16%). TLCs in S2 mixture, R_f = 0.74. m. p. 460 - 463 K. ^{1}H NMR (400 MHz, D_2O), δ(ppm): 8.12 (1H, d, J = 8 Hz, 6-**H**Py), 7.39 (5H, s, Ph), 7.10 (1H, d, J = 8 Hz, 5-**H**Py), 5.07 (2H, s,

C**H$_2$**Ph), 4.51 (2H, t, *J* = 8 Hz, C**H$_2$**NPy), 3.34 (2H, t, *J* = 8 Hz, C**H$_2$**NH$_2$), 2.36 (3H, s, C**H$_3$**). ^{13}C NMR (400 MHz, D_2O), δ(ppm): 166.39, 150.03, 143.29, 142.28, 135.21, 129.62, 129.26, 128.84, 114.09, 75.39, 52.37, 38.00, 12.91. *m/z* (ESI-MS) = 259 (M+1).

3'-(aminopropyl)-3-benzyloxy-2-methyl-4-pyridinone (3)

A solution of **1** (10.41 g, 48.16 mol) in a ethanol/water mixture (6/4 mL) was added drop by drop to a solution of 1,3-diaminopropane (4.50 mL, 52.97 mmol) in a 17 mL of EtOH, 13 mL of H_2O and NaOH aqueous solution (c_{NaOH}= 2 mol L^{-1}). The reaction mixture was left on stirring under reflux at *T* = 348 K for 20 hours, according to the reaction reported in Figure 2.16. The experimental procedure followed for the workup was the same reported for the 3'-(aminoethyl)-3-benzyloxy-2-methyl-4-pyridinone (**2**). The recrystallization of the white precipitate with ethanol-acetonitrile gave the product in the form of hydrochloride salt (2.66 g, η = 18%). TLC control of the reaction was carried out using S2 mixture, R_f = 0.45. m.p. 463 – 466 K.^{1}H NMR (400 MHz, D_2O), δ(ppm): 8.13 (1H, d, *J* = 8 Hz, 6-**H**Py), 7.38 (5H, s, Ph), 7.11 (1H, d, *J* = 8 Hz, 5-**H**Py), 5.08 (2H, s, C**H$_2$**Ph), 4.28 (2H, t, *J* = 8 Hz, C**H$_2$**NPy), 2.99 (2H, t, *J* = 8 Hz, C**H$_2$**NH$_2$), 2.34 (3H, s, C**H$_3$**), 2.09 (2H, m, CH$_2$C**H$_2$**NH$_2$). ^{13}C NMR (400 MHz, D_2O), δ(ppm): 164.96, 150.10, 142.97, 141.92, 135.19, 129.69, 129.27, 128.82, 113.56, 75.43, 53.21, 36.21, 27.28, 12.90. *m/z* (ESI-MS) = 273 (M+1).

8.4 Coupling with N-Z-L-aspartic anhydride

(S)-4-((2-(3-(benzyloxy)-2-methyl-4-oxopyridin-1(4H)-yl)ethyl)amino)-2-(((benzyloxy) carbonyl)amino)-4-oxobutanoic acid (4)

3'-(aminoethyl)-3-benzyloxy-2-methyl-4-pyridinone (0.76 g, 2.59 mmol), in the form of hydrochloride salt, was neutralized with potassium hydroxide (0.22 g, 3.92 mmol) in 10 mL of dry MeOHon stirring under nitrogen for 15 hours. After filtering this solution to remove the white precipitate of KCl and evaporating the solvent under vacuum, 10 mL of N-dimethylformamide (DMF), dried with molecular sieves and distilled, were added to the flask. Meanwhile, N-Z-L-aspartic anhydride (0.78 g, 3.13 mmol), was dissolved in 5 mL of dried and distilled DMF and added dropwise to the neutralized and protected 3,4-hydroxypyridinone, according to the first step of the reaction reported in Figure 8.2. The mixture was left at *T* = 333 K on stirring and under nitrogen. After 3 hours, the starting materials were completely consumed and only one major product was formed. The solvent was evaporated under vacuum at ca. *T* = 363 K and the solid product (0.57g, η = 44%) was

obtained after recrystallization with methanol-diethyl ether and its filtration. S3 mixture was used like eluent for TLC control of the reaction, R_f = 0.30. m. p. 370 – 372 K. ^{1}H NMR (400 MHz, Methanol-d_4), δ(ppm): 7.94 (1H, d, *J* = 8 Hz, 6-**H**Py), 7.46 (5H, s, $Ph_{protected\ aspartic\ anhydride}$), 7.37 (5H, s, Ph), 6.91 (1H, d, *J* = 8 Hz, 5-**H**Py), 5.13 (2H, s, C$\mathbf{H_2}Ph_{protected\ aspartic\ anhydride}$), 5.11 (2H, s, C$\mathbf{H_2}$Ph), 4.56 (1H, t, *J* = 4 Hz, C**H**NH), 4.31 (2H, t, *J* = 8 Hz, C$\mathbf{H_2}$NPy), 3.52 (2H, d, *J* = 8 Hz, C$\mathbf{H_2}$CHNH), 2.77 (2H, t, *J* = 8 Hz, C$\mathbf{H_2}$NHCO), 2.42 (3H, s, C$\mathbf{H_3}$). ^{13}C NMR (400 MHz, Methanol-d_4), δ(ppm): 172.47, 172.24, 171.26, 168.48, 156.93, 147.97, 147.31, 144.91, 136.45, 128.71, 128.66, 128.23, 128.10, 127.65, 127.49, 113.88, 74.13, 65.85, 54.09, 51.55, 38.36, 35.96, 12.01. *m/z* (ESI-MS) = 508 (M+1).

(S)-2-amino-4-((2-(3-hydroxy-2-methyl-4-oxopyridin-1(4H)-yl)ethyl)amino)-4-oxobutanoic acid (5)

To a solution of **4** (0.60 g, 1.18 mmol) in 50 mL of dry methanol, 10% Pd/C (0.13 g, 1.20 mmol) was added and the mixture was stirred under hydrogen (4.5 atm) for 3 hours at room temperature, following the second step of the reaction in Figure 8.2. After the filtration of the reaction mixture and the evaporation of the solvent under reduced pressure, the solid product (0.20 g, η = 52%) was obtained through a recrystallization with MeOH-Et_2O. TLCs were performed using S3 mixture as mobile phase, R_f = 0.38. m.p. 390 – 393 K.^{1}H NMR (400 Hz, D_2O), δ(ppm): 7.66 (1H, d, *J* = 8 Hz, 6-**H**Py), 6.69 (1H, d, *J* = 8 Hz, 5-**H**Py), 4.60 (1H, t, *J* = 4 Hz, C**H**NH), 4.29 (2H, t, *J* = 8 Hz, C$\mathbf{H_2}$NPy), 3.86 (2H, t, C$\mathbf{H_2}$CHNH), 2.68 (2H, t, *J* = 8 Hz, C$\mathbf{H_2}$NHCO), 2.47 (3H, s, C$\mathbf{H_3}$). ^{13}C NMR (400 MHz, D_2O), δ(ppm): 174.56, 172.65, 171.47, 169.59, 164.25, 143.25, 139.26, 111.54, 54.36, 51.32, 38.15), 35.05, 11.08. *m/z* (ESI-MS) = 328 (M+1).

(S)-4-((3-(3-(benzyloxy)-2-methyl-4-oxopyridin-1(4H)-yl)propyl)amino)-2-(((benzyloxy) carbonyl)amino)-4-oxobutanoic acid (6)

For the neutralization of compound **3** (1.00 g, 3.24 mmol) as hydrochloride salt, with KOH (0.25 g, 4.45 mmol) in 20 mL of dry MeOH, the same procedure than the compound **2** was followed. N-Z-L-aspartic anhydride (0.98 g, 3.93 mmol) dissolved in 5 mL of dry and distilled DMF was added drop by drop to the neutralized 3'-(aminopropyl)-3-benzyloxy-2-methyl-4-pyridinone in 10 mL of the same solvent, according to the first step of the reaction reported in Figure 8.2. The mixture was left at *T* = 333 K on stirring and under nitrogen. After 3 hours the DMF was evaporated under vacuum at about *T* = 366 K and with the

recrystallization with methanol-diethyl ether it was possible to obtain the desired product (0.27 g, η = 16%). The eluent used for the TLC control of the reaction was S3 mixture, R_f = 0.45. m.p. 378 – 381 K.^{1}H NMR (400 MHz, Methanol-d_4), δ(ppm): 8.05 (1H, d, *J* = 8 Hz, 6-**H**Py), 7.37 (5H, s, $Ph_{protected\ aspartic\ anhydride}$), 7.33 (5H, s, Ph), 7.27 (1H, d, *J* = 8 Hz, 5-**H**Py), 5.16 (2H, s, C**H$_2$**$Ph_{protected\ aspartic\ anhydride}$), 5.12 (2H, s, C**H$_2$**Ph), 4.63 (1H, t, *J* = 8 Hz, C**H**NH), 4.12 (2H, t, *J* = 8 Hz, C**H$_2$**NPy), 3.21 (2H, d, *J* = 8 Hz, C**H$_2$**CHNH), 2.81 (2H, t, *J* = 8 Hz, C**H$_2$**NHCO), 2,34 (3H, s, C**H$_3$**), 1.97 (2H, m, CH_2C**H$_2$**NH_2). ^{13}C NMR (400 MHz, Methanol-d_4), δ(ppm): 172.97, 172.27, 167.93, 157.02, 147.46, 144.37, 140.90, 136.72, 136.19, 128.81, 128.35, 128.21, 128.07, 127.64, 127.38, 113.93, 74.18, 66.6, 53.20, 51.92, 37.60, 35.38, 29.80, 11.85. *m/z* (ESI-MS) = 522 (M+1).

(S)-2-amino-4-((3-(3-hydroxy-2-methyl-4-oxopyridin-1(4H)-yl)propyl)amino)-4-oxobutanoic acid (7)

To a solution of **6** (0.22 g, 0.42 mmol) in 50 mL of dry methanol, 10% Pd/C (0.06 g, 0.53 mmol) was added and the mixture was stirred under H_2 (4.5 atm) for 3 hours at room temperature. After filtrating the reaction mixture and evaporating the methanol under reduced pressure, the solid product (0.10 g, η = 70%) was obtained through a recrystallization with MeOH-Et_2O. TLCs in mobile phase S3 mixture, R_f = 0.35. m.p. 400 – 403 K. ^{1}H NMR (400 MHz, Methanol-d_4), δ(ppm): ^{1}H NMR (400 MHz, D_2O), δ(ppm): 7.78 (1H, d, *J* = 8 Hz, 5-**H**Py), 6.72 (1H, d, *J* = 8 Hz, 6-**H**Py), 4.15 (1H, t, *J* = 8 Hz, C**H**NH), 3.95 (2H, t, *J* = 8 Hz, C**H$_2$**NPy), 3.23 (2H, t, *J* = 8 Hz, C**H$_2$**CHNH), 2.78 (2H, t, *J* = 8 Hz, C**H$_2$**NHCO), 2,45 (3H, s, C**H$_3$**), 1.97 (2H, m, CH_2C**H$_2$**NH_2). ^{13}C NMR (400 MHz, D_2O), δ(ppm): 175.02, 172.92, 169.38, 165.15, 143.76, 139.79, 138.59, 137.80, 53.00, 48.90, 36.73, 35.09, 29.13, 11.78. *m/z* (ESI-MS) = 342 (M+1).

8.5. Coupling with DTPA bisanhydride

Diethylenetriaminepentaacetic bisanhydride

DTPA bisanhydride was synthesized according to a method already described in literature.[151-153] The reaction reported in Figure 8.3, started from the corresponding carboxylic acid, in the presence of acetic anhydride, that is used as dehydrating agent and solvent and pyridine, which increases the rate of the reaction through association with the carboxylic acid functions of DTPA to form an acylpyridinium salt.[151]

Acetic anhydride (4.90 mL, 51.72 mmol) and dry pyridine (6.30 mL, 77.52 mmol) were added in a three necks flask to diethylenetriaminepentaacetic acid (5.08 g, 12.92 mmol) and the reaction mixture was left under nitrogen and on stirring at T = 338 K for 5 hours. The reaction mixture was filtered and the solid white product (3.46 g, η = 75%) was washed with acetic anhydride (3 x 10 mL) and with dry acetonitrile (3 x 10 mL) and dried at about T = 313 K. ^{1}H NMR (400 MHz, Methanol-d_4), δ (ppm): 3.98 (8H, s, C**H$_2$**COOCO), 3.70 (2H, s, C**H$_2$**COOH), 3.41 (4H, t, 2 x C**H$_2$**CH_2NCH_2COOH), 3.25 (4H, t, 2 x CH_2C**H$_2$**NCH_2COOH). FT-IR (KBr, Figure 8.6), wavenumber (cm^{-1}): 1820 (asymmetric C=O stretching anhydride), 1776 (symmetric C=O stretching anhydride), 1640 (C=O stretching carboxylic acid), 1332 (C-O stretching), 1112 (C-N stretching), 955 (O-H bending).

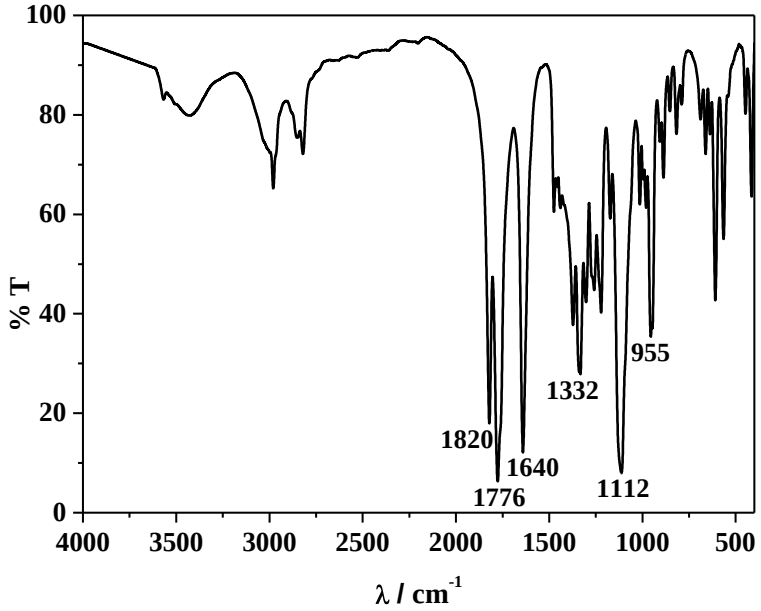

Figure 8.6. FT-IR spectrum of diethylenetriaminepentaacetic bisanhydride.

15-(3-(benzyloxy)-2-methyl-4-oxopyridin-1(4H)-yl)-3-(2-((3-(3-(benzyloxy)-2-methyl-4-oxopyridin-1(4H)-yl)propyl)amino)-2-oxoethyl)-6,9-bis(carboxymethyl)-11-oxo-3,6,9,12-tetraazapentadecan-1-oic acid (8)

3'-(aminopropyl)-3-benzyloxy-2-methyl-4-pyridinone (1.45 g, 4.68 mmol) as hydrochloride salt was neutralized with potassium hydroxide (0.40 g, 7.13 mmol) in 20 mL of dry methanol, on stirring under nitrogen for 15 hours. The white precipitate of potassium chloride formed was filtered, the solvent evaporated under vacuum and the mixture was dissolved in 10 mL of dry and distilled DMF. Meanwhile, diethylenetriaminepentaacetic bisanhydride (DTPA

bisanhydride, 0.67 g, 1.87 mmol) was dissolved in 20 mL of the same solvent and added dropwise to the reaction mixture, followed by triethylamine (TEA, 0.14 mL, 3.75 mmol), previously dried with KOH under nitrogen for 12 hours. The reaction mixture was stirred at *T* = 323 K and under N_2 and after 3 hours the solvent was evaporated under vacuum at about *T* = 363 K. Because of the use of an excess of compound **3** to favor the formation of the bis-3,4-hydroxypyridinone derivative, a little percentage of starting material remained in the reaction mixture and some preparative TLCs were performed to purify it, choosing as eluent S4 mixture, R_f = 0.35. After running this TLCs and scratched the areas in the silica related to the desired product, they were dissolved in MeOH and filtered, the solvent was evaporated and the pure product (0.38 g, η = 9%) obtained. The reaction scheme is reported in Figure 8.4. ^{1}H NMR (400 MHz, D_2O), δ(ppm): 7.65 (2H, d, *J* = 8 Hz, 2 x 6-**H**Py), 7.32 (10H, s, 2 x Ph), 6.50 (2H, d, *J* = 8 Hz, 2 x 5-**H**Py), 4.93 (4H, s, 2 x C**H$_2$**Ph), 3.89 (4H, t, *J* = 8 Hz, 2 x C**H$_2$**NPy), 3.60 (2H, s, *J* = 4 Hz, C**H$_2$**CONH), 3.41 (2H, s, C**H$_2$**$COOH_{centre}$), 3.29 (2H, s, C**H$_2$**$COOH_{side}$), 3.14 (4H, t, *J* = 8 Hz, 2 x NCH_2C**H$_2$**N), 3.10 (4H, t, *J* = 8 Hz, 2 x NC**H$_2$**CH_2N), 2.81 (4H, t, *J* = 8 Hz, 2 x C**H$_2$**NH), 1.96 (6H, s, 2 x C**H$_3$**), 1.76 (4H, m, 2 x CH_2C**H$_2$**CH_2). ^{13}C NMR (400 MHz, D_2O), δ(ppm): 177.75, 177.65, 172.91, 171.48, 145.43, 144.70, 140.70, 135.73, 130.08, 129.39, 128.49, 115.99, 73.90, 57.54, 56.90, 52.03, 36.28, 36.16, 29.41, 29.23, 16.90, 12.01. *m/z* (ESI-MS) = 902 (M+1).

6,9-bis(carboxymethyl)-15-(3-hydroxy-2-methyl-4-oxopyridin-1(4H)-yl)-3-(2-((3-(3-hydroxy-2-methyl-4-oxopyridin-1(4H)-yl)propyl)amino)-2-oxoethyl)-11-oxo-3,6,9,12-tetraazapentadecan-1-oic acid (9)

To a solution of **8** (0.38 g, 0.42 mmol) in 50 mL of dry methanol, 10% Pd/C (0.09 g, 0.84 mmol) was added and the mixture was stirred under hydrogen (4.5 atm) for 3 hours at room temperature. The reaction mixture was filtered, the methanol was evaporated under reduced pressure and the solid product (0.18 g, η = 59%) dried very well. The eluent used for TLC control of the reaction was S4 mixture, R_f = 0.20. m.p. 461 – 463 K**.** ^{1}H NMR (400 MHz, D_2O), δ(ppm): 7.66 (2H, d, *J* = 8 Hz, 2 x 6-**H**Py), 6.51 (2H, d, *J* = 8 Hz, 2 x 5-**H**Py), 4.09 (4H, t, *J* = 8 Hz, 2 x C**H$_2$**NPy), 3.48 (2H, s, C**H$_2$**CONH), 3.36 (2H, s, C**H$_2$**$COOH_{centre}$), 3.33 (2H, s, C**H$_2$**$COOH_{side}$), 3.27 (4H, t, *J* = 8 Hz, 2 x NCH_2C**H$_2$**N), 3.25 (4H, t, *J* = 8 Hz, 2 x NC**H$_2$**CH_2N), 3.18 (4H, t, *J* = 8 Hz, 2 x C**H$_2$**NH), 2.39 (6H, s, 2 x C**H$_3$**), 1.96 (4H, m, 2 x CH_2C**H$_2$**CH_2). ^{13}C NMR (400 MHz, D_2O), δ(ppm): 177.97, 177.66, 171.85, 168.47, 138.13, 134.36, 112.56, 112.23, 52.41, 52.22, 48.91, 36.49, 36.41, 29.62, 28.95, 28.15, 11.52. *m/z* (ESI-MS) = 722 (M+1).

8.6. T3P-catalyzed coupling with nitrilotriacetic acid (NTA)

15-(3-(benzyloxy)-2-methyl-4-oxopyridin-1(4H)-yl)-3-(2-((3-(3-(benzyloxy)-2-methyl-4-oxopyridin-1(4H)-yl)propyl)amino)-2-oxoethyl)-6,9-bis(carboxymethyl)-11-oxo-3,6,9,12-tetraazapentadecan-1-oic acid (10)

To a mixture of nitrilotriacetic acid (NTA) (0.35 g, 1.83 mmol) dissolved in 25 mL of dried and distilled DCM, *N*-methylmorpholine (NMM, 0.80 mL, 7.32 mmol) was added under nitrogen. Few minutes later, when the reaction mixture became a clear solution, n-propylphosphonic anhydride (T3P, 1.20 mL, 4.02 mmol) was added dropwise under nitrogen and the reaction was stirred for 30 minutes. Product **3** (0.56 g, 1.83 mmol) as hydrochloride salt which has been neutralized with potassium hydroxide (0.12 g, 2.20 mmol) in 20 mL of dry methanol, on stirring under nitrogen for 15 hours, was filtered to remove the precipitate of KCl. The solvent was evaporated under vacuum, the mixture dissolved and added in dry DCM and added to the NTA clear solution under nitrogen atmosphere. The reaction was stirred at room temperature for 5 hours and the course of the reaction was monitored by TLC, by using S3 mixture. DCM layer was washed with brine solution and the reaction mixture was purified through column chromatography over silica in 9-10 % MeOH-DCM system to give the desired compound **10** (0.88 g, η = 69%). m. p. 351 – 355 K. ^{1}H NMR (400 MHz, Methanol-d_4), δ (ppm): 7.73 (2H, d, *J* = 8 Hz, 2 x 6-**H**Py), 7.30-7.38 (10H, m, 2 x Ph), 6.46 (2H, d, 8 Hz, 2 x 5-**H**Py), 5.05 (4H, s, 2 x C**H$_2$**Ph), 3.99 (4H, t, *J* = 8 Hz, 2 x C**H$_2$**N), 3.43 (2H, s, C**H$_2$**COOH), 3.29 (4H, s, 2 x NC**H$_2$**CO), 3.23 (4H, t, *J* = 8 Hz, 2 x C**H$_2$**NH), 2.16 (6H, s, 2 x C**H$_3$**), 1.86 (4H, t, *J* = 8 Hz, 2 x CH_2C**H$_2$**CH_2).^{13}C NMR (400 MHz, Methanol-d_4), δ (ppm): 177.56, 173.41, 172.71, 145.70, 143.59, 139.95, 137.04, 128.88, 128.02, 116.04, 73.07, 59.68, 51.61, 35.60, 30.00,11.40. *m/z* (ESI-MS) = 699 (M - H).

6,9-bis(carboxymethyl)-15-(3-hydroxy-2-methyl-4-oxopyridin-1(4H)-yl)-3-(2-((3-(3-hydroxy-2-methyl-4-oxopyridin-1(4H)-yl)propyl)amino)-2-oxoethyl)-11-oxo-3,6,9,12 tetraazapentadecan-1-oic acid (11)

In a hydrogenation flask, the product **10** (0.70 g, 1 mmol) was dissolved in methanol and 10% Pd/C was added (0.21 g, 2 mmol) and stirred under hydrogen (4.5 atm) for 3 hours at room temperature. The reaction mixture was filtered, the methanol was evaporated under reduced pressure and the solid product (0.49 g, η = 95%) dried. m. p. 368 – 370 K. ^{1}H NMR (400 MHz, Methanol-d_4), δ (ppm): 7.57 (2H, d, *J* = 8 Hz, 2 x 6-**H**Py), 6.30 (2H, d, *J* = 8 Hz, 2 x 5-**H**Py), 3.99 (4H, t, *J* = 8 Hz, 2 x C**H$_2$**N), 3.30 (2H, s, C**H$_2$**COOH), 3.18-321 (8H, m, 2 x C**H$_2$**NH and 2 x NC**H$_2$**CO), 2.31 (6H, s, 2 x C**H$_3$**HPy), 1.86 (4H, t, *J* = 8 Hz, 2 x

$CH_2C\mathbf{H_2}CH_2$). ^{13}C NMR (400 MHz, DMSO-d_6), δ (ppm): 173.70, 171.22, 169.29, 145.99, 138.07, 129.05, 111.09, 58.70, 56.40, 51.10, 35.88, 30.70, 11.70. *m/z* (ESI-MS) = 520 (M +1).

Chapter 9

Protonations of 3-Hydroxy-4-Pyridinones

Before studying and analyzing the different M^{n+}/3-hydroxy-4-pyridinone systems it was necessary to investigate the acid-base behavior of these ligands in solution. Protonation constants of all the ligands and other four compounds synthesized[154,155] by the group of Prof. M. Amélia Santos were determined by UV - Vis spectrophotometric and spectrofluorimetric measurements. The structures of the ligands are reported in Figure 9.1.

Monosubstituted 3-hydroxy-4-pyridinones

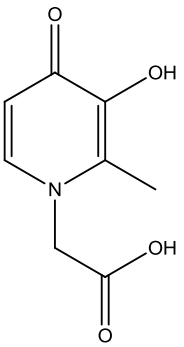

2-(3-hydroxy-2-methyl-4-oxopyridin-1(4H)-yl)acetic acid

(KC)

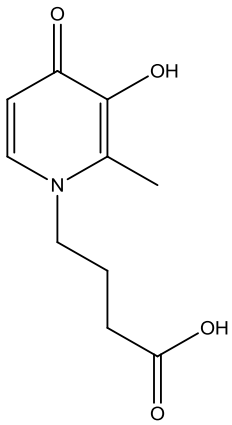

4-(3-hydroxy-2-methyl-4-oxopyridin-1(4H)-yl)butanoic acid

(PropKC)

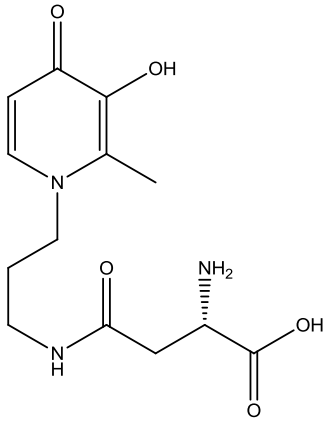

(S)-2-amino-4-((3-(3-hydroxy-2-methyl-4-oxopyridin-1(4H)-yl)propyl)amino)-4-oxobutanoic acid

(A5, product 7)

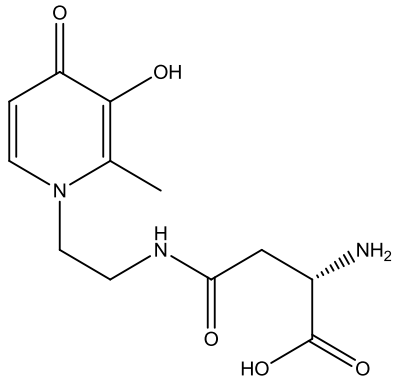

(S)-2-amino-4-((2-(3-hydroxy-2-methyl-4-oxopyridin-1(4H)-yl)ethyl)amino)-4-oxobutanoicacid

(*A6, product 5*)

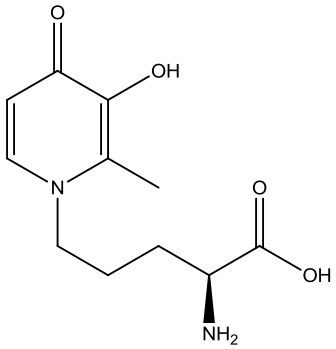

(S)-2-amino-5-(3-hydroxy-2-methyl-4-oxopyridin-1(4H)-yl)pentanoic acid

(*Py-Orn*)

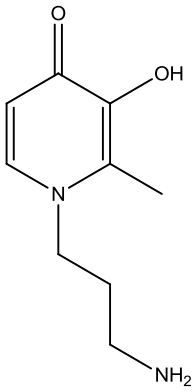

1-(3-aminopropyl)-3-hydroxy-2-methylpyridin-4(1H)-one

(*A3*)

Disubstituted 3-hydroxy-4-pyridinones

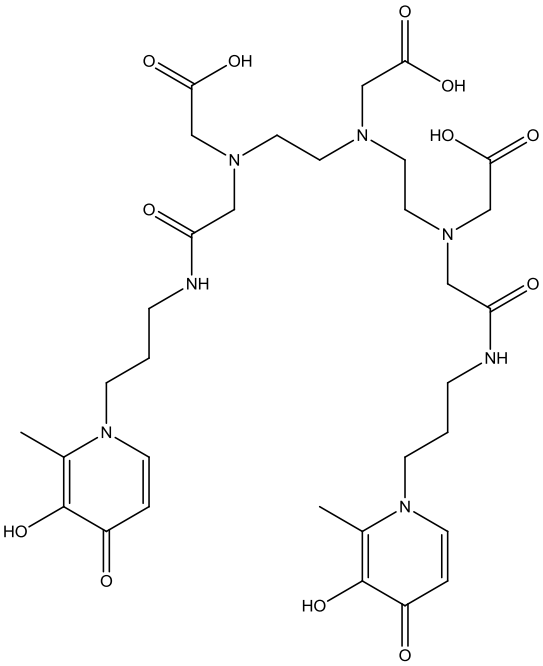

6,9-bis(carboxymethyl)-15-(3-hydroxy-2-methyl-4-oxopyridin-1(4H)-yl)-3-(2-((3-(3-hydroxy-2-methyl-4-oxopyridin-1(4H)-yl)propyl)amino)-2-oxoethyl)-11-oxo-3,6,9,12-tetraazapentadecan-1-oic acid

(*A7, product 9*)

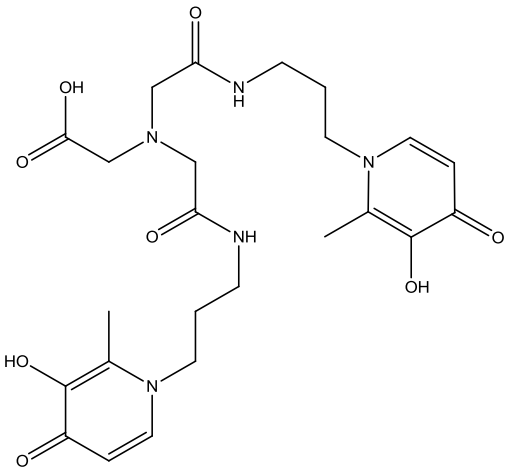

2-(bis(2-((3-(3-hydroxy-2-methyl-4-oxopyridin-1(4H)-yl)propyl)amino)-2-oxoethyl)amino)acetic acid

(*A8, product 11*)

Figure 9.1. Structures of the 3-hydroxy-4-pyridinones.

9.1. Protonation constants of the ligands

The study of the acid – base properties of the 3-hydroxy-4-piridinonone compounds was performed at I = 0.15 mol L^{-1} in $NaCl_{(aq)}$ at T = 298.15 and 310.15 K (physiological conditions) by UV – Vis spectrophotometry in the wavelength range $200 \leq \lambda / nm \leq 400$, and by spectrofluorimetric measurements in the range of $300 \leq \lambda / nm \leq 520$, with an excitation wavelength of 278 nm ($\lambda_{max\ excitation}$) and also other checks were performed at isosbestic points. The experiments were carried out, in the pH range 2.0 - 10.7, by titrating with NaOH standard solution a volume containing the ligand, strong acid (hydrochloric acid) and the ionic medium. The concentration range of the 3-hydroxy-4-piridinonones used in the UV – Vis spectrophotometric and spectrofluorimetric measurements was $1.2 \cdot 10^{-5} \leq c_L / mol\ L^{-1} \leq 5.5 \cdot 10^{-5}$ and $0.0005 \leq c_L / mol\ L^{-1} \leq 0.001$, respectively.

9.2. Monosubstituted 3,4-hydroxypyridinone derivatives

9.2.1. Spectrophotometric analysis

All the 3-hydroxy-4-pyridinones synthetized were obtained as neutral species; usually on their structures the protonable groups are the –OH of the heterocyclic ring, the amino and carboxylic groups eventually present on the alkylic moiety, and also the pyridyl nitrogen atom (proton supplied by excess of mineral acid).[154]

In the case of a monosustituted ligand with these four functional groups, the protonation constants refer to the following equilibria:

$$H^+ + L^{2-} = HL^- \qquad K_1^H \qquad (9.1)$$

$$H^+ + HL^- = H_2L^0 \qquad K_2^H \qquad (9.2)$$

$$H^+ + H_2L^0 = H_3L^+ \qquad K_3^H \qquad (9.3)$$

$$H^+ + H_3L^+ = H_4L^{2+} \qquad K_4^H \qquad (9.4)$$

and

$$H^+ + L^{2-} = HL^- \qquad \beta_1^H \qquad (9.5)$$

$$2H^+ + L^{2-} = H_2L^0 \qquad \beta_2^H \qquad (9.6)$$

$$3H^+ + L^{2-} = H_3L^+ \qquad \beta_3^H \qquad (9.7)$$

$$4H^+ + L^{2-} = H_4L^{2+} \qquad \beta_4^H \qquad (9.8)$$

The monosustituted ligands studied are *KC, PropKC, A5, A6, Py-Orn and A3*, whose structures are reported in Figure 9.1. The compounds with the simplest lateral chain are *KC* and *PropKC*, and in particular the last one differs for the presence of two extra -CH_2 groups on the lateral chain respect to *KC*; their protonation constants refer to the equilibria of eqs. (9.1-9.3) and (9.5-9.7). The analysis of the spectrophotometric data of *KC* and *PropKC* allowed the determination of three protonation constants related to the hydroxyl group, the carboxylic group and the pyridyl nitrogen atom and the experimental protonation constants at I = 0.15 mol L^{-1} in $NaCl_{(aq)}$, at T = 298.15 and 310.15±0.15 K are reported in Table 9.1. Analyzing the results, it was possible to note that the acid-base properties of the ligands are influenced by the lateral chain length, in particular, the logK^H values increase with increasing the -CH_2- groups.

Santos at al.[154] reported the acid-base behavior of *PropKC* and other 3-hydroxy-4-pyridinones having different length in the lateral chain, in particular the 2-(3-hydroxy-2-ethyl-4-oxopyridin-1(4H)-yl)acetic acid (*EthylKC)*, which has an ethyl group in the lateral chain. The protonation constant values of *EthylKC* (logK_1^H = 9.83, logK_2^H = 4.13 and logK_3^H = 3.34 at I = 0.10 mol L^{-1} in $KNO_{3(aq)}$ and T = 298.15 K) fall between the *KC* (only one -CH_2 group) and *PropKC* (propyl group) values.

The refined protonation constant values of *PropKC* can be compared with Santos data, obtained by UV–Vis spectrophotometry at I = 0.10 mol L^{-1} in $KNO_{3(aq)}$ and T = 298.15 K. The author charaterized the protonable groups and reported for *PropKC* logK_1^H = 9.91±0.02 (hydroxyl group), logK_2^H = 4.38±0.05 (carboxylic group) and logK_3^H = 3.53±0.06 (pyridyl nitrogen atom) that are in good agreement with logK_1^H = 9.95, logK_2^H = 4.41 and logK_3^H = 3.38, obtained in this thesis.

In Figure 9.2, the distribution of the *PropKC* species, at I = 0.15 mol L^{-1} in $NaCl_{(aq)}$ and T = 298.15 K, is showed. The graph evidences that all the species reach high formation percentages (≥ 60%) and the H(*PropKC*) is the main species and is present in all pH range investigated (2.5-10.7).

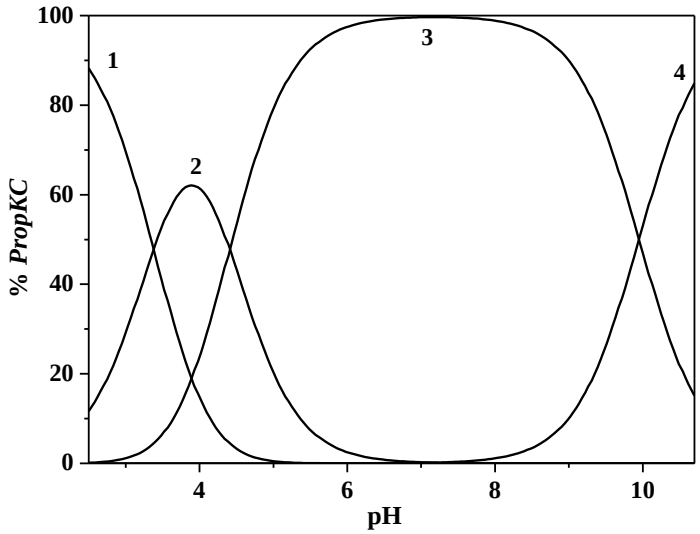

Figure 9.2. Speciation diagram of *PropKC* species at I = 0.15 mol L^{-1} in $NaCl_{(aq)}$ and T = 298.15 K ($c_L = 3.0 \cdot 10^{-5}$ mol L^{-1}).
Species: 1. H_3(*PropKC*); 2. H_2(*PropKC*); 3. H(*PropKC*); 4. (*PropHC*).

A5, *A6* and *Py-Orn* ligands unlike *KC* and *PropKC*, have an amino group on the alkylic chain, so four functional groups were considered. *A5* and *A6* compounds are structurally very similar to each other with the difference of an extra -CH_2 group on the alkylic chain of *A5*, as shown in Figure 9.1.

The protonation constants of *A5* and *A6* determined by spectrophotometric technique at I = 0.15 mol L^{-1} in $NaCl_{(aq)}$, and T = 298.15 and 310.15±0.15K are reported in Table 9.1. As can be seen for *KC* and *PropKC*, the values increase with increasing the length of the alkylic chain, this behavior is showed in Figure 9.3, where the distribution diagram of *A5* and *A6*, at I = 0.15 mol L^{-1} in $NaCl_{(aq)}$ and T = 298.15 K, is reported.

The effect of the lateral chain on protonable species is evidenced on H_2L and HL species that for *A5* (3 -CH_2 groups) are shifted towards higher pH values than *A6* (2 -CH_2 groups).

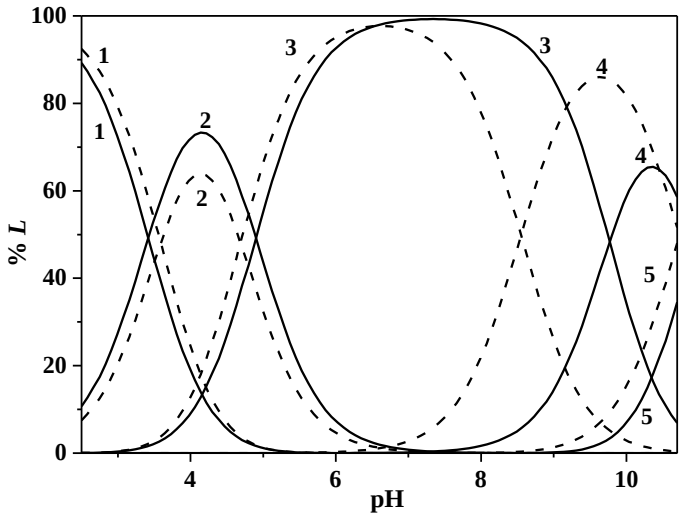

Figure 9.3. Speciation diagram of *A5* (solid line) and *A6* (dashed line) at I = 0.15 mol L^{-1} in $NaCl_{(aq)}$ and T = 298.15 K ($c_L = 3.0 \cdot 10^{-5}$ mol L^{-1}).
Species: 1. H_4L; 2. H_3L; 3. H_2L; 4. HL; 5. L.

As an example, the profile of the titration curves of the spectrophotometric measurements of *A6* at different pH values are reported in Figure 9.4.

This figure shows that the absorption spectrum (absorbance (A) *vs.* wavelenghts (λ)) varies significantly with pH; this behavior can be explained taking into account that the protonated species of the ligand absorb at different wavelengths.

From the analysis of these spectra, it is possible to evidence that increasing pH values the band at 278 nm ($\lambda_{max\ absorption}$) undergoes by a bathochromic shift, and an increase of the absorbances up to pH ~ 6. Some isosbestic points at different wavelenghts (*e.g.* at λ = 231, 240, 255, 281, 295 nm) occur.

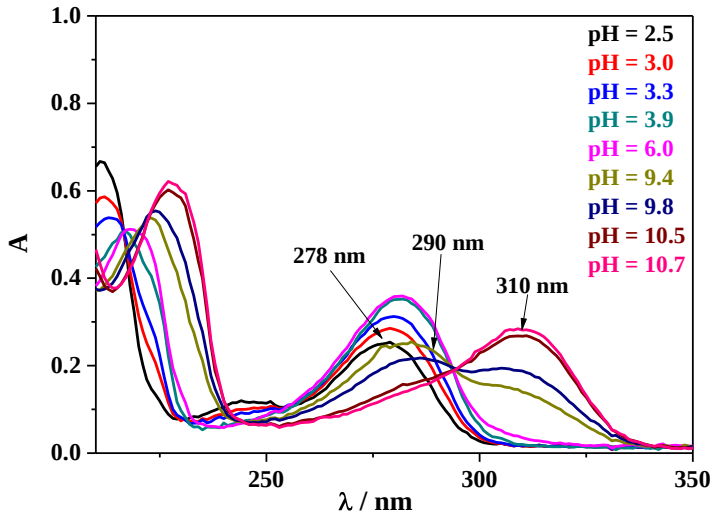

Figure 9.4. Spectrophotometric titration of *A6* (c_L = 3.0·10^{-5} mol L^{-1}) at I = 0.15 mol L^{-1} in $NaCl_{(aq)}$, T = 298.15 K, and at different pH values.

From deconvolution procedures of the spectrophotometric data, it was possible to calculate the molar absorbivities (ε/ mol^{-1} L cm^{-1}) of each species and as example in Figure 9.5, the variation of ε in the wavelength range 200 - 400 nm, at I = 0.15 mol L^{-1} and T = 298.15 K for *A6* is reported. The values of the molar absorbivities in these conditions are: ε_{max}(*A6*) = 10855 (λ = 313 nm), ε_{max}(H(*A6*)) = 6386 (λ = 291 nm), ε_{max}(H_2(*A6*)) = 6785 (λ = 290 nm), ε_{max}(H_3(*A6*)) = 9192 (λ = 282 nm), ε_{max}(H_4(*A6*)) = 5622 (λ = 278 nm), the charges of the species are omitted for simplicity.

The absoption spectra and the trend of the molar absorbivity obtained for all the monosubtituted ligands are analogous of that reported in Figures 9.4 and 9.5, respectively.

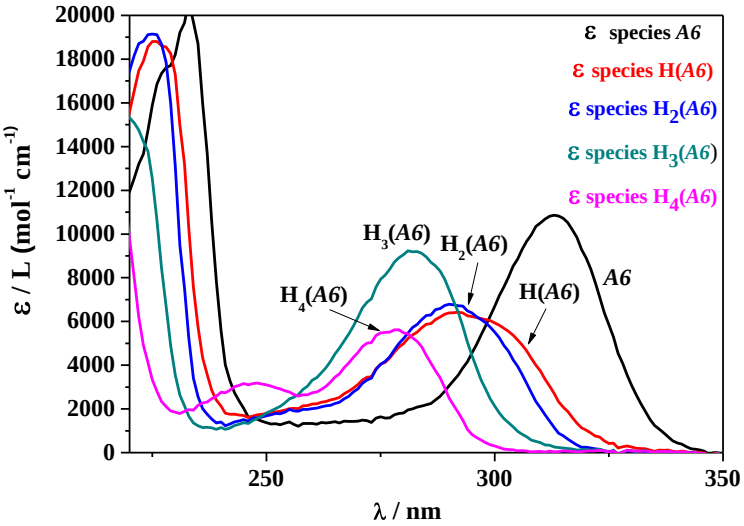

Figure 9.5. Molar absorbivity of the different *A6* species *vs.* λ at I = 0.15 mol L^{-1} in $NaCl_{(aq)}$ and T = 298.15 K.

The last two monosubstituted 3-hydroxy-4-pyridinones studied are *A3* and *Py-Orn* (see Figure 9.1), that differ for a carboxylic group on the end of the lateral chain of *Py-Orn*.

The experimental data carried out at I = 0.15 mol L^{-1} in $NaCl_{(aq)}$ and T = 298.15 and 310.15±0.15 K, by spectrophotometric measurements are reported in Table 9.2 together with the other compounds.

The refined constant values of the hydroxylic, amino and pyridyl nitrogen groups for *Py-Orn* and *A3* are in good agreement between them.

In literature[155], the protonation constants of *A3* are reported in $KCl_{(aq)}$ at I = 0.10 mol L^{-1} and T = 298.15 K and the values of $\log K_1^H$ = 10.07, $\log K_2^H$ = 9.09 and $\log K_3^H$ = 3.20.

Table 9.1. Protonation constants[a)] of the monosubstituted 3,4-hydroxypyridinones obtained by UV – Vis spectrophotometry at I = 0.15 mol L^{-1} in $NaCl_{(aq)}$ and T = 298.15 and 310.15±0.15K

Ligand	T / K	$\log\beta_1^H$ ($\log K_1^H$)	$\log\beta_2^H$ ($\log K_2^H$)	$\log\beta_3^H$ ($\log K_3^H$)	$\log\beta_4^H$ ($\log K_4^H$)
KC	298.15	9.41±0.08[b)]	12.65±0.12 (3.24)	15.71±0.13 (3.06)	
	310.15	10.37±0.10	13.45±0.03 (3.08)	16.18±0.02 (2.73)	
PropKC	298.15	9.949±0.007	14.36±0.09 (4.41)	17.74±0.03 (3.38)	
	310.15	10.029±0.003	13.62±0.01 (3.59)	16.54±0.04 (2.92)	
A5	298.15	10.93±0.02	20.70±0.06 (9.77)	25.60±0.01 (4.90)	29.02±0.01 (3.42)
	310.15	10.93±0.02	17.71±0.07 (6.78)	22.50±0.05 (4.79)	25.93±0.05 (3.43)
A6	298.15	10.73±0.03	19.52±0.08 (8.79)	24.17±0.08 (4.65)	27.43±0.08 (3.26)
	310.15	10.99±0.02	17.05±0.03 (6.06)	21.02±0.04 (3.97)	24.08±0.05 (3.06)
Py-Orn	298.15	11.10±0.09	20.44±0.07 (9.34)	24.60±0.05 (4.16)	27.87±0.04 (3.27)
	310.15	11.13±0.03	17.93±0.04 (6.80)	22.00±0.03 (4.07)	25.30±0.05 (3.30)
A3	298.15	11.08±0.02	20.468±0.005 (9.39)	23.679±0.03 (3.21)	
	310.15	10.57±0.07	16.53±0.08 (5.96)	19.53±0.05 (3.00)	

[a)] $\log K_r^H$ and $\log\beta r^H$ refer to eqs. (9.1-9.8); [b)] ±Std. deviation.

In general, the temperature effect on the protonation constant values of the 3,4-hydroxypyridinones is different between the hydroxylic group and the others (carboxylic, amino and pyridyl nitrogen groups). In fact, analyzing the data reported in Table 9.1, it is possible to observe that the $\log\beta_1^H$ values increase with increasing the temperature while for the other protonation contants this trend in not respected.

To show better the temperature effect on the distribution of the species, as an example in Figure 9.6 the distribution diagram of *A6* at I = 0.15 mol L^{-1} in $NaCl_{(aq)}$ at T = 298.15 K and T = 310.15 K is reported. The graph evidences that the formation species at T = 310.15 K are shifted towards lower pH values.

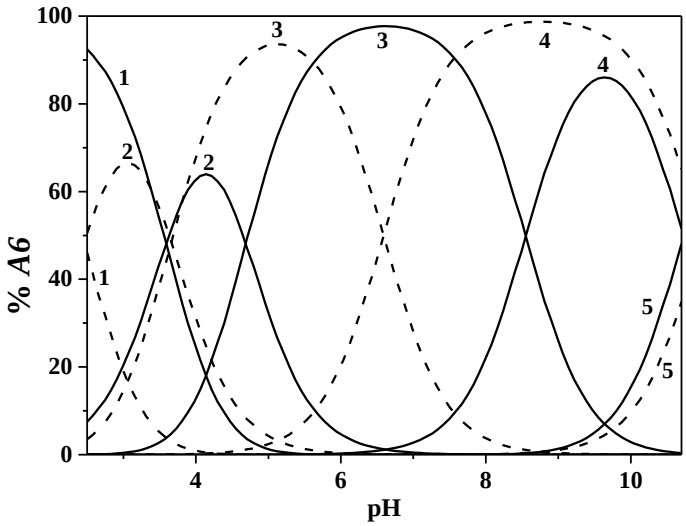

Figure 9.6. Speciation diagram of *A6* (c_L = 3.0·10^{-5} mol L^{-1}) at I = 0.15 mol L^{-1} in $NaCl_{(aq)}$ and T = 298.15 K (solid line) and T = 310.15 K (dashed line).
Species: 1. H_4*(A6);* 2. H_3*(A6)*; 3. H_2*(A6)*; 4. H*(A6)*; 5. *(A6)*.

9.2.2. Spectrofluorimetric analysis

To confirm the speciation models and to verify the repeteability of the UV – Vis spectrophofotometric measurements, also spectrofluorimetric titrations were performed. As maximum absorbance wavelenght, 278 nm ($\lambda_{max\ excitation}$) has been chosen, and also some checks of absorption at the isosbestic points were carried out to verify if the behavior of the species is the same of that at 278 nm ($\lambda_{max\ excitation}$).
At each point of the titration (mL of strong base NaOH), the variation of the emission intensity (CPS) towards wavelenght (nm) was recorded. All the monosubstituted ligands evidenced a lowering of the signal along the pH scale with a light shift of the $\lambda_{max\ emission}$ from 379 nm to 376 nm increasing the basicity of the solution.
In Figure 9.7 a tridimensional titration curve of the ligand *A6* is reported at I = 0.15 mol L^{-1} in $NaCl_{(aq)}$ and T = 298.15 K.

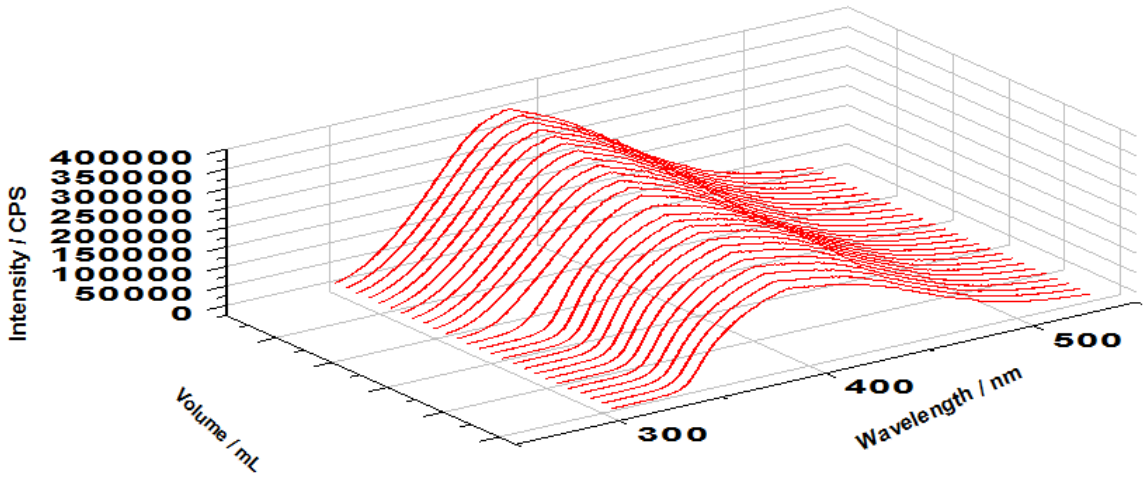

Figure 9.7. Emission intensity (CPS) of *A6* (c_L = 0.0001 mol L^{-1}) as a function of the wavelength (nm) at different pH values.

Experimental data analysis performed by Hyperquad computer program led to the refinement of protonation constants.

Spectrofluorimetric values confirmed the trend of the UV-Vis data, therefore the protonation constants for the carboxylic, amino groups and pyridyl nitrogen atom, decrease with increasing the temperature. Concerning the hydroxylic group, the protonation constants increase incresing the temperature in the case of *KC* and *PropKC*, while an inverse tendency was observed for the other ligands.

The experimental spectrofluorimetric protonation constants of the monosubtituted 3-hydroxy-4-pyridinones studied at I = 0.15 mol L^{-1} in $NaCl_{(aq)}$ at T = 298.15 and 310.15 K are reported in Table 9.2.

Table 9.2. Spectrofluorimetric protonation constants[a)] of the mono 3,4-hydroxypyridinones at I = 0.15 mol L^{-1} in $NaCl_{(aq)}$ and T = 298.15 and 310.15±0.15K

Ligand	T / K	$\log\beta_1^H$ ($\log K_1^H$)	$\log\beta_2^H$ ($\log K_2^H$)	$\log\beta_3^H$ ($\log K_3^H$)	$\log\beta_4^H$ ($\log K_4^H$)
KC	298.15	9.35±0.05[b)]	12.64±0.20	15.48±0.07	
			(3.29)	(2.84)	
	310.15	10.37±0.02	13.97±0.01	16.78±0.01	
			(3.60)	(2.81)	
PropKC	298.15	9.90±0.04	14.38±0.04	17.73±0.12	
			(4.48)	(3.35)	
	310.15	10.05±0.02	13.88±0.01	16.44±0.01	
			(3.83)	(2.56)	
A5	298.15	11.03±0.01	20.38±0.02	25.99±0.04	29.69±0.08
			(9.35)	(5.61)	(3.70)
	310.15	10.47±0.01	17.96±0.06	22.00±0.07	25.15±0.09
			(7.49)	(4.04)	(3.12)
A6	298.15	10.73±0.03	19.50±0.13	24.18±0.03	27.62±0.04
			(8.77)	(4.68)	(3.44)
	310.15	10.397±0.002	17.34±0.03	20.69±0.04	22.94±0.07
			(6.94)	(3.35)	(2.25)
Py-Orn	298.15	11.00±0.01	19.77±0.03	24.38±0.03	27.75±0.03
			(8.77)	(4.61)	(3.37)
	310.15	10.05±0.02	17.02±0.05	21.17±0.04	24.27±0.01
			(7.00)	(4.15)	(3.10)
A3	298.15	11.20±0.03	20.51±0.03	23.70±0.03	
			(9.31)	(3.17)	
	310.15	10.62±0.20	16.93±0.04	19.74±0.08	
			(6.31)	(2.81)	

[a)] $\log K_r^H$ and $\log\beta r^H$ refer to eqs. (9.1-9.8); [b)] ±Std. deviation.

9.3. Disubstituted 3-hydroxy-4-pyridinone derivatives

9.3.1. Spectrophotometric analysis

The disubstituted derivatives *A7* and *A8* present a major number of protonable groups than the corresponding mono 3,4-hydroxypyridinone compounds.

Regarding *A7*, the possible groups should be ten, but it was possible to refine only height protonation constants, probably because the other two constants could be determined at pH < 2. This hypothesis is supported by Bretti et al.[156] who reported for the not substituted diethylenetriaminepentaacetic acid (DTPA) at I = 0.16 mol L^{-1} in $NaCl_{(aq)}$ and T = 298.15 K the values of $\log K_5^H$ =1.99±0.01 and $\log K_6^H$ =1.21±0.01.

The values of the other refined constants are in good agreement with Bretti et al. data, that in the case of the central atom of nitrogen of the DTPA reported $\log K^H$ = 9.88±0.03, while for the same group $\log K^H$ = 9.60 is here reported. The differences in the protonation constant values of the other groups could be due to electronic effects and for the substitution of two carboxylic groups of the DTPA with two 3-hydroxy-4-pyridinone chains.

The protonation constants of *A7* refer to the following equilibria:

$$H^+ + H_{(r-1)}L^{((r-1)-5)} = H_rL^{(r-5)} \qquad K_1^H \qquad (9.9)$$

and

$$rH^+ + L^{5-} = H_rL^{(r-5)} \qquad \beta_1^H \qquad (9.10)$$

Regard *A8*, for all the possible protonable groups: $\log K_1^H$ and $\log K_2^H$ for the two –OH groups of the heterocyclic ring, $\log K_3^H$ for the nitrogen atom of the NTA chain, $\log K_4^H$ for the carboxylic group and, $\log K_5^H$ and $\log K_6^H$ for the pyridyl nitrogen atom, the protonation constants were determined.

The experimental results were in agreement with the data obtained for analogous functional groups in the case of the monosubstituted and of the DTPA derivatives; if compared with NTA literature data at I = 0.10 mol L^{-1} in Na^+ salt electrolyte[140] some differences are evidenced, probably for the same reasons already cited for *A7* compound (electronic effects and substitution of two carboxylic groups of the NTA with two 3-hydroxy-4-pyridinone chains). In fact, for example, $\log K_3^H$ = 7.15 (central nitrogen atom) of *A8* should be compared with the $\log K_1^H$ = 9.46±0.07 of NTA. The $\log K_4^H$= 4.56, that could be referred to the –COOH group, presents a difference of about two logarithmic units than the literature data of $\log K_2^H$= 2.52±0.09 of the not substituted acid.

The protonation constants for *A8* refer to the following equilibria:

$$H^+ + H_{(r-1)}L^{((r-1)-3)} = H_rL^{(r-3)} \qquad K_1^H \qquad (9.11)$$

and

$$rH^+ + L^{3-} = H_rL^{(r-3)} \qquad \beta_1^H \qquad (9.12)$$

Table 9.3 reports the protonation constants of these two ligands, determined by UV – Vis spectrophotometry at I = 0.15 mol L^{-1} in $NaCl_{(aq)}$ and T = 298.15 K.

Table 9.3. UV – Vis spectrophotometric protonation constants[a)] of *A7* and *A8* at I = 0.15 mol L^{-1} in $NaCl_{(aq)}$ and T = 298.15 K

	A7	*A8*
$\log\beta_1^H$ ($\log K_1^H$)	11.08±0.10[b)]	10.84±0.03
$\log\beta_2^H$ ($\log K_2^H$)	21.73±0.02 (10.65)	20.501±0.007 (9.66)
$\log\beta_3^H$ ($\log K_3^H$)	31.336±0.008 (9.60)	27.65±0.14 (7.15)
$\log\beta_4^H$ ($\log K_4^H$)	38.18±0.07 (6.85)	32.21±0.07 (4.56)
$\log\beta_5^H$ ($\log K_5^H$)	42.55±0.10 (4.37)	35.72±0.09 (3.51)
$\log\beta_6^H$ ($\log K_6^H$)	46.07±0.01 (3.52)	38.59±0.07 (2.87)
$\log\beta_7^H$ ($\log K_7^H$)	49.08±0.03 (3.01)	
$\log\beta_8^H$ ($\log K_8^H$)	51.46±0.03 (2.38)	

[a)] $\log K_r^H$ and $\log\beta r^H$ refer to eqs. (9.9-9.12);
[b)] ±Std. deviation.

The absorpion spectra recovered for these ligands are characterized by a similar trend than that of the monosubstituted products and, also in these cases, a bathochromic shift of the λ_{max}

$_{absorption}$ = 278 nm and isosbestic points at different wavelenghts occurred. Furthermore, the intensity of absorbance measured is for both the ligands about two fold the value found for monosubstituted ligands, owing to the presence of two 3,4-hydroxypyridinone chains on the molecules.

The calculation of the molar absorbance ε (mol^{-1} L cm^{-1}) of each species was performed. Figure 9.8 shows the ε of the different species of *A8*, where *A8*, H_2(*A8*), H_3(*A8*) and H_4(*A8*) species absorb more than the H(*A8*), H_5(*A8*) and H_6(*A8*) ones.

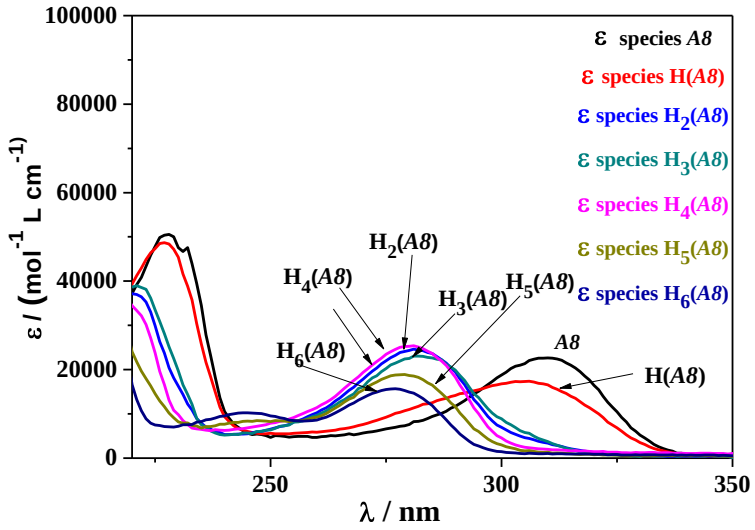

Figure 9.8. Molar absorbivity of *A8* species *vs.* wavelength at I = 0.15 mol L^{-1} in $NaCl_{(aq)}$ and T = 298.15 K.

In the wavelength range 200 - 400 nm, as it can be seen in Figure 9.8, the molar absorbivity values of the different species at the maximum absorbation wavelength of each band are the following: ε_{max}(*A8*) = 22568 (λ = 309 nm), ε_{max}(H(*A8*)) = 17032 (λ = 302 nm), ε_{max}(H_2(*A8*)) = 24365 (λ = 281 nm), ε_{max}(H_3(*A8*)) = 22382 (λ = 279 nm), ε_{max}(H_4(*A8*)) = 25049 (λ = 278 nm), ε_{max}(H_5(*A8*)) = 18770 (λ = 278 nm), ε_{max}(H_6(*A8*)) = 15689 (λ = 278 nm). The charges of the species have been omitted for simplicity.

In the literature, Santos et al.[50] reported the protonation constants, at I = 0.20 mol L^{-1} in $KCl_{(aq)}$ and T = 298.15 K, of a derivative of the ethylenediaminetetraacetic acid, the so-called EDTAPr(3,4-HP)$_2$,: logK_1^H = 10.12±0.01, logK_2^H = 9.53±0.01, logK_3^H = 7.04±0.01, logK_4^H = 4.03±0.02, logK_5^H = 3.38±0.02 and logK_6^H = 2.84±0.02, that are in quite good agreement with the values reported in Table 9.3 at I = 0.15 mol L^{-1} in $NaCl_{(aq)}$ and T = 298.15 K.

Also for disubstituted ligands, the temperature effect on the speciation was studied by performing UV – Vis spectrophotometric measurements at I = 0.15 mol L^{-1} in $NaCl_{(aq)}$ and T = 310.15 K (physiological conditions). Protonation constant values for all the species determined at T = 310.15 K show a common trend for both the compounds; in fact, the values of the $\log K_1^H$ and $\log K_2^H$, probably related to the –OH groups, slightly increase with increasing temperature, while an inverse behavior characterizes the other protonation constant values, that are lower than those at T = 298.15 K. In Table 9.4 the protonation constants of the ligands determined by the UV – Vis spectrophotometric measurements at I = 0.15 mol L^{-1} in $NaCl_{(aq)}$ and T = 310.15 K are reported.

Table 9.4. UV – Vis spectrophotometric protonation constants[a)] of *A7* and *A8* at I = 0.15 mol L^{-1} in $NaCl_{(aq)}$ and T = 310.15 K

	A7	*A8*
$\log\beta_1^H$ ($\log K_1^H$)	11.29±0.10[b)]	10.95±0.02
$\log\beta_2^H$ ($\log K_2^H$)	22.34±0.07 (11.05)	20.99±0.03 (10.04)
$\log\beta_3^H$ ($\log K_3^H$)	31.31±0.05 (8.97)	27.13±0.03 (6.14)
$\log\beta_4^H$ ($\log K_4^H$)	37.99±0.01 (6.68)	31.25±0.01 (4.12)
$\log\beta_5^H$ ($\log K_5^H$)	41.94±0.07 (3.95)	34.54±0.02 (3.29)
$\log\beta_6^H$ ($\log K_6^H$)	45.41±0.01 (3.47)	36.95±0.04 (2.41)
$\log\beta_7^H$ ($\log K_7^H$)	47.89±0.07 (2.481)	
$\log\beta_8^H$ ($\log K_8^H$)	50.16±0.04 (2.23)	

[a)] $\log K_r^H$ and $\log\beta r^H$ refer to eqs. (9.9-9.12);
[b)] ±Std. deviation.

The effect of the temperature on the acid – base properties of the two disubstituted 3-hydroxy-4-pyridinone derivatives is shown in the distribution diagram, Figure 9.9, at I = 0.15 mol L^{-1}

in $NaCl_{(aq)}$ at T = 298.15 K and T = 310.15 K. As already seen for the other ligands studied, the distribution of the species at T = 310.15 K is shifted towards more acidic pH values.

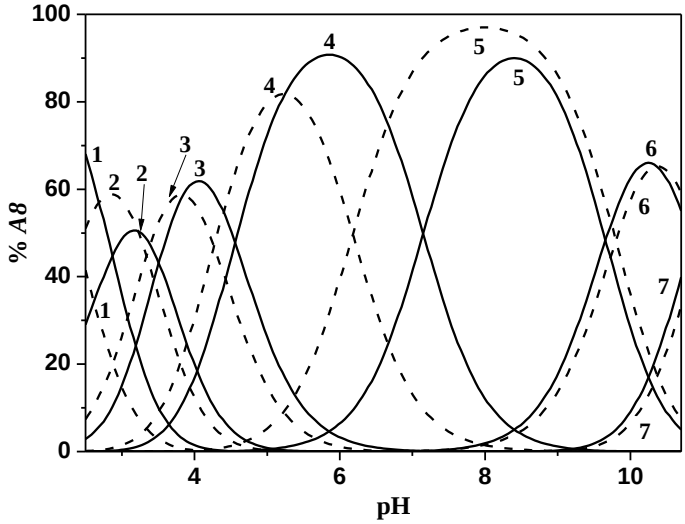

Figure 9.9. Speciation diagram of *A8* at I = 0.15 mol L^{-1} in $NaCl_{(aq)}$ and T = 298.15 K (solid line) and T = 310.15 K (dashed line). $c_L = 1.0 \cdot 10^{-5}$ mol L^{-1}.
Species: 1. H_6(*A8*); 2. H_5(*A8*); 3. H_4(*A8*); 4. H_3(*A8*); 5. H_2(*A8*), 6. H(*A8*); 7. (*A8*).

9.3.2. Spectrofluorimetric measurements

Spectrofluorimetric measurements were performed at I = 0.15 mol L^{-1} in $NaCl_{(aq)}$ at T = 298.15 K and T = 310.15 K. Owing to the complexity of these two systems, it was possible to refine only some of the protonation constants. As example, for *A7* at T = 298.15 K it was not possible to determine the $\log K_1^H$ and $\log K_5^H$ while, $\log K_2^H = 10.93 \pm 0.02$, $\log K_3^H = 9.32 \pm 0.01$, $\log K_4^H = 6.87 \pm 0.02$, $\log K_6^H = 3.51 \pm 0.07$, $\log K_7^H = 3.22 \pm 0.05$ and $\log K_8^H = 2.12 \pm 0.07$ values were obtained. The corresponding UV – Vis spectrophotometric data are: $\log K_2^H = 10.65$, $\log K_3^H = 9.60$, $\log K_4^H = 6.85$, $\log K_6^H = 4.37$, $\log K_7^H = 3.52$ and $\log K_8^H = 2.38$. Concerning *A8*, at T = 298.15 K it was possible to refine three protonation constants namely $\log K_3^H = 7.33 \pm 0.01$, $\log K_5^H = 3.78 \pm 0.02$ and $\log K_6^H = 2.60 \pm 0.03$, against the UV – Vis data, $\log K_3^H = 7.15$, $\log K_5^H = 3.51$, $\log K_6^H = 2.87$.

Chapter 10

M^{n+} / 3-Hydroxy-4-Pyridinone systems

10.1. Al^{3+}/ monosubstituted 3-hydroxy-4-pyridinone complexes

10.1.1. Experimental details

The interactions of Al^{3+} with 3,4-hydroxypyridinones were investigated experimentally by carrying out potentiometric (ISE–H^+) measurements at I = 0.15 mol L^{-1} in $NaCl_{(aq)}$, T = 298.15±0.15 K and at different concentrations of metal cation ($0.0005 \leq c_{Al^{3+}}$ / mol $L^{-1} \leq 0.001$) and ligands ($0.001 \leq c_L$/ mol $L^{-1} \leq 0.004$).

Afterwards, the speciation models of the systems were confirmed by UV – Vis spectrophotometric titrations, in the same range of wavelengths of the protonation reactions of the ligands ($200 \leq \lambda$ / nm ≤ 400) and in the same experimental conditions of ionic strength, supporting electrolyte and temperature of potentiometric measurements, but at lower concentrations of metal cation ($5.0 \cdot 10^{-6} \leq c_{Al^{3+}}$ / mol $L^{-1} \leq 1.5 \cdot 10^{-5}$) and ligands ($1.0 \cdot 10^{-5} \leq c_L$/ mol $L^{-1} \leq 2.1 \cdot 10^{-5}$).

10.1.2. Stability of Al^{3+}/monosustituted 3-hydroxy-4-pyridinone systems

The study of the interactions of Al^{3+} with the monosubstituted ligands, at I = 0.15 mol L^{-1} in $NaCl_{(aq)}$ and T = 298.15 K, allowed to determined $Al_pL_qH_r$ complexes having different stoichiometry.

Concerning Al^{3+}/*KC* complexes, the elaboration of experimental data led to the determination of two species, namely Al(*KC*) and $Al(KC)_2$ (charged omitted for simplicity), which refer to the following equilibrium:

$$pAl^{3+} + q(KC)^{2-} + rH^{+} = Al_p(KC)_qH_r^{(3p+r-2q)} \qquad \beta_{pqr} \quad (10.1)$$

The speciation model build from potentiometric measurements, was considered reliable in the pH range 2.0 – 5.0, because of the formation of the scarcely soluble species $Al(OH)_{3(s)}$. It did not occur during UV – Vis spectrophotometric experiments, inasmuch the concentration of metal cation and ligand were lower than potentiometry so, it was possible to determine the formation constants of the Al^{3+}/*KC* complexes in the pH range 2.0 – 11.0. The experimental stability constants, reported in Table 10.1, are in a good agreement between the two analytical techniques.

Table 10.1. Experimental stability constants[a)] of Al^{3+}/*KC* complexes by potentiometric and UV – Vis spectrophotometric data, at I = 0.15 mol L^{-1} in $NaCl_{(aq)}$ and T = 298.15 K

Species	Potentiometry (ISE – H^+)	UV – Vis Spectrophotometry
	$\log\beta_{pqr}$	$\log\beta_{pqr}$
Al(*KC*)	12.39±0.02[b)]	12.79±0.01
$Al(KC)_2$	24.41±0.05	24.79±0.04

[a)] $\log\beta_{pqr}$ refers to eq. (10.1); [b)] ±Std. Deviation.

The study of the Al^{3+}/*PropKC* interactions in the experimental conditions already mentioned allowed to define a speciation model constituted by five species, namely Al(*PropKC*), $Al(PropKC)_2$, $Al(PropKC)_2H$, $Al(PropKC)_2H_2$ and $Al(PropKC)_3$, in the pH range 2.0 – 9.2 and 2.0 – 11.0 for potentiometric and UV – Vis spectrophotometric data, respectively.
The stability constants of the complexes refer to the following equilibrium:

$$pAl^{3+} + q(PropKC)^{2-} + rH^{+} = Al_p(PropKC)_qH_r^{(3p+r-2q)} \qquad \beta_{pqr} \quad (10.2)$$

The experimental stability constants calculated by BSTAC, STACO and Hyperquad computer programs from potentiometric and UV – Vis spectrophotometric data, respectively, at I = 0.15 mol L^{-1} in $NaCl_{(aq)}$ and T = 298.15 K, are reported in Table 10.2.

Table 10.2. Experimental stability constants[a)] of Al^{3+}/*PropKC* complexes by potentiometric and UV – Vis spectrophotometric data, at I = 0.15 mol L^{-1} in $NaCl_{(aq)}$ and T = 298.15 K

Species	Potentiometry (ISE – H^+)	UV – Vis Spectrophotometry
	$\log\beta_{pqr}$	$\log\beta_{pqr}$
Al(*PropKC*)	12.30±0.04[b)]	12.85±0.01
Al(*PropKC*)$_2$	23.44±0.07	22.90±0.03
Al(*PropKC*)$_2$H	27.03±0.12	28.37±0.07
Al(*PropKC*)$_2$H$_2$	30.92±0.03	30.20±0.05
Al(*PropKC*)$_3$	31.66±0.18	31.80±0.07

[a)] $\log\beta_{pqr}$ refers to eq. (10.2); [b)] ±Std. Deviation.

The formation constants of Al^{3+}/*PropKC* complexes obtained are in agreement (considering the different ionic medium and ionic strength value) with the literature data by Santos et al.[154] who reported: $\log\beta_{110}$ = 13.03±0.03, $\log\beta_{120}$ = 22.97±0.02, $\log\beta_{121}$ = 27.34±0.03, $\log\beta_{122}$ = 30.26±0.08 and $\log\beta_{130}$ = 31.27±0.03, determined by UV – Vis spectrophotometric measurements at I = 0.10 mol L^{-1} in $KNO_{3(aq)}$ and T = 298.15 K.

In Figure 10.1 the absorption spectra (absorbance *vs.* wavelenght) of the Al^{3+}/*PropKC* system, at I = 0.15 mol L^{-1} in $NaCl_{(aq)}$ and T = 298.15 K, at different pH values, are reported.

The absorption spectra, as for the protonation reactions of the ligands, vary significantly with pH and it is due to the fact that the complexes absorb in different wavelength ranges and form in different pH regions. In the spectra, the absorption band at 278 nm shows a bathochromic shift, and some isosbestic points (at 241, 244, 282, 299 nm wavelenghts values) indicate the formation of the different complex species.

Santos et al.[154], for Al^{3+}/*EthylKC* system reported the formation constant values of $\log\beta_{110}$ = 13.04±0.04 and $\log\beta_{120}$ = 24.06±0.04 determined by UV-Vis spectrophotometry at I = 0.10 mol L^{-1} in $KNO_{3(aq)}$ and T = 298.15 K. These values are in good agreement accordance with the stability constants of the Al(*KC*) and Al(*PropKC*) species, here found.

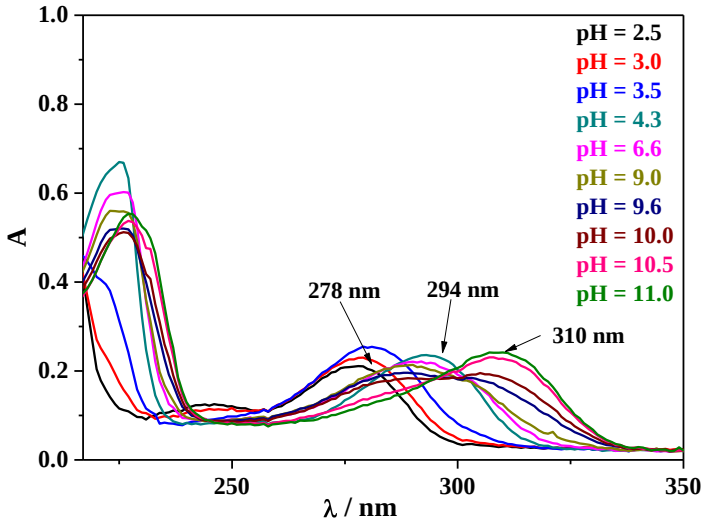

Figure 10.1. Absorption spectra of Al^{3+}/*PropKC* complexes at I = 0.15 mol L^{-1} in $NaCl_{(aq)}$, T = 298.15 K and different pH values. $c_{Al^{3+}} = 7.0 \cdot 10^{-6}$ mol L^{-1}; $c_{PropKC} = 2.1 \cdot 10^{-5}$ mol L^{-1}.

The study of the Al^{3+}/*A5*, Al^{3+}/*A6*, Al^{3+}/*Py-Orn* and Al^{3+}/*A3* systems allowed to determine a common speciation model that consider two species, namely Al*L*H and Al*L* in the pH range 2.0 – 7.0 and 2.0 – 11.0, from potentiometric and UV – Vis spectrophotometric data, respectively. In the case of Al^{3+}/*A5* and Al^{3+}/*A3* systems, considering the solubility product of the scarcely soluble species in the calculations, the formation of $Al(OH)_{3(s)}$ should start at pH ~ 6.5 and pH ~ 4.9, respectively but the precipitate was not observed during the measurements. Its absence in the experiments may be explained considering the slow kinetic of formation of $Al(OH)_{3(s)}$.[141]

The experimental stability constants determined from potentiometric and UV-Vis spectrophotometric data at I = 0.15 mol L^{-1} in $NaCl_{(aq)}$ and T = 298.15 K are reported in Table 10.3 and refer to the following equilibria:

$$pAl^{3+} + q(A5)^{2-} + rH^{+} = Al_p(A5)_qH_r^{(3p+r-2q)} \qquad \beta_{pqr} \qquad (10.3)$$

$$pAl^{3+} + q(A6)^{2-} + rH^{+} = Al_p(A6)_qH_r^{(3p+r-2q)} \qquad \beta_{pqr} \qquad (10.4)$$

$$pAl^{3+} + q(Py\text{-}Orn)^{2-} + rH^{+} = Al_p(Py\text{-}Orn)_qH_r^{(3p+r-2q)} \qquad \beta_{pqr} \qquad (10.5)$$

$$pAl^{3+} + q(A3)^{-} + rH^{+} = Al_p(A3)_qH_r^{(3p+r-q)} \qquad \beta_{pqr} \qquad (10.6)$$

Table 10.3. Experimental stability constants[a)] of Al^{3+}/*A5*, Al^{3+}/*A6*, Al^{3+}/*Py-Orn* and Al^{3+}/*A3* complexes determined by potentiometry and UV-Vis spectrophotometry at I = 0.15 mol L^{-1} in $NaCl_{(aq)}$ and T = 298.15 K

	Potentiometry (ISE – H^+)		UV – Vis Spectrophotometry	
Systems	$\log\beta_{111}$	$\log\beta_{110}$	$\log\beta_{111}$	$\log\beta_{110}$
Al^{3+}/*A5*	24.27±0.03[b)]	17.50±0.10	24.50±0.01	17.65±0.10
Al^{3+}/*A6*	23.28±0.02	17.94±0.10	23.66±0.01	17.94±0.04
Al^{3+}/(*Py-Orn*)	23.48±0.03	18.32±0.03	23.47±0.01	18.88±0.02
Al^{3+}/*A3*	20.98±0.02	15.08±0.09	20.05±0.10	15.08±0.09

[a)] $\log\beta_{pqr}$ refers to eqs. (10.3 – 10.6); [b)] ±Std. Deviation.

The UV – Vis spectrophotometric data confirmed the speciation models and the stability constant values obtained from potentiometric data are in good agreement with spectrophotometric ones. In the case of the Al(*A5)* and Al(*A6)* species, the trend is opposite to that observed for *KC* and *PropKC*, in fact the stability constant values refined decrease increasing the length of the alkyl chain. The analysis of Figure 10.2 allows to understand better the species distribution in the Al^{3+}/*A5* and Al^{3+}/*A6* systems from potentiometric data, at I = 0.15 mol L^{-1} in $NaCl_{(aq)}$ and T = 298.15 K.

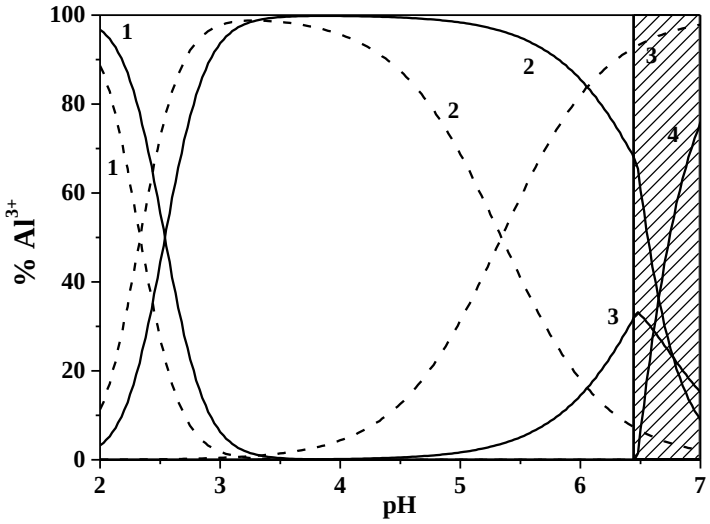

Figure 10.2. Speciation diagram of Al^{3+}/*A5* (solid line) and Al^{3+}/*A6* (dashed line) systems at I = 0.15 mol L^{-1} in $NaCl_{(aq)}$ and T = 298.15 K. $c_{Al^{3+}}$ = 0.0008 mol L^{-1}; c_L = 0.002 mol L^{-1}. Species: 1. free Al^{3+}; 2. Al*L*H; 3. Al*L*; 4. $Al(OH)_{3(s)}$.

The higher stability of the Al^{3+}/*A6* system avoids the formation of the scarcely soluble species $Al(OH)_{3(s)}$, that instead, in the case of Al^{3+}/*A5* complexation, starts form at pH ~ 6.4 (shaded zone in Figure 10.2), but it is not experimentally observed because of its already mentioned slow kinetics.[141]

In Figure 10.3 the distribution of the Al^{3+}/*Py-Orn* complexes from potentiometric data, at I = 0.15 mol L^{-1} in $NaCl_{(aq)}$ and T = 298.15 K, is shown. The Al(*Py-Orn*)H species is present in solution along the entire pH range of the titration, while the Al(*Py-Orn*) complex starts to form at pH ~ 2.7.

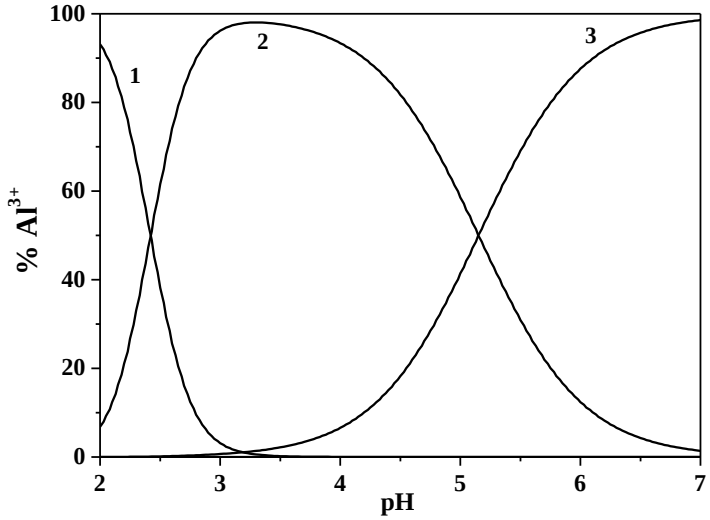

Figure 10.3. Speciation diagram of Al^{3+}/*Py-Orn* complexes at I = 0.15 mol L^{-1} in $NaCl_{(aq)}$ and T = 298.15 K. $c_{Al^{3+}}$ = 0.0008 mol L^{-1}; c_L = 0.002 mol L^{-1}. Species: 1. free Al^{3+}; 2. Al(*Py-Orn)*H; 3. Al(*Py-Orn*).

Figure 10.4 shows the distribution of the species for the interaction between Al^{3+} and the *A3* ligand, that in comparison with the other ligands does not contain carboxylic groups.

In Figure 10.4, it can be noted that the precipitation of $Al(OH)_{3(s)}$, not observed experimentally, should start from pH ~ 4.9.

The formation percentages of Al^{3+}, Al(*A3*)H and Al(*A3*) species are 95%, 96% and 8% at pH ~ 2, ~ 4.1 and ~ 4.9, respectively.

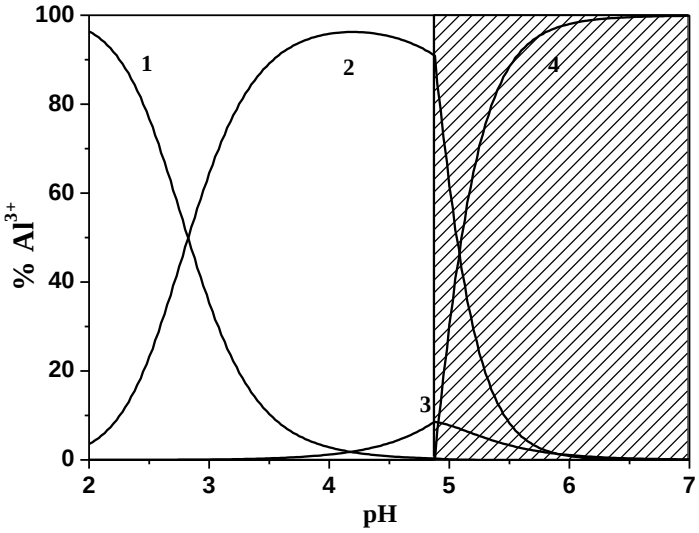

Figure 10.4. Speciation diagram of Al^{3+}/*A3* system at I = 0.15 mol L^{-1} in $NaCl_{(aq)}$ and T = 298.15 K. $c_{Al^{3+}}$ = 0.0008 mol L^{-1}; c_L = 0.002 mol L^{-1}. Species: 1. free Al^{3+}; 2. Al(*A3*)H; 3. Al(*A3*); 4. $Al(OH)_{3(s)}$.

10.2. M^{2+} and Al^{3+}/Disubstituted 3-hydroxy-4-pyridinone complexes

10.2.1. Experimental details

The M^{2+}/*A7* and M^{2+}/*A8* systems were studied experimentally by performing UV – Vis spectrophotometric titrations, in the same range of wavelengths of the ligands protonation measurements ($200 \leq \lambda$ / nm ≤ 400), at I = 0.15 mol L^{-1} in $NaCl_{(aq)}$, T = 298.15 K and different concentrations of bivalent metal cations such as Ca^{2+}, Zn^{2+} and Cu^{2+} ($5.0 \cdot 10^{-6} \leq c_{M^{2+}}$ / mol $L^{-1} \leq 1.5 \cdot 10^{-5}$) and ligands ($1.0 \cdot 10^{-5} \leq c_L$/ mol $L^{-1} \leq 2.1 \cdot 10^{-5}$), in the pH range 2.0 – 11.0, and in no case the formation of scarcely soluble species occurred during the experiments.

The investigation on the interactions of Al^{3+}/disubstituted 3-hydroxy-4-pyridinones was performed by carrying out potentiometric (ISE–H^+) and UV-Vis spectrophotometric measurements at I = 0.15 mol L^{-1} in $NaCl_{(aq)}$, T = 298.15 K and at the same concentration ranges of ligands and metal cations used for the study of the Al^{3+}/monosubstituted 3-hydroxy-4-pyridinones complexes.

The values of the protonation constants of the two ligands used for the calculations are reported in Table 9.4, while the hydrolysis reactions of the metal cations was already investigated and the several data were published in the literature. [138-140]

The stability constants of the complexes with the four metal cations refer to the following equilibrium:

$$pM^{n+} + qL^{z-} + rH^{+} = M_pL_qH_r^{(pn+r-qz)} \qquad \beta_{pqr} \quad (10.7)$$

10.2.2. M^{2+}/disubstituted 3-hydroxy-4-pyridinones systems

The elaboration of the experimental data using the Hyperquad computer program for the study of the interactions between *A7* and the bivalent metal cations (M^{2+}), showed a common speciation model constituted by three species, namely the M(*A7*)H, M(*A7*) and M_2(*A7*).

The experimental formation constants of the M^{2+}/*A7* complexes, obtained by UV-Vis spectrophotometric measurements, at I = 0.15 mol L^{-1} in $NaCl_{(aq)}$ and T = 298.15 K are reported in Table 10.4.

Table 10.4. Experimental stability constants[a)] of M^{2+}/*A7* complexes determined by UV-Vis spectrophotometry, at I = 0.15 mol L^{-1} in $NaCl_{(aq)}$ and T = 298.15 K

Species	Ca^{2+}	Zn^{2+}	Cu^{2+}
	$\log\beta_{pqr}$	$\log\beta_{pqr}$	$\log\beta_{pqr}$
M(*A7*)H	29.93±0.05[b)]	28.76±0.02	32.85±0.10
M(*A7*)	19.60±0.03	18.59±0.09	20.48±0.03
M_2(*A7*)	36.88±0.07	35.74±0.05	41.97±0.05

[a)] $\log\beta_{pqr}$ refers to eq. (10.7); [b)] ±Std. Deviation.

From the analysis of the experimental data, it was possible to note that the stability constant values follow the trend: Cu^{2+} > Ca^{2+}> Zn^{2+}. The formation constant of Cu(*A7*) species is higher than the other ones, this is due to the higher affinity of copper towards the amino groups. As an example, the distribution of the Cu^{2+}/*A7* complex species is reported in Figure 10.5, at I = 0.15 mol L^{-1} in $NaCl_{(aq)}$ and T = 298.15 K.

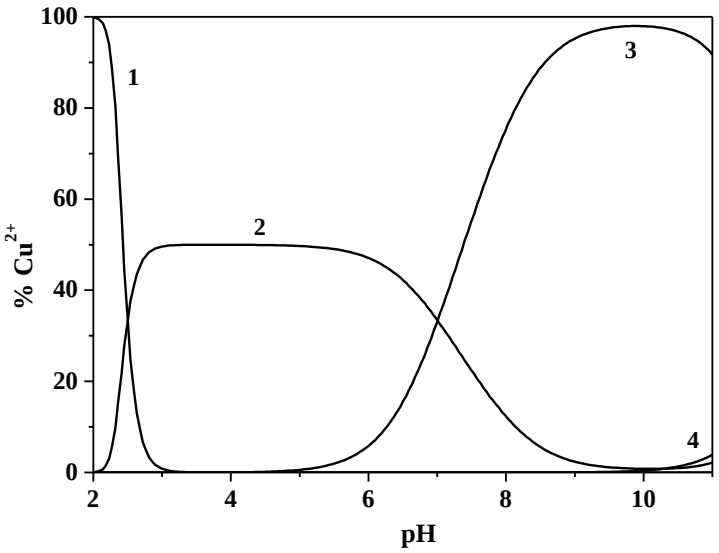

Figure 10.5. Speciation diagram of Cu^{2+}/*A7* complexes at I = 0.15 mol L^{-1} in $NaCl_{(aq)}$ and T = 298.15 K. $c_{Cu^{2+}}$ = 7.0·10^{-6} mol L^{-1}; c_{A7} = 1.8·10^{-5} mol L^{-1}. Species: 1. free Cu^{2+}; 2. Cu_2(*A7*); 3. Cu(*A7*)H; 4. Cu(*A7*).

The binuclear Cu_2(*A7*) species reaches the 50% at pH ~ 4.3, while the protonated Cu(*A7*)H is the main species: it forms at pH ~ 4.7 and achieves the 98% of formation at pH ~ 9.8.

At last, the Cu(*A7*) complex is the minor species and its formation percentage does not exceed the 10%, in all experimental conditions of the UV – Vis spectrophotometric measurements performed.

As an example, the profile of the titration curves of the UV-Vis spectrophotometric measurements of Ca^{2+}/*A7* at different pH values at I = 0.15 mol L^{-1} in $NaCl_{(aq)}$ and T = 298.15 K, is reported in Figure 10.6. Also in this case, the same behavior (bathochromic shift) of both protonation and formation reactions is observed.

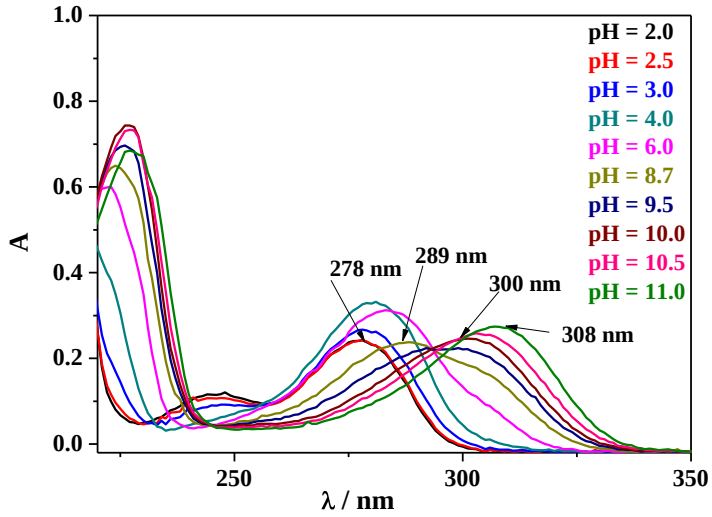

Figure 10.6. Absorption spectra of Ca^{2+}/*A7* complexes at I = 0.15 mol L^{-1} in $NaCl_{(aq)}$, T = 298.15 K and different pH values. $c_{Ca^{2+}}$ =8.0·10^{-6} mol L^{-1}; c_{A7} = 2.0·10^{-5} mol L^{-1}.

In the case of M^{2+}/*A8* systems, the formation of the M(*A8*)H_2, M(*A8*)H, M(*A8*) and M_2(*A8*) species was determined. Concerning the Cu^{2+}/*A8* system, the Cu(*A8*)H_2 species was not found. The experimental formation constants of the complexes obtained by UV-Vis spectrophotometry, at I = 0.15 mol L^{-1} in $NaCl_{(aq)}$ and T = 298.15 K, are reported in Table 10.5.

Table 10.5. Experimental stability constants[a)] of M^{2+}/*A8* complexes determined by UV-Vis spectrophotometric data, at I = 0.15 mol L^{-1} in $NaCl_{(aq)}$ and T = 298.15 K

Species	Ca^{2+}	Zn^{2+}	Cu^{2+}
	$\log\beta_{pqr}$	$\log\beta_{pqr}$	$\log\beta_{pqr}$
M(*A8*)H_2	33.95±0.04	34.32±0.03	/
M(*A8*)H	29.70±0.02	29.77±0.02	31.73±0.02
M(*A8*)	19.83±0.01	19.85±0.07	21.08±0.01
M_2(*A8*)	36.37±0.02	36.42±0.05	41.62±0.01

[a)] $\log\beta_{pqr}$ refers to eq. (10.7); [b)] ±Std. Deviation.

The stability constant values related to the Ca^{2+}/*A8* and Zn^{2+}/*A8* systems are similar, while the stability of the Cu^{2+}/*A8* complexes is higher. As an example of distribution of the species, in

Figure 10.7 the speciation diagram of Ca^{2+}/*A8* complexes at I = 0.15 mol L^{-1} in $NaCl_{(aq)}$ and T = 298.15 K, is reported.

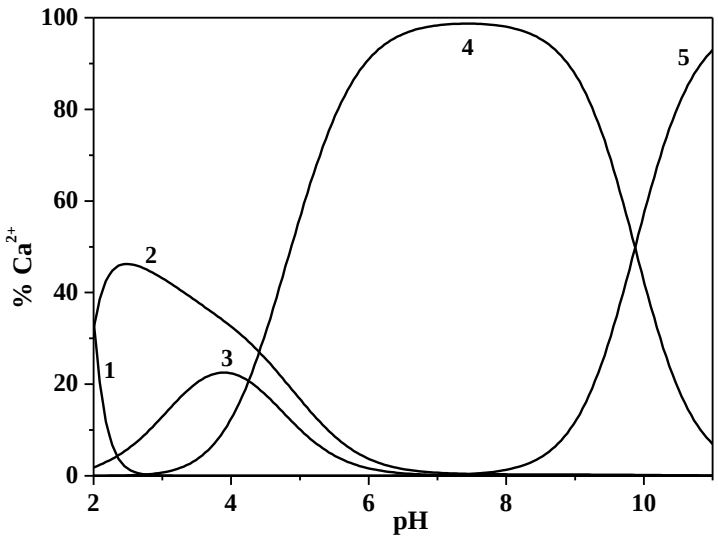

Figure 10.7. Speciation diagram of Ca^{2+}/*A8* complexes at I = 0.15 mol L^{-1} in $NaCl_{(aq)}$ and T = 298.15 K. $c_{Ca^{2+}}$ = $8.0 \cdot 10^{-6}$ mol L^{-1}; c_{A8} = $2.0 \cdot 10^{-5}$ mol L^{-1}. Species: 1. free Ca^{2+}; 2. Ca_2(*A8*); 3. Ca(*A8*)H_2; 4. Ca(*A8*)H; 5. Ca(*A8*).

For all the complexes the formation percentages exceeds the 25%. The main species are the Ca(*A8*)H, that forms at pH ~ 2.3 and is present during all the pH range investigated and the Ca(*A8*) that achieves the 90% of formation at pH ~ 11.

Similarly to the M^{2+}/*A7* systems, also the investigation on the interactions between the three metal cations and the ligand *A8*, revealed very similar absorption spectra to each other and, in all the cases, the profile of the titration curves varies significantly with pH and the usual band at $\lambda_{max\ absorption}$ = 278 nm which undergoes to a bathochromic shift.

10.2.3. Al^{3+}/ disubstituted 3-hydroxy-4-pyridinones systems

The study of the interactions of Al^{3+} with the two disubstituted ligands *A7* and *A8*, at I = 0.15 mol L^{-1} in $NaCl_{(aq)}$ and T = 298.15 K, showed in both cases a common speciation model, constituted by three species, such as Al(*L*)H_2, Al(*L*)H and Al_2(*L*), in the pH range 2.0 – 7.5 and 2.0 – 11.0, for potentiometric and UV – Vis spectrophotometric measurements, respectively, without the formation of scarcely soluble species.

The analysis of potentiometric data by BSTAC and STACO computer programs and of UV – Vis spectrophotometric ones using the Hyperquad, led to the refinement of the stability constant values of the complexes which are in good accordance between the two analytic techniques, as reported in Table 10.6.

Table 10.6. Experimental stability constants[a)] of Al^{3+}/*A7* and Al^{3+}/*A8* systems determined by potentiometric and UV – Vis spectrophotometric data, at I = 0.15 mol L^{-1} in $NaCl_{(aq)}$ and T = 298.15 K

Species	Potentiometry (ISE – H^+)	UV – Vis Spectrophotometry
	$\log\beta_{pqr}$	$\log\beta_{pqr}$
Al(*A7*)H_2	43.75±0.05[b)]	44.49±0.01
Al(*A7*)H	39.53±0.10	39.54±0.02
Al_2(*A7*)	47.10±0.08	47.259±0.008
Al(*A8*)H_2	31.31±0.05	31.77±0.07
Al(*A8*)H	28.85±0.02	29.24±0.02
Al_2(*A8*)	30.95±0.01	31.18±0.03

[a)] $\log\beta_{pqr}$ refers to eq. (10.7); [b)] ±Std. Deviation.

Figures 10.8 and 10.9 show the distribution of the species *vs.* pH, determined by potentiometric data at I = 0.15 mol L^{-1} in $NaCl_{(aq)}$ and T = 298.15 K of Al^{3+}/*A7* and Al^{3+}/*A8* complexes, respectively.

In the first case, Figure 10.8 shows that Al^{3+} is already complexed at acidic pH. The binuclear Al_2(*A7*) and the diprotonated Al(*A7*)H_2 species reach formation percentages of 48% and 77% at pH ~ 2 and pH ~ 3.5, respectively. The Al(*A7*)H is the main species reaching the 98% at pH ~ 2.4.

In the case of the Al^{3+}/*A8* system, Figure 10.9 shows that Al_2(*A8*) reaches the 36% of formation at pH ~ 2.6. The Al(*A8*)H_2 species is the species with the lower formation percentage, in fact it achieves 13% at pH ~ 3.1.

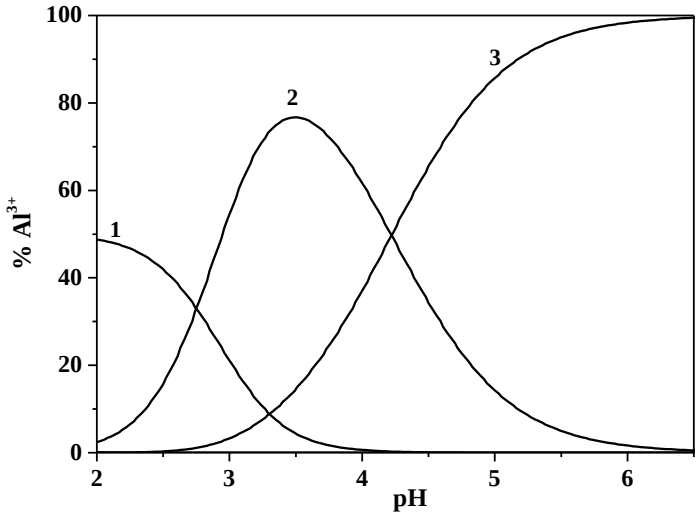

Figure 10.8. Speciation diagram of Al^{3+}/*A7* complexes at I = 0.15 mol L^{-1} in $NaCl_{(aq)}$ and T = 298.15 K. $c_{Al^{3+}}$ = 0.0008 mol L^{-1}; c_{A7} = 0.002 mol L^{-1}. Species: 1. Al_2(*A7*); 2. Al(*A7*)H_2; 3. Al(*A7*)H.

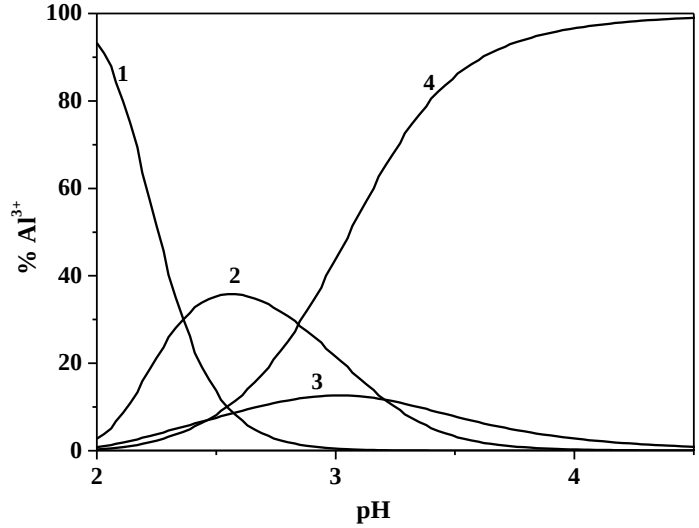

Figure 10.9. Speciation diagram of Al^{3+}/*A8* complexes at I = 0.15 mol L^{-1} in $NaCl_{(aq)}$ and T = 298.15 K. $c_{Al^{3+}}$ = 0.0008 mol L^{-1}; c_{A8} = 0.002 mol L^{-1}. Species: 1. free Al^{3+}; 2. Al_2(*A8*); 3. Al(*A8*)H_2; 4. Al(*A8*)H.

In the literature, Gama et al.[39] published some data about the complexes of Al^{3+} with similar disubstituted 3-hydroxy-4-pyridinones, such as ligand derivatives of the

ethylenediaminetetraacetic acid, so-called EDTAPr(3,4-$HP)_2$. The Author obtained the same speciation model of that reported here, also in that case it was not possible determined the Al*L* species. The speciation scheme presented in the literature reported other species, here not determined, as Al(*L*)H_3 and Al(*L*)H_4 and polynuclear $Al_2(L)_3H$ and $Al_2(L)_3$ species.

Chapter 11

Sequestering ability: $pL_{0.5}$

11.1. Sequestering ability of ligands towards metal cations

The simple analysis of the stability constants of metal - ligand complexes is not always sufficient to evaluate, , the sequestering ability of a ligand towards a metal cation, because of the network of interactions that takes place in a multicomponent system, furthermore the binding ability of a ligand depends on pH, ionic strength, temperature. Therefore, it is particularly difficult, often impossible, to compare the sequestering ability of two different systems by the simple analysis of the stability constants, especially if the metal - ligand systems have different speciation. The problem becomes bigger if the system of interest is located in multicomponent solutions, where there is the simultaneous presence of the metal component and / or more organic and inorganic ligands.

To overcome this difficulty in the past, the research group[13] proposed the $pL_{0.5}$, an empirical parameter which represents the total concentration of ligand necessary to sequester the 50% of a metal cation present in trace (10^{-12} mol L^{-1}) in solution. This parameter is described through a sigmoidal type Boltzmann equation, reported in eq. (11.1):

$$x_M = \frac{1}{1+10^{(pL-pL_{0.5})}} \qquad (11.1)$$

where x_M is the mole fraction of metal complexed by the ligand, pL = -log c_L and $pL_{0.5}$ = -log c_L, when x_M = 0.5. The sequestering ability can be graphically represented by a dose – response curve, represented in Figure 11.1, characterized by asymptotes equal to 1 for pL→-∞ and 0 for pL → +∞, obtained by plotting the mole fraction or the percentage of the metal complexed *vs.* the pL values.

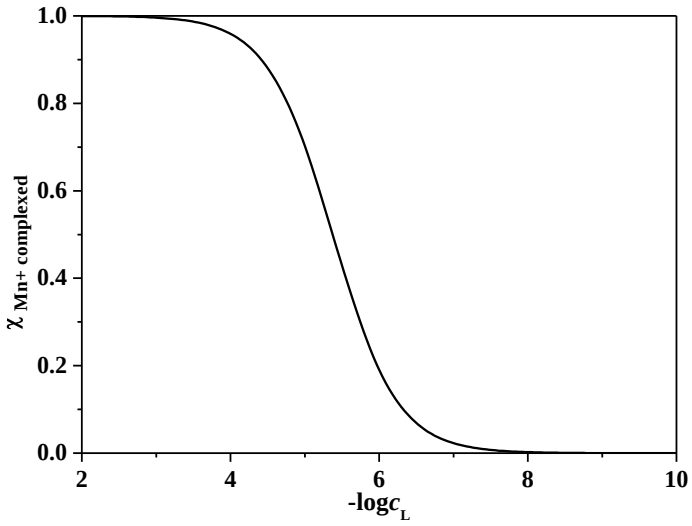

Figure 11.1. Typical dose-response curve representing the sequestering ability of a ligand towards a metal cation.

High $pL_{0.5}$ values are linked to a greater sequestering ability of a ligand towards a metal cation than lower values. It is a quantitative parameter which allows to determine the sequestering ability of a ligand in different experimental conditions (pH, ionic strength, ionic medium, temperature), and it is independent by the analytical concentration of the ion when it is present in trace.

Moreover, all the interactions in the system such as the protonation of the ligand, the hydrolysis of the metal cation and the interactions with other components, are taken into account in the speciation model, but are excluded from the calculation of $pL_{0.5}$ values. In this way, this parameter, can quantify the sequestering ability of a ligand, regardless of all the competition reactions and the speciation model, and allows the comparison between the sequester ability of different ligands.

The quantification of the sequestering ability is of great importance both in the remediation of polluted sites, detoxification processes and water treatment. All these processes involve the use of a chelating agent, and the knowledge of this parameter can be useful for optimizing the working conditions.

The sequestering ability of all the ligands, commercially available or synthetized and reported in this thesis, towards the metal cations Ca^{2+}, Zn^{2+}, Cu^{2+} and Al^{3+} was studied in different experimental conditions.

11.1.1. M^{n+}/commercially available ligands systems

The study of the sequestering ability of the commercially available ligands such as Gantrez® AN169 (GTZ^{4-}), citric acid (Cit^{3-}) and orthosilicic acid ($H_2SiO_4^{2-}$) towards the metal cations was performed at different pH values, temperatures and ionic strengths.

Table 11.1 reports the $pL_{0.5}$ values for some metal – ligand systems studied in this thesis, calculated at various experimental conditions in $NaCl_{(aq)}$.

Table 11.1. $pL_{0.5}$ values of M^{n+}/commercially available ligands systems at different pH values, temperatures and ionic strengths in $NaCl_{(aq)}$

System	T / K	I / mol L^{-1}	pH	$pL_{0.5}$
Zn^{2+}/GTZ^{4-}	298.15	0.10	7.4	5.35
Zn^{2+}/GTZ^{4-}	298.15	0.25	7.4	5.05
Zn^{2+}/GTZ^{4-}	298.15	1.00	7.4	4.75
Al^{3+}/GTZ^{4-}	298.15	1.00	2.5	0.16
Al^{3+}/GTZ^{4-}	298.15	1.00	3.5	2.64
Al^{3+}/GTZ^{4-}	298.15	1.00	4.0	3.62
Al^{3+}/GTZ^{4-}	298.15	1.00	5.0	5.37
Al^{3+}/GTZ^{4-}	298.15	1.00	6.0	6.29
Al^{3+}/Cit^{3-}	298.15	1.00	4.0	5.82
Al^{3+}/Cit^{3-}	283.15	0.25	5.0	7.08
Al^{3+}/Cit^{3-}	298.15	0.25	5.0	7.66
Al^{3+}/Cit^{3-}	318.15	0.25	5.0	8.34
$Al^{3+}/H_2SiO_4^{2-}$	298.15	0.10	4.0	1.82
$Al^{3+}/H_2SiO_4^{2-}$	298.15	1.00	4.0	1.11

The analysis of the $pL_{0.5}$ values evidences that for all the metal – ligand systems the sequestering ability decreases with increasing the ionic strength in $NaCl_{(aq)}$ and increases with increasing the pH and the temperature.

Some examples of the sequestering ability of the ligands towards the metal cations in different experimental conditions are shown in Figures 11.2 – 11.3.

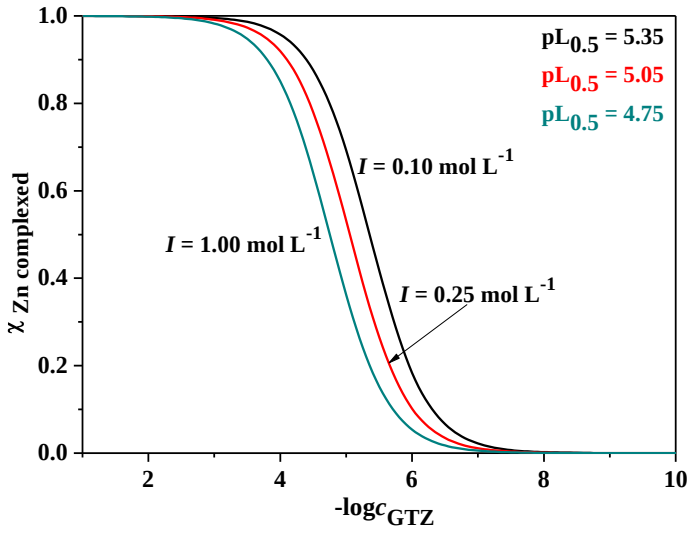

Figure 11.2. Sequestration diagram of Gantrez® AN169 towards Zn^{2+} at pH = 7.4. Molar fraction of metal cation complexed *vs.* the total ligand concentration (as -log*c*) at different ionic strengths in $NaCl_{(aq)}$ and T = 298.15 K.

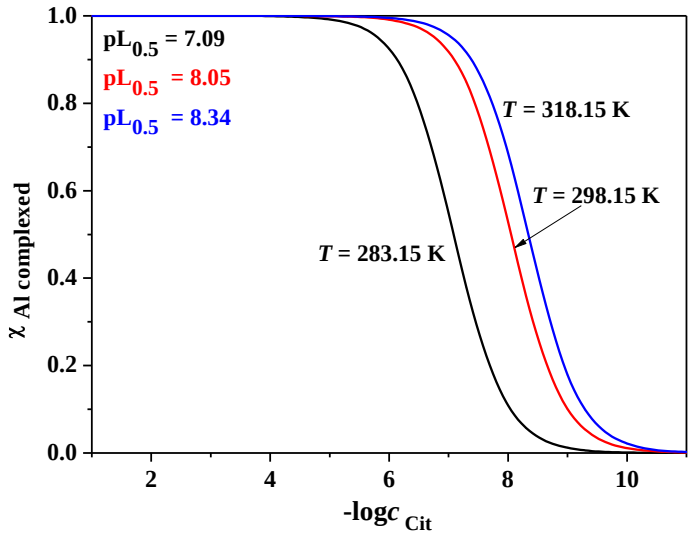

Figure 11.3. Sequestration diagram of citric acid towards Al^{3+} at pH = 5.0. Molar fraction of metal cation complexed *vs.* the total ligand concentration (as -log*c*) at I = 1.00 mol L^{-1} in $NaCl_{(aq)}$ and different temperatures.

In the case of the Mg^{2+}/GTZ^{4-} and Sn^{2+}/GTZ^{4-} systems it was not possible to calculate the $pL_{0.5}$ values because at the trace concentrations of these metals, the formation percentage of the $M_2(GTZ)_{(aq)}$ species is not significative.

An alternative way to have information about the tendency of the ligand to sequester the bivalent metal cations (also considering the case of Zn^{2+} for comparisons) was to calculate the sum of the formation percentages of the complexes, and their mole fractions, at fixes c_M = 0.001 mol L^{-1} and different concentrations of ligands ($0.001 \leq c_L$ / mol $L^{-1} \leq 0.006$), at I = 0.10 mol L^{-1} in $NaCl_{(aq)}$ and T = 298.15 K. Plotting these values *vs.* the –log*c*, it was possible to see that the ligand tends to sequester better the metal cations in the order:

$$Sn^{2+} > Zn^{2+} > Mg^{2+}.$$

Concerning the Al^{3+}/L^{z-} systems, as reported in Figure 11.4, at pH = 4.0, I = 1.00 mol L^{-1} in $NaCl_{(aq)}$ and T = 298.15 K, it is possible to observe that the sequestering ability follows this order:

$$Cit^{3-} > GTZ^{4-} > H_2SiO_4^{2}.$$

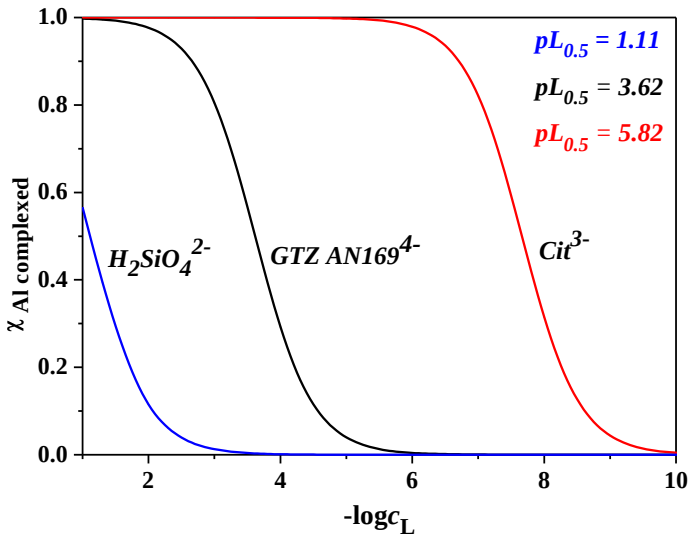

Figure 11.4. Sequestration diagram of orthosilicic acid, Gantrez® AN169 and citric acid towards Al^{3+} at pH = 4.0. Molar fraction of metal cation complexed *vs.* the total ligand concentration (as -log*c*) at I = 1.00 mol L^{-1} in $NaCl_{(aq)}$ and T = 298.15 K.

11.1.2. M^{n+}/synthetic ligands systems

The study of the sequestering ability of the 3-hydroxy-4-pyridinone ligands towards Al^{3+} and, in the case of the disubstituted derivatives *A7* and *A8*, also to bivalent metal cations (M^{2+} = Ca^{2+}, Zn^{2+}, Cu^{2+}), was performed at different pH values, at I = 0.15 mol L^{-1} in $NaCl_{(aq)}$ and T = 298.15 K.

For the Al^{3+}/3-hydroxy-4-pyridinones complexes, the $pL_{0.5}$ values increase with increasing pH values until the sequestering ability of the ligands starts to decrease, owing to the precipitation of $Al(OH)_{3(s)}$.

Table 11.2 reports the $pL_{0.5}$ values of Al^{3+}/3,4-hydroxypyridinone systems calculated at different pH, I = 0.15 mol L^{-1} in $NaCl_{(aq)}$ and T = 298.15 K.

In Figure 11.5 an example of dose – response sequestering ability curve of the ligand *A3* towards Al^{3+} at different pH values is reported.

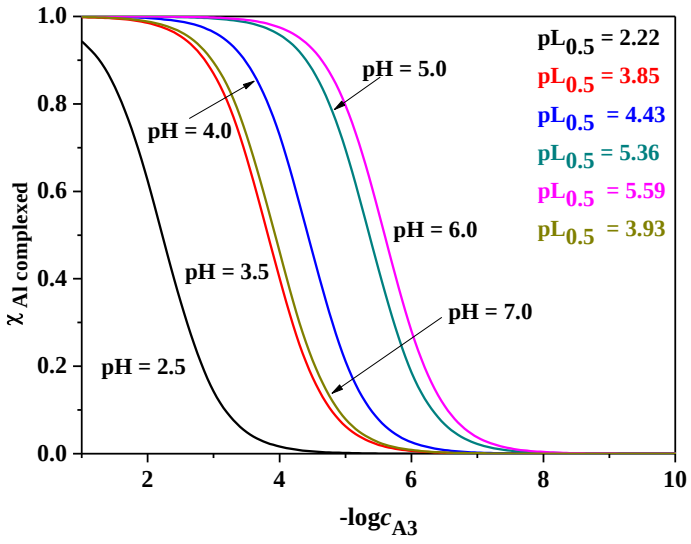

Figure 11.5. Sequestration diagram of *A3* ligand towards Al^{3+} at different pH values. Molar fraction of metal cation complexed *vs.* the total ligand concentration (as -log*c*) at I = 0.15 mol L^{-1} in $NaCl_{(aq)}$ and T = 298.15 K.

Table 11.2. $pL_{0.5}$ values of Al^{3+}/3,4-hydroxypyridinone systems at different pH, I = 0.15 mol L^{-1} in $NaCl_{(aq)}$ and T = 298.15 K

System	pH	$pL_{0.5}$
Al^{3+}/*KC*	4.0	7.36
Al^{3+}/*PropKC*	4.0	5.77
Al^{3+}/*A5*	2.0	2.70
Al^{3+}/*A5*	3.5	5.39
Al^{3+}/*A5*	4.0	6.50
Al^{3+}/*A5*	5.0	8.12
Al^{3+}/*A5*	6.0	8.33
Al^{3+}/*A5*	7.0	6.29
Al^{3+}/*A6*	4.0	6.96
Al^{3+}/*Py-Orn*	2.5	3.04
Al^{3+}/*Py-Orn*	3.5	5.62
Al^{3+}/*Py-Orn*	4.0	6.61
Al^{3+}/*Py-Orn*	5.0	8.01
Al^{3+}/*Py-Orn*	6.0	8.66
Al^{3+}/*Py-Orn*	7.0	7.17
Al^{3+}/*A3*	2.5	2.22
Al^{3+}/*A3*	3.0	3.85
Al^{3+}/*A3*	4.0	4.43
Al^{3+}/*A3*	5.0	5.36
Al^{3+}/*A3*	6.0	5.59
Al^{3+}/*A3*	7.0	3.93
Al^{3+}/*A7*	4.0	12.32
Al^{3+}/*A7*	7.0	12.66
Al^{3+}/*A8*	2.5	2.87
Al^{3+}/*A8*	4.0	8.42
Al^{3+}/*A8*	7.0	9.82

The variations of $pL_{0.5}$ as a function of different parameters such as pH, temperature and ionic strength, as already written, often follow linear or polynomial patterns, as can be seen in

Figure 11.6 for the dependence of $pL_{0.5}$ on pH for the Al^{3+}/*A3* system, at I = 0.15 mol L^{-1} in $NaCl_{(aq)}$ and T = 298.15 K.

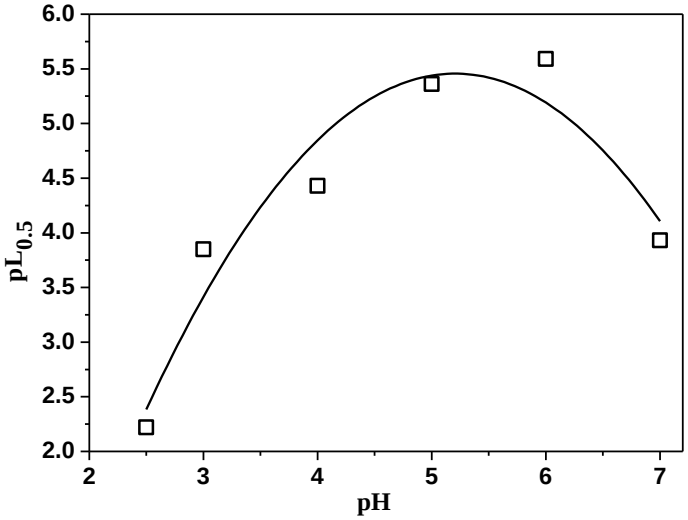

Figure 11.6. Trend of $pL_{0.5}$ vs. pH values of Al^{3+}/*A3* system at I = 0.15 mol L^{-1} in $NaCl_{(aq)}$ and T = 298.15 K.

From the analysis of the calculated $pL_{0.5}$ values in the same experimental conditions, at pH = 4.0, I = 0.15 mol L^{-1} in $NaCl_{(aq)}$ and T = 298.15 K, it is possible to note that the presence of carboxylic groups increases the sequestering ability of the ligands towards Al^{3+}.

As it can be observed in Figure 11.7 and from the data in Table 11.2, the $pL_{0.5}$ values for the Al^{3+}/*A3* system, are lower than the other ones. This is due to the fact that no carboxylate groups are present on *A3*. Furthermore, also the length of the alkyl moiety has an important role.

The ligands *KC* and *A6* have one and two $–CH_2$ groups on the alkyl chain, respectively, and conversely to all the other compounds that have propyl groups, show a bigger sequestering ability, that decrease with increasing the length of the alkyl chain.

In the case of Al^{3+}/*A7* and Al^{3+}/*A8* systems, the $pL_{0.5}$ values and are very high because of the presence of the moieties derived from the DTPA and NTA complexones, of the two 3,4-hydroxypyridinone chains and of the absence of amino groups.

On this basis, in the same experimental conditions already mentioned, it is possible to observe that the sequestering ability follows this order:

A7 > *A8* > *KC* > *A6* > *Py-Orn* > *A5* > *PropKC* >*A3*

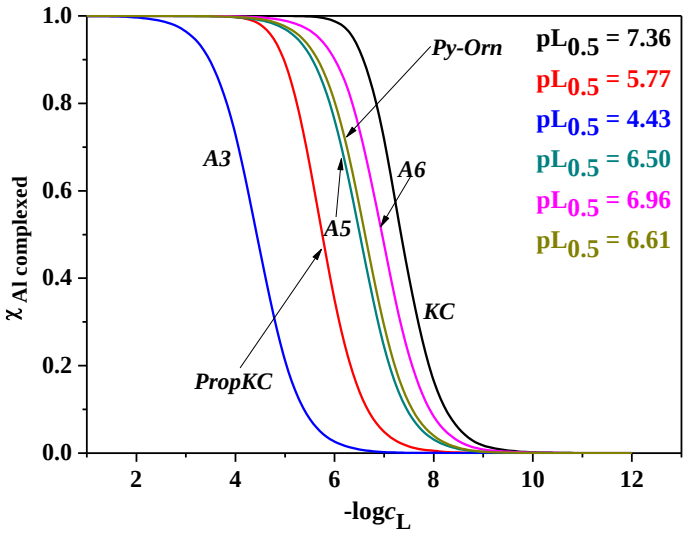

Figure 11.7. Sequestration diagram of monosubstituted 3-hydroxy-4-pyridinone ligands towards Al^{3+} at pH = 4.0. Molar fraction of metal cation complexed *vs.* the total ligands concentration (as -log*c*) at I = 0.15 mol L^{-1} in $NaCl_{(aq)}$ and T = 298.15 K.

In the case of the M^{2+}/disubstituted 3-hydroxy-4-pyridinones, the $pL_{0.5}$ are higher than the corresponding values calculated for the Al^{3+}/*A7* and Al^{3+}/*A8* systems. They increase with increasing pH until pH ≥ 7 where the sequestering ability starts to assume similar values to each other and no formation of scarcely soluble species interferes with the sequestration of the bivalent metal cations by both the ligands.

Table 11.3 reports the $pL_{0.5}$ values of M^{2+}/disubstituted 3,4-hydroxypyridinones systems calculated at different pH values, I = 0.15 mol L^{-1} in $NaCl_{(aq)}$ and T = 298.15 K, while in Figure 11.8 the trend of the $pL_{0.5}$ determined for the Ca^{2+}/*A7* systems *vs.* pH values is reported.

From the analysis of the $pL_{0.5}$ values, obtained at pH = 7.0, I = 0.15 mol L^{-1} in $NaCl_{(aq)}$ and T = 298.15 K for the sequestration of the ligand *A7* towards Ca^{2+}, Cu^{2+} and Zn^{2+}, it is possible to observe that the sequestering ability of the ligand follows the order:

$$Cu^{2+} > Ca^{2+} > Zn^{2+}.$$

Instead, from the comparison of the $pL_{0.5}$ obtained for the M^{2+}/*A8* systems in the same experimental conditions, it is possible to note that the $pL_{0.5}$ values of 12.97, 13.01 and 13.03 calculated for Ca^{2+}, Zn^{2+} and Cu^{2+}, respectively, at pH = 7.0, I = 0.15 mol L^{-1} in $NaCl_{(aq)}$ and T = 298.15 K, are very similar to each other.

Table 11.3. $pL_{0.5}$ values of Al^{3+}/3,4-hydroxypyridinone ligands systems at different pH, I = 0.15 mol L^{-1} in $NaCl_{(aq)}$ and T = 298.15 K

System	pH	$pL_{0.5}$
Ca^{2+}/*A7*	4.0	0.36
Ca^{2+}/*A7*	5.0	4.21
Ca^{2+}/*A7*	6.0	10.43
Ca^{2+}/*A7*	7.0	12.97
Ca^{2+}/*A7*	8.0	13.02
Ca^{2+}/*A7*	9.0	13.03
Ca^{2+}/*A8*	7.0	13.03
Zn^{2+}/*A7*	7.0	12.78
Zn^{2+}/*A8*	7.0	13.01
Cu^{2+}/*A7*	7.0	13.02
Cu^{+}/*A8*	7.0	13.03

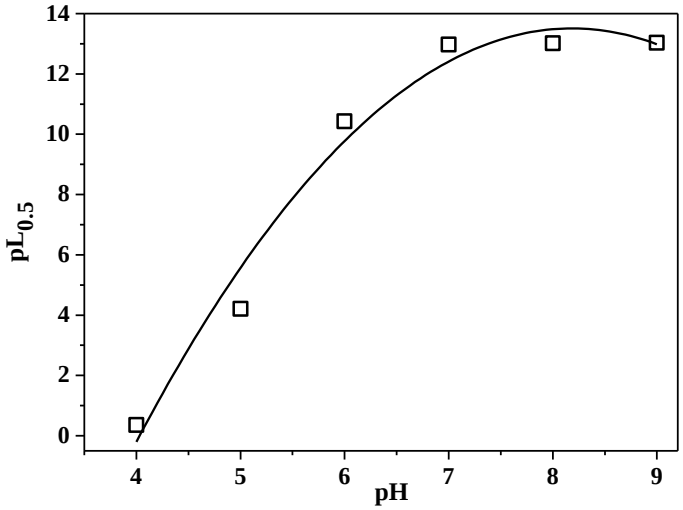

Figure 11.8. Trend of $pL_{0.5}$ vs. pH values of Ca^{2+}/*A7* system at I = 0.15 mol L^{-1} in $NaCl_{(aq)}$and T = 298.15 K.

Chapter 12

Conclusions

The research work performed during the three years of PhD course has been focused on the study of speciation of bivalent and trivalent metal cations in the presence of ligands (L^{z-}) of different interest in ionic medium NaCl aqueous solutions, since it is the main inorganic component of many natural[6,7] and biological fluids.[8]
The ligands of interest can be divided in two categories:

1. ligands commercially available, such as the Gantrez®AN169, the citric acid and the orthosilicic acid;

2. ligands of synthesis, the 3-hydroxy-4-pyridinones, derivatives of the 1,2-dimethyl-3-hydroxy-4-pyridinone, better known as Deferiprone.

For all the systems, the study dealt with the determination of the acid – base properties of the ligands and the metal cations (protonation and hydrolysis, respectively), at different ionic strengths and temperatures. The dependence of the determined stability constants on these parameters has been modeled by a modified Debye-Hückel equation.
The investigated metal-ligand systems investigated were:

1. Mg^{2+}/ Gantrez® AN169;
2. Sn^{2+}/ Gantrez® AN169;
3. Zn^{2+}/ Gantrez® AN169;
4. Al^{3+}/ Gantrez® AN169;
5. Al^{3+}/ citric acid;
6. Al^{3+}/ orthosilicic acid;
7. Al^{3+}/ monosubstituted 3-hydroxy-4-pyridinones;

8. Al^{3+}/ disubstituted 3-hydroxy-4-pyridinones;
9. Ca^{2+}/ disubstituted 3-hydroxy-4-pyridinones;
10. Zn^{2+}/ disubstituted 3-hydroxy-4-pyridinones;
11. Cu^{2+}/ disubstituted 3-hydroxy-4-pyridinones.

Concerning the interactions of Gantrez® AN169 with bivalent metal cations, the formation of the $M_2(GTZ)$ species was observed for all the cations, while in the case of the Zn^{2+}/GTZ^{4-} system the $Zn(GTZ)H_2$ and $Zn(GTZ)$ species also were determined. The speciation scheme obtained from the investigation of Al^{3+}/GTZ^{4-} interactions was more complexes since four species, namely $Al(GTZ)H$, $Al(GTZ)$, $Al(GTZ)(OH)_2$ and $Al_2(GTZ)_2(OH)_2$ were formed.

The Al^{3+}/citric acid system was studied at different ionic strengths and temperatures and five species were determined, such as $Al(Cit)H$, $Al(Cit)_{(aq)}$, $Al(Cit)OH$, $Al(Cit)_2$ and $Al_3(Cit)_3(OH)_4$. The stability constants obtained are in agreement with the data already reported in the literature. Finally, in the case of the Al^{3+}/orthosilicic acid only the protonated $[AlH(H_2SiO_4)]^{2+}$ species was determined.

Regarding the 3-hydroxy-4-pyridinone products, their synthesis was performed under the supervision of the Prof. Maria Amélia Santos, at the Centro de Química Estrutural of the Instituto Superior Técnico (Universidade de Lisboa). The compounds obtained were 3-hydroxy-4-pyridinone derivatives of aspartic anhydride, of diethylenetriaminepentaacetic bisanhydride (DTPA bisanhydride) and of nitrilotriacetic acid (NTA), respectively. The study of the acid – base properties and of the binding ability of these and other similar synthetic compounds towards the Al^{3+} showed various speciation models, on the basis of the different structures and functional groups present on the molecules. Considering the Al*L* species stability of the complexes follows the trend (at I = 0.15 mol L^{-1} in $NaCl_{(aq)}$ and T = 298.15 K):

$$(Py\text{-}Orn) > (A5) > (A6) > (A3) > (KC) \sim (PropKC)$$

Furthermore, the interactions of the derivatives of DTPA bisanhydride and NTA with bivalent metal cations such as Ca^{2+}, Cu^{2+} and Zn^{2+} were investigated. The complexes formed were protonated, simple metal – ligand and polynuclear species.

At I = 0.15 mol L^{-1} in $NaCl_{(aq)}$ and T = 298.15 K, the stability of the $M^{2+}/A7$ species follows the trend:

$$Cu(A7) > Ca(A7) > Zn(A7)$$

while in the case of $M^{2+}/A8$ systems the order is the following:

$$Cu(A8) > Zn(A8) \sim Ca(A8).$$

Finally, the sequestering ability of all the ligands studied towards the metal cations was investigated by the calculation of the $pL_{0.5,}$ an empirical parameter already proposed by our research group, which represents the total concentration of ligand necessary to sequester the 50% of a given metal cation present in trace in solution. In the case of the Mg^{2+}/GTZ^{4-} and Sn^{2+}/GTZ^{4-} systems, the classical calculation of $pL_{0.5}$ was not possible because the formation percentage of the $M_2(GTZ)$ species was null for c_M is in trace (10^{-12} mol L^{-1}, as it is for the $pL_{0.5}$ calculation). Nevertheless, the sequestration diagrams equally were built, but considering a fixed c_M (not trace). The sequestering ability of the Gantrez® AN169 towards the M^{2+}, at pH ~ 5.8, follows the trend:

$$Sn^{2+} > Zn^{2+} > Mg^{2+}.$$

In the case of the Al^{3+}/L^{z-} systems, at pH = 4.0, I = 1.00 mol L^{-1} in $NaCl_{(aq)}$ and T = 298.15 K, the trend is:

$$Cit^{3-} > GTZ^{4-} > H_2SiO_4^{2}.$$

Concerning the investigation on Al^{3+}/3-hydroxy-4-pyridinone products, at pH = 4.0, I = 0.15 mol L^{-1} in $NaCl_{(aq)}$ and T = 298.15 K, the sequestering ability trend is:

$$A7 > A8 > KC > A6 > Py\text{-}Orn > A5 > PropKC > A3$$

Moreover, the study of the behavior of the ligand *A7* towards Ca^{2+}, Cu^{2+} and Zn^{2+} at pH = 7.0, I = 0.15 mol L^{-1} in $NaCl_{(aq)}$ and T = 298.15 K showed that the sequestering ability of this ligand is:

$$Cu^{2+} > Ca^{2+} > Zn^{2+}.$$

Instead, in the case of the $M^{2+}/A8$ systems, it was possible to note that the sequestering ability of *A8* towards Ca^{2+}, Zn^{2+} and Cu^{2+} is very similar ($pL_{0.5}$ = 12.97, 13.01 and 13.03, respectively).

Bibliography

1. Kot, A.; Namiesnik, J., The role of speciation in analytical chemistry. *Trends in Analytical Chemistry* **2000,** 19, 69-79.

2. Templeton, D. M.; Ariese, F.; Cornelis, R.; Danielsson, L. G.; Muntau, H.; Van Leeuwen, H. P.; Łobinsky, R., Guidelines for terms related to chemical speciation and fractionation of elements. Definitions, structural aspects, and methological approaches. *Pure and Applied Chemistry* **2000,** 72, (8), 1453-1470.

3. Michalke, B., Element Speciation Analysis. In *Elements and Their Compounds in the Environment*, Merian, E.; Anke, M.; Ihnat, M.; Stoeppler, M., Eds. Wiley-VCH Verlag GmbH: **2008**, 1643-1673..

4. Stoecker, B., Chromium. In *Elements and Their Compounds in the Environment*, Wiley-VCH Verlag GmbH: **2008**, 709-729.

5. Walter, P. B.; Knutson, M. D.; Paler-Martinez, A.; Lee, S.; Xu, Y.; Viteri, F. E.; Ames, B. N., Iron deficiency and iron excess damage mitochondria and mitochondrial DNA in rats. *Proceedings of the National Academy of Sciences U.S.A.* **2002,** 99, (4), 2264-2269.

6. Buffle, J., *Complexation Reactions in Aquatic Systems: an Analytical Approach*. Ellis Horwood: Chichester, **1988**.

7. Millero, F. J., *Physical Chemistry of Natural Waters*. John Wiley & Sons, Inc.: New York, **2001**.

8.Lentner, C., *Geigy Scientific Tables*, 8th Edition. CIBA-Geigy: Basilea, Switzerland, **1981**.

9. Ashland Inc., Performance & Industrial Chemicals-Reference Guide. **2005**, 45.

10. Campbell, M. K.; Farrell, S. O., The citric acid cycle. In *Biochemistry*, 6th Edition; Thomson Brooks/Cole: **2009**, 545-575.

11. Jurkic, L. M.; Cepanec, I.; Pavelic, S. K.; Pavelic, K., Biological and therapeutic effects of ortho-silicic acid and some ortho-silicic acid-releasing compounds: New perspectives for therapy. *Nutrition & Metabolism* **2013,** 10, (1), 2.

12. Santos, M. A.; Chaves, S., 3-hydroxypyridinone derivatives as metal sequestering agents for therapeutic use. *Future Medicinal Chemistry* **2015,** 7, (3), 383-410.

13. Crea, F.; De Stefano, C.; Foti, C.; Milea, D.; Sammartano, S., Chelating agents for the sequestration of mercury(II) and monomethyl mercury(II). *Current Medicinal Chemistry* **2014,** 21, (33), 3819-3836.

14. Acevedo, R. A.; Machón, L.; Chávez, N., Effectiveness of a mouthwash containing Triclosan and Gantrez in the reduction of biofilm and gingivitis: a clinical pilot study. *The Journal of Contemporary Dental Practice* **2009,** 10, (6), E033-40.

15. Glicksman, M., *Advanced in Food Research*. Academic Press. Inc. (London) LTD.: New York, **1963**, 12, 346-348.

16. Mattey, M.; Kristiansen, B., A Brief Introduction to Citric Acid Biotechnology. In *Citric Acid and Biotechnology*, Kristiansen, B.; Mattey, M.; Linde, J., Eds. Taylor and Francis: New York, **1998**.

17. Rudy, H., Citric acid, occurrence, preparation chemistry, physiology, pharmacology, toxicology, pharmaceutical and therapeutic use. *Pharmazie* **1949,** 4, 393-399.

18. Thunberg, T., Occurrence and significance of citric acid in animal organism. *Physiological Reviews* **1953,** 33, 1-12.

19. Apelblat, A., *Citric acid*. Springer: **2014**.

20. Parkes, S., On citric acid. *Philosophical Magazine and Journal of Science* **1815,** 1, (46), 48-60.

21. Grimoux, E.; Adams, P., Synthese de l'ácide citrique. *Comptes rendus hebdomadaires des séances de l'Académie* **1880,** 90, 1252.

22. Krupavathi M.; Sarva Mangala, D., Production of Citric Acid – A Short Review. *International Journal of Development Research* **2015,** 5, (04), 4002-4006.

23. Mailloux, R. J.; Bériault, R.; Lemire, J.; Singh, R.; Chénier, D. R.; Hamel, R. D.; Appanna, V. D., The Tricarboxylic Acid Cycle, an Ancient Metabolic Network with a Novel Twist. *PLoS ONE* **2007,** 2, (8), e690.

24. Akram, M., Citric Acid Cycle and Role of its Intermediates in Metabolism. *Cell Biochemistry and Biophysics* **2014,** 68, (3), 475-478.

25. Greenwood, N. N.; Earnshaw, A., *Chemistry of the elements.* 2nd Edition; Betterworth-Heinemann: Oxford, **1997**.

26. Bowen, H. J. M.; Peggs, A., Determination of the silicon content of food. *Journal of the Science of Food and Agriculture* **1984,** 35, (11), 1225-1229.

27. Jugdaohsingh, R.; Anderson, S. H. C.; Tucker, K. L.; Elliott, H.; Kiel, D. P.; Thompson, R. P. H.; Powell, J. J., Dietary silicon intake and absorption. *The American Journal of Clinical Nutrition* **2002,** 75, 887-893.

28. Reffitt, D. M.; Jugdaohsingh, R.; Thompson, R. P. H.; Powell, J. J., Silicic acid: its gastrointestinal uptake and urinary excretion in man and effects on aluminium excretion. *Journal of Inorganic Biochemistry* **1999,** 76, (2), 141-147.

29. Dobbie, J. W.; Smith, M. J., The silicon content of body fluids. *Scottish Medical Journal* **1982,** 27, (1), 17-19.

30. Carlisle, E. M., Silicon: An Essential Element for the Chick. *Science* **1972,** 178, (4061), 619-621.

31. Eisinge, J.; Clairet, D., Effects of silicon, fluoride, etidronate and magnesium on bone mineral density: a retrospective study. *Magnesium Research* **1993,** 6, (3), 247-249.

32. Gonzalez-Muñoz, M. J.; Meseguer, I.; Sanchez-Reus, M. I.; Schultz, A.; Olivero, R.; Benedí, J.; Sánchez-Muniz, F. J., Beer consumption reduces cerebral oxidation caused by aluminum toxicity by normalizing gene expression of tumor necrotic factor alpha and several antioxidant enzymes. *Food and Chemical Toxicology* **2008,** 46, (3), 1111-1118.

33. Maehira, F.; Ishimine, N.; Miyagi, I.; Eguchi, Y.; Shimada, K.; Kawaguchi, D.; Oshiro, Y., Anti-diabetic effects including diabetic nephropathy of anti-osteoporotic trace minerals on diabetic mice. *Nutrition* **2011,** 27, (4), 488-495.

34. Smith, W. O.; Hammarsten, J. F., Intracellular magnesium in delirium tremens and uremia. *American Journal of Medicine* **1959,** 237, 413.

35. Schwarz, K., Silicon, Fibre, and Atherosclerosis. *The Lancet* **1977,** 309, (8009), 454-457.

36. Schwarz, K.; Ricci, B. A.; Punsar, S.; Karvonen, M. J., Inverse Relation of Silicon in Drinking Water and Atherosclerosis in Finland. *The Lancet* **1977,** 309, (8010), 538-539.

37. Railsback, L. B. Some Fundamentals of Mineralogy and Geochemistry, **2006**.

38. Pavelic, K.; Colic, M.; Subotic, B., Studies in Surface Science and Catalysis. In Elsevier: Amsterdam, **2001**, 135.

39. Gama, S.; Dron, P.; Chaves, S.; Farkasc, E.; Santos, M. A., A bis(3-hydroxy-4-pyridinone)-EDTA derivative as a strong chelator for M^{3+} hard metal ions: complexation ability and selectivity. *Dalton Transactions* **2009**, 6141-6150.

40. Neilands, J. B., Microbial Iron Compounds. *Annual Review of Biochemistry* **1981,** 50, (1), 715-731.

41. Porter, J. B.; Huehns, E. R., The toxic effects of desferrioxamine. *Baillière's Clinical Haematology* **1989,** 2, (2), 459-474.

42. Kontoghiorghes, G. J. Process for producing pyrid-4-ones. **1989**.

43. Santos, M. A., Iões Metálicos em Medicina: Do Diagnóstico à Terapia. *Quimica* **2014,** 132, 23-32.

44. Williamson, A. W., XXII.—On etherification. *Quarterly Journal of the Chemical Society* **1852,** 4, (3), 229-239.

45. Williamson, A. W., Ueber die Theorie der Aetherbildung. *Justus Liebigs Annalen der Chemie* **1851,** 77, (1), 37-49.

46. Harris, R. L. N., Potential wood growth inhibitors. Improved synthesis of mimosine and related 4(1H)-pyridinones. *Australian Journal of Chemistry* **1976,** 29, (6), 1335-1339.

47. Saghaie, L.; Sadeghi, M. M.; Nikazma, A., Synthesis, analysis and determination of partition coefficients of N-arylhydroxypyridinone derivatives as iron chelators. *Reasearch in Pharmaceutical Sciences* **2006,** 1, 40-48.

48. Santos, M. A.; Esteves, M. A.; Vaz, M. C. T.; Goncalves, M. L. S. S., A new iron(III) ion sequestering ligand: synthesis, solution chemistry and electrochemistry. *Journal of the Chemical Society, Dalton Transactions* **1993**, (6), 927-932.

49. Santos, M. A.; Gama, S.; Gano, L.; Cantinho, G.; Farkas, E., A new bis(3-hydroxy-4-pyridinone)-IDA derivative as a potential therapeutic chelating agent. Synthesis, metal-complexation and biological assays. *Dalton Transactions* **2004**, (21), 3772-3781.

50. Santos, M. A.; Gama, S.; Gano, L.; Farkas, E., Bis(3-hydroxy-4-pyridinone)-EDTA derivative as a potential therapeutic Al-chelating agent. Synthesis, solution studies and biological assays. *Journal of Inorganic Biochemistry* **2005,** 99, (9), 1845-1852.

51. Al-Warhi, T. I.; Al-Hazimi, H. M. A.; El-Faham, A., Recent development in peptide coupling reagents. *Journal of Saudi Chemical Society* **2012,** 16, 97-116.

52. Dunetz, J. R.; Xiang, Y.; Baldwin, A.; Ringling, J., General and Scalable Amide Bond Formation with Epimerization-Prone Substrates Using T3P and Pyridine. *Organic Letters* **2011,** 13, (19).

53. Valeur, E.; Bradley, M., Amide bond formation: beyond the myth of coupling reagents. *Chemical Society Reviews* **2009,** 38, 606-631.

54. Peterlik, M.; Stoeppler, M., Calcium. In *Elements and Their Compounds in the Environment*, Merian, E.; Anke, M.; Ihnat, M.; Stoeppler, M., Eds. Wiley-VCH Verlag GmbH: **2008**; 599-618.

55. Anke, M.; Kramer-Beselia, K.; Losch, E.; Muller, R.; Muller, M.; Seifert, M., Calcium supply, intake, balance and requirement of man. First information: Calcium content of plant food. In *Macro and Trace Elements.*, Schubert, V. H., Ed. Leipzig, **2002**; 1386-1391.

56. Anke, M.; Kramer-Beselia, K.; Dorn, W.; Hoppe, C., Calcium supply, intake, balance and requirement of man. Second information: Calcium content of animal food. In *Macro and Trace Elements.*, Schubert, V. H., Ed. Leipzig, **2002**; 1392-1397.

57. Weaver, C. M., Calcium. *American Society for Nutrition* **2011,** 2, 290–292.

58. Weaver, C. M.; Heaney, R. P., Calcium. In *Modern nutrition in health disease.*, 10th Edition; Shils, M. E.; Shike, M.; Ross, A. C.; Caballero, B.; Cousins, R. J., Eds. Lippincott Williams & Wilkins: Baltimore (MD), **2006**, 194-210.

59. Peacock, M., Calcium Metabolism in Health and Disease. *Clinical Journal of the American Society of Nephrology* **2010,** 5, S23-S30.

60. Kruse, H. D.; Schmidt, M. M.; McCollum, E. V., Studies on magnesium deficiency in animals. 4. Reaction to galvanic stimuli following magnesium deprivation. *American Journal of Physiology* **1933,** 105, 635-642.

61. Hirschfelder, A. D.; Haury, V. G., Clinical manifestations of high and low plasma magnesium: Dangers of epsom salt purgation in nephritis. *Journal of the American Medical Association* **1934,** 102, (14), 1138-1141.

62. Flink, E. B., Magnesium deficiency syndrome in man. *Journal of the American Medical Association* **1956,** 160, 1406-1409.

63. Vormann, J., Magnesium. In *Elements and Their Compounds in the Environment*, Merian, E.; Anke, M.; Ihnat, M.; Stoeppler, M., Eds. Wiley-VCH Verlag GmbH: **2008**, 587-598.

64. Shils, M. A., Magnesium. In *Handbook of Nutritionally Essential Mineral Elements.*, O'Dell, B. J.; Sunde, R., Eds. Marcel Dekker: **1997,** 117-152, New York, Basel, Hong Kong.

65. Gunther, T., Biochemistry and pathobiochemistry of magnesium. *Artery* **1981,** 9, 167-181.

66. Fraser, R.; MacIntyre, I., *Biochemical disorders in human disease.* 3rd Edition; London, Churchill, **1970**.

67. Paymaster, N. J., Magnesium metabolism: a brief review. *Annals of the Royal College of Surgeons of England* **1976,** 58, 309-314.

68. Vormann, J.; Förster, C.; Zippel, U.; Lozo, E.; Günther, T.; Merker, H.-J.; Stahlmann, R., Effects of Magnesium Deficiency on Magnesium and Calcium Content in Bone and Cartilage in Developing Rats in Correlation to Chondrotoxicity. *Calcified Tissue International* **1997,** 61, (3), 230 -238.

69. Peganova, S.; Eder, K., Zinc. In *Elements and Their Compounds in the Environment*, Wiley-VCH Verlag GmbH: **2008**, 1203-1239.

70. Adriano, D. C., Zinc. In *Trace Elements in the Terrestrial Environment*, Springer New York: New York, NY, **1986**, 421-469.

71. Malle, K. G., Zink in der Umwelt. *Acta Hydrochimica et Hydrobiologica* **1992,** 20, 196-204.

72. Yeats, P. A., The distribution of trace metals in ocean waters. *Science of The Total Environment* **1988,** 72, 131-149.

73. Henkin, R. I., *Zinc*. Univ. Park. Press: Baltimore, MD, **1979**.

74. Siegert, E.; Anke, M.; Szentmihalyi, S.; Regius, A.; Lokay, D.; Powel, J.; Gruen, M., The zinc supply of plants and animals in Middle Europe. In *Trace Element Symposium*, University of Leipzig-Jena, Germany, **1986**, 487-493.

75. Wastney, M. E.; Aamodt, R. L.; Rumble, W. F.; Henkin, R. I., Kinetic analysis of zinc metabolism and its regulation in normal humans. *The American Journal of Physiology* **1986,** 251, (2), R398-408.

76. Scherz, H.; Kloos, G.; Senser, F., *Food Composition and Nutrition Tables 1986/1987*. Wissenschaftliche VerlagsGmbH: Stuttgart, **1986**.

77. Kaltenberg, J.; Plum, L. M.; Ober-Blöbaum, J. L.; Hönscheid, A.; Rink, L.; Haase, H., Zinc signals promote IL-2-dependent proliferation of T cells. *European Journal of Immunology* **2010,** 40, (5), 1496-1503.

78. Agren, M. S., Studies on zinc in wound healing. *Acta dermato-venereologica. Supplementum* **1990,** 154, 1-36.

79. Powell, S. R., The antioxidant properties of zinc. *The Journal of Nutrition* **2000,** 130, (5S Suppl), 1447S-1454S.

80. Singh, M.; Das, R. R., Zinc for the common cold. *The Cochrane Database of Systematic Reviews* **2011,** 16, (2).

81. Tuerk, M. J.; Fazel, N., Zinc deficiency. *Current Opinion in Gastroenterology* **2009,** 25, (2), 136-143.

82. National Institute of Health, Zinc - Fact Sheet for Health Professionals. *Office of Dietary Supplements* **2013**.

83. Cigala, R. M.; Crea, F.; De Stefano, C.; Lando, G.; Milea, D.; Sammartano, S., The inorganic speciation of tin(II) in aqueous solution. *Geochimica et Cosmochimica Acta* **2012,** 87, 1-20.

84. Anger, J. P., Tin. In *Elements and Their Compounds in the Environment*, Merian, E.; Anke, M.; Ihnat, M.; Stoeppler, M., Eds. Wiley-VCH Verlag GmbH: **2008**, 1113-1124.

85. Auteur, C. A.; Auteur, P. M., L'étain et les organoétains en milieu marin: biogéochimie et écotoxicologie. *Rapports scientifiques et techniques de l'IFREMER,* **1989**.

86. Lantzy, R. J.; Mackenzie, F. T., Atmospheric trace metals: global cycles and assessment of man's impact. *Geochimica et Cosmochimica Acta* **1979,** 43, (4), 511-525.

87. Howe, P.; Wood, M.; Watts, P., Tin and inorganic tin compounds. In *Concise International Chemical Assessment Document 65.*, World Health Org., Ed. Geneva, **2005**.

88. Senesil, G. S.; Baldassarre, G.; Senesi, N.; Radina, B., Trace element inputs into soils by anthropogenic activities and implications for human health. *Chemosphere* **1999,** 39, (2), 343-377.

89. Veysseyre, A.; Moutard, K.; Ferrari, C.; Van de Velde, K.; Barbante, C.; Cozzi, G.; Capodaglio, G.; Boutron, C., Heavy metals in fresh snow collected at different altitudes in the Chamonix and Maurienne valleys, French Alps: initial results. *Atmospheric Environment* **2001,** 35, (2), 415-425.

90. Maguire, R. J.; Tkacz, R. J.; Chau, Y. K.; Bengert, G. A.; Wong, P. T. S.; Chau, Y. K.; Kramar, O.; Bengert, G. A., Occurrence of organotin compounds in water and sediment in Canada. *Chemosphere* **1986,** 15, 253-274.

91. Giordano, R.; Lombardi, G.; Ciaralli, L.; Beccaloni, E.; Sepe, A.; Ciprotti, M.; Costantini, S., Major and trace elements in sediments from Terra Nova Bay, Antarctica. *The Science of the Total Environment* **1999,** 227, (1), 29-40.

92. Eisler, R., Tin hazards to fish, wildlife, and invertebrates: a synoptic review. *Biological Report* **1989**, 85.

93. Ichihashi, H.; Nakamura, Y.; Kannan, K.; Tsumura, A.; Yamasaki, S., Multi-elemental concentrations in tissues of Japanese common squid (Todarodes pacificus). *Archives of Environmental Contamination and Toxicology* **2001,** 41, (4), 483-490.

94. Burger, J.; Gochfeld, M., Metals in Laysan albatrosses from Midway Atoll. *Archives of Environmental Contamination and Toxicology* **2000,** 38, (2), 254-259.

95. Burger, J.; Gochfeld, M., Metal levels in feathers of cormorants, flamingos and gulls from the coast of Namibia in southern Africa. *Environmental Monitoring and Assessment* **2001,** 69, (2), 195-203.

96. Cardellicchio, N.; Decataldo, A.; Di Leo, A.; Giandomenico, S., Trace elements in organs and tissues of striped dolphins (Stenella coeruleoalba) from the Mediterranean Sea (southern Italy). *Chemosphere* **2002,** 49, (1), 85-90.

97. Malcolm, H. M.; Boyd, I. L.; Osborn, D.; French, M. C.; Freestone, P., Trace metals in Antarctic fur seal (Arctocephalus gazella) livers from Bird Island, South Georgia. *Marine Pollution Bulletin* **1994,** 28, (6), 375-380.

98. Blunden, S.; Wallace, T., Tin in canned food: a review and understanding of occurrence and effect. *Food and Chemical Toxicology* **2003,** 41, 1651-1662.

99. Momčilović, B., Copper. In *Elements and Their Compounds in the Environment*, Merian, E.; Anke, M.; Ihnat, M.; Stoeppler, M., Eds. Wiley-VCH Verlag GmbH: **2008**, 731-750.

100. Horn, R. A., *The Chemistry of Our Environment*. John Wiley & Sons: New York, **1978**.

101. Förstner, U.; Wittmann, G. T. W., *Metal Pollution in the Aquatic Environment.* Springer-Verlag: Berlin, **1981**.

102. Peres, I.; Pilan, J. C., Copper LC50 to Cyprinus carpio. Influence of hardness, seasonal variation, proposition of maximum acceptable toxicant concentration. *Environmental Technology* **1991,** 12, 161-167.

103. Playle, R. C.; Gensemer, R. W.; Dixon, D. G., Copper accumulation of gills of fathead minnows: influence of water hardness, complexation and pH of the gill micro- environment. *Environmental Toxicology and Chemistry* **1992,** 11, 381-391.

104. Buckley, J. T.; Roch, M.; McCarter, M.; Rendel, C. A.; Matheson, A. T., Chronic exposure of coho salmon to sublethal concentrations of copper.--I. Effect on growth, on accumulation and distribution of copper, and on copper tolerance. *Comparative Biochemistry and Physiology - Part C: Toxicology & Pharmacology* **1982,** 72, (1), 15-19.

105. Turniund, J. R.; Keyes, W. R.; Anderson, H. L.; Acord, L. L., Copper absorption and retention in young men at three levels of dietary copper by use of the stable isotope ^{65}Cu. *American Society for Clinical Nutrition* **1989,** 49, 870-878.

106. Cox, D. W., Genes of the copper patway. *The American Journal of Human Genetics* **1995,** 56, 828-834.

107. Gow, P. J.; Smallwood, R. A.; Angus, P. W.; Smith, A. L.; Wall, A. J.; Sewell, R. B., Diagnosis of Wilson's disease: an experience over three decades. *Gut* **2000,** 46, 415-419.

108. L. S.; Pegler, S. P.; Lellis, R. F.; Krebs, V. L.; Robertson, S.; Morgan, T.; Honjo, R. S.; Bertola, D. R.; Kim, C. A., Menkes disease: importance of diagnosis with molecular analysis in the neonatal period. *Revista Da Associacao Medica Brasileira* **1992**.

109. Alt, E. R.; Sternlieb, I.; Goldfisher, S., The Cytopathology of Metal Overload. *International Review of Experimental Pathology* **1990,** 31, 165-88.

110. Goldstein, S.; Czapski, G., The role and mechanism of metal ions and their complexes in enhancing damage in biological systems or in protecting these systems from the toxicity of O_2^-. *Free Radical Biology & Medicine* **1986,** 2, (1), 3-11.

111. Yokel, R. A., Aluminum. In *Elements and Their Compounds in the Environment*, Merian, E.; Anke, M.; Ihnat, M.; Stoeppler, M., Eds. Wiley-VCH Verlag GmbH: **2008,** 635-658.

112. Agency for Toxic Substances and Disease Registry, Toxicological Profile for Aluminum., Department of Health and Human Services., Ed. **1999**.

113. - -Vargas, M., Direct fluorimetric determination of dissolved aluminum in seawater at nanomolar levels. *Analytica Chimica Acta* **1997,** 355, (2–3), 157-161.

114. Davison, A. M.; Oli, H.; Walker, G. S.; Lewins, A. M., Water Supply Aluminium Concentration, Dialysis Dementia, and Effect of Reverse-Osmosis Water Treatment. *The Lancet* **1982,** 320, (8302), 785-787.

115. Barnett, P. R.; Skougstad, M. W.; Miller, K. J., Chemical Characterization of a Public Water Supply. *Journal of American Water Works Association* **1969,** 61, (2), 60-67.

116. Gensemer, R. W.; Playle, R., The Bioavailability and Toxicity of Aluminum in Aquatic Environments. *Critical Reviews in Environmental Science and Technology* **1999,** 29, 315-450.

117. Jansen, S.; Broadley, M. R.; Robbrecht, E.; Smets, E., Aluminum hyperaccumulation in angiosperms: A review of its phylogenetic significance. *The Botanical Review* **2002,** 68, (2), 235-269.

118. Duggan, J. M.; Dickeson, J. E.; Tynan, P. F.; Houghton, A.; Flynn, J. E., Aluminium beverage cans as a dietary source of aluminium. *Medical Journal of Australia* **1992,** 156, (9), 604-605.

119. Institute of Medicine, Committee on Food Chemicals Codex, *Food Chemical Codex.* National Academy Press: Washington, DC, **1981**.

120. Allen, E. A.; Boardman, M. C.; Plunkett, B. A., Comparison of two chelating agents immobilized on controlled-pore glass for the preconcentrationof aluminium from aqueous solutions. *Analytica Chimica Acta* **1987,** 196, 323-327.

121. Crisponi, G.; Nurchi, V. M.; Bertolasi, V.; Remelli, M.; Faa, G., Chelating agents for human diseases related to aluminium overload. *Coordination Chemistry Reviews* **2012,** 256, (1–2), 89-104.

122. Kawahara, M., Effects of aluminum on the nervous system and its possible link with neurodegenerative diseases. *Journal of Alzheimer's Disease* **2005,** 8, (2), 171-182.

123. Savory, J.; Herman, M. M.; Katsetos, C. D.; Will, M. R., *Aluminum in Chemistry Biology and Medicine.* Cortina International/Raven Press: Verona/New York, **1991**.

124. Skoog, D. A.; Holler, F. J.; Crouch, S. R., *Principles of Instrumental Analysis.* 6th Edition; Thomson Brookx/Cole: **1998**.

125. Harris, D. C., *Quantitative Chemical Analysis.* 7th Edition.; W. H. Freeman and Company: **2007**.

126. Flaschka, H. A., *EDTA Titration*. Pergamon Press: London, **1959**.

127. De Stefano, C.; Foti, C.; Giuffrè, O.; Mineo, P.; Rigano, C.; Sammartano, S., Binding of Tripolyphosphate by Aliphatic Amines: Formation, Stability and Calculation Problems. *Annali di Chimica (Rome)* **1996,** 86, 257-280.

128. De Stefano, C.; Mineo, P.; Rigano, C.; Sammartano, S., Ionic Strength Dependence of Formation Constants. XVII. The Calculation of Equilibrium Concentrations and Formation Constants. *Annali di Chimica (Rome)* **1993,** 83, 243-277.

129. De Stefano, C.; Princi, P.; Rigano, C.; Sammartano, S., Computer Analysis of Equilibrium Data in Solution. ESAB2M: An Improved Version of the ESAB Program. *Annali di Chimica (Rome)* **1987,** 7, 643-675.

130. De Stefano, C.; Sammartano, S.; Mineo, P.; Rigano, C., Computer Tools for the Speciation of Natural Fluids. *Marine Chemistry - An Environmental Analytical Chemistry Approach.* Kluwer Academic Publishers: Amsterdam: **1997**.

131. Alderighi, L.; Gans, P.; Ienco, A.; Peters, D.; Sabatini, A.; Vacca, A., Hyperquad simulation and speciation (HySS): a utility program for the investigation of equilibria involving soluble and partially soluble species. *Coordination Chemistry Reviews* **1999,** 184, (1), 311-318.

132. Gans, P.; Sabatini, A.; Vacca, A., Investigation of equilibria in solution. Determination of equilibrium constants with the HYPERQUAD suite programs. *Talanta* **1996,** 43, 1739-1753.

133. Davies, C. W., *Ion Association.* Butterworths: London, **1962**.

134. De Robertis, A.; Foti, C.; Sammartano, S.; Gianguzza, A., *Marine Chemistry, an Environmental Analitic Chemistry Approach.* Kluwer Accademic Publishers: Amsterdam, 1997.

135. Crea, F.; De Stefano, C.; Manfredi, G.; Sammartano, S., Sequestration of some biogenic amines and poly(allyl)amine by high molecular weight polycarboxylic ligands in aqueous solution. *Journal of Molecular Liquids* **2010,** 151, (2-3), 138-144.

136. Crea, F.; De Stefano, C.; Gianguzza, A.; Pettignano, A.; Piazzese, D.; Sammartano, S., Acid-base properties of synthetic and natural polyelectrolytes: experimental results and models for the dependence on different aqueous media. *Journal of Chemical and Engineering Data* **2009,** 54, (2), 589-605.

137. Cigala, R. M.; Crea, F.; De Stefano, C.; Milea, D.; Sammartano, S.; Scopelliti, M., Speciation of tin(II) in aqueous solution: thermodynamic and spectroscopic study of simple and mixed hydroxocarboxylate complexes. *Monatshefte Fur Chemie* **2013,** 144, 761-772.

138. Baes, C. F.; Mesmer, R. E., The Hydrolysis of Cations. *John Wyley & Sons, New York* **1976**.

139. Cigala, R. M.; De Stefano, C.; Giacalone, A.; Gianguzza, A., Speciation of Al^{3+} in fairly concentrated solutions (20 – 200 mmol L^{-1}) at I = 1 mol L^{-1} ($NaNO_3$), in the acidic pH range, at different temperatures. *Chemical Speciation and Bioavailability* **2011,** 23, (11), 33-37.

140. Martell, A. E.; Smith, R. M.; Motekaitis, R. J., NIST Critically selected stability constants of metal complexes database, 8.0. *National Institute of Standard and Technology*: Garthersburg, MD, **2004**.

141. Öhman, L. O. Equilibrium Studies Of Ternary Aluminium (III) Hydroxo Complexes With Ligands Related To Conditions In Natural Waters. Doctor of Philosophy Thesis, University of Umeà, Sweden, **1983**.

142. Berto, S.; Crea, F.; Daniele, P. G.; De Stefano, C.; Prenesti, E.; Sammartano, S., Potentiometric and spectrophotometric characterization of the UO_2^{2+}-citrate complexes in aqueous solution, at different concentrations, ionic strengths and supporting electrolytes. *Radiochim. Acta* **2012,** 100, 13-28.

143. Daniele, P. G.; De Robertis, A.; De Stefano, C.; Gianguzza, A.; Sammartano, S., Studies on Polyfunctional O-Ligands. Formation Thermodynamics of Simple and Mixed Alkali Metal Complexes with Citrate at Different Ionic Strengths in Aqueous Solution. *Journal of Chemical Research* **1990**, (S) 300 (M) 2316-2350.

144. Ohman, L. O.; Sjoberg, S., Equilibrium And Structural Studies Of Silicon(IV) And Aluminum(III) In Aqueous-Solution .9. A Potentiometric Study Of Mono-Nuclear And Poly-Nuclear Aluminum(III) Citrates. *Journal of the Chemical Society, Dalton Transactions* **1983**, 2513-2517.

145. Gregor, J. E.; Powell, H. K. J., Aluminium(III)-Citrate Complexes: a Potenziometric and ^{13}C N.M.R.-Study. *Australian Journal of Chemistry*, **1986**, 39, 1851-1864.

146. Lakatos, A.; Banyai, I.; Decock, P.; Kiss, T., Time-Dependent Solution Speciation of the Al^{III}-Citrate System: Potentiometric and NMR Studies. *European Journal of Inorganic Chemistry* **2001**, 461-469.

147. Wiese, G.; Vieth, J. A., Komplexbildung zwischen Zitronensäure und Aluminium. *Zeitschrift für Naturforschung* **1975,** 306, 446-453.

148. Spadini, L.; Schindler, P. W.; Sjöberg, S., On the Stability of the $AlOSi(OH)_3^{2+}$ Complex in Aqueous Solution. *Aquatic Geochemistry* **2005**, 21-31.

149. Armarego, W. L. F.; Perrin, D. D., *Purification of Laboratory Chemicals*. 4th Edition; Butterworth-Heinemann Press: Oxford, **1999**.

150. Gottlieb, H. E.; Kotlyar, V.; Nudelman, A., NMR Chemical Shifts of Common Laboratory Solvents as Trace Impurities. *Journal of Organic Chemistry* **1997,** 62, (21), 7512-7515.

151. Montembault, V.; Soutif, J.-C.; Brosse, J.-C., Synthesis of chelating molecules as agents for magnetic resonance imaging, 31. Polycondensation of diethylenetriaminepentaacetic acid bisanhydride with diols and diamines. *Reactive and Functional Polymers* **1996,** 29, (1), 29-39.

152. Andersen, E. R.; Holmaas, L. T.; Olaisen, V., Process for the production of DTPA-bisanhydride. In Google Patents: **2006**.

153. Roosen, J.; Binnemans, K., Adsorption and chromatographic separation of rare earths with EDTA and DTPA-functionalized chitosan biopolymers., *Journal of Materials Chemistry A* **2013**, 12, 1-5.

154. Santos, M. A.; Gil, M.; Marques, S.; Gano, L.; Cantinho, G.; Chaves, S., N-Carboxyalkyl derivatives of 3-hydroxy-4-pyridinones: synthesis, complexation with Fe(III), Al(III) and Ga(III) and in vivo evaluation. *Journal of Inorganic Biochemistry* **2002,** 92, (1), 43-54.

155. Santos, M. A.; Grazina, R.; Neto, A. Q.; Cantinho, G.; Gano, L.; Patrıcio, L., Synthesis, chelating properties towards gallium and biological evaluation of two N-substituted 3-hydroxy-4-pyridinones. *Journal of Inorganic Biochemistry* **2000,** 304, (78), 303-311.

156. Bretti, C.; De Stefano, C.; Foti, C.; Sammartano, S., Total and Specific Solubility and Activity Coefficients of Neutral Species of $(CH_2)_{2i-2}N_i(CH_2COOH)_{i+2}$ Complexons in Aqueous NaCl Solutions at Different Ionic Strengths, $(0 \leq I \leq 5)$ mol·L^{-1}, and 298.15 K. *Journal of Chemical & Engineering Data* **2011,** 56, 437-443.